STROMAL-EPITHELIAL DYNAMICS IN RESPONSE TO
FRACTIONATED RADIOTHERAPY

BY

MUQEEM ABDUL QAYYUM

DISSERTATION

Submitted in partial fulfillment of the requirements
for the degree of Doctor of Philosophy in Bioengineering
in the Graduate College of the
University of Illinois at Urbana-Champaign, 2012

Urbana, Illinois

Doctoral Committee:

Professor Michael Insana, Chair
Professor William O'Brien
Professor Ann Nardulli
Associate Professor Peter Wang
Adjunct Assistant Professor Masab Garada

ABSTRACT

Radiotherapy is central to the management of a number of human cancers, either as an adjuvant or primary treatment modality. The principal objective in irradiating tumors is to permanently inhibit their proliferative ability. More than half of all malignancies are primarily treated with radiation, but the heterotypic nature of tumor cells greatly complicates their response to radiotherapy. The need for reliable parameters to predict tumor and normal tissue response to radiation is therefore a prime concern of clinical oncology.

Post-operative radiotherapy has commonly been used for early stage breast cancer to treat residual disease. There is continued debate as to what might be the proper dose per fraction as well as the total dose of radiation that needs to be prescribed to prevent disease recurrence. Countries outside the US have adopted increased dose fractionation (i.e., hypofractionation) schemes for early stage breast cancer as a standard of practice; however there is a lack of confidence in these approaches in the United States.

The tumor microenvironment plays a significant role in regulating the progression of carcinomas, although the mechanisms are not entirely clear. The primary objective of this work was to characterize, through mechanobiological and radiobiological modeling, a test bed for radiotherapy fractionation techniques assessment. Our goal is to understand how the tumor microenvironment responds to dose fractionation schemes for Breast Conserving Therapy (BCT). Although carcinomas are the major concern for oncology, in this project, the goal is to understand how the stromal microenvironment influences behavior of the cancer cell populations. By classifying 3-D cellular co-cultures as having a reactive or quiescent stroma using the mechanobiology profile (culture stiffness,

cellular activation, differentiation, and proliferation) we aim to differentiate the effectiveness of various fractionation schemes.

The benefits of understanding heterotypic signaling in post-surgical breast cancer recurrence would be to assist radiation oncologists in designing an improved therapeutic strategy. To relate the parameters of cellular function to therapeutic prescriptions which offer an enhanced clinical outcome would address the lack of knowledge regarding recurrence of disease, tumor control and whether the tumor microenvironment requires more aggressive treatments.

In our work to date, we have developed a three-dimensional co-culture model to determine how alternative dose fractionations affect the post-surgical microenvironment. This work suggests that 3-D co-cultures provide the microenvironmental cues needed to reexamine the radiobiological basis underlying radiation therapy.

The findings suggest dose escalation to the tumor region may deactivate the reactive stroma, thus minimizing the cancer promoting environment. Large-fraction irradiation may be used to sterilize residual tumor cells and inhibit activation of intracellular transduction pathways that are promoted during the post-surgical wound-healing period. Wound-healing mechanisms are characterized by angiogenesis, fibroplasia, collagen production and granulation tissue formation all of which impact patient prognosis. In fact, tumor dose escalation trials have been proven to reduce local recurrence rates and thus new approaches to partial breast irradiation and tumor bed boosting using external-beam electrons and intensity-modulated radiotherapy (IMRT) techniques are currently under use. These techniques minimize absorbed dose to healthy breast tissues. Treating the residual cancer cells and the reactive stroma that has been stimulated by wound healing requires that we look at the interplay between cell types as well as the mechanical and biochemical factors driving disease.

We have discovered that the reason hypofractionation schemes (larger irradiation fractions per day with less total dose) offer therapeutic advantages to some patients could be that it is more effective at treating the reactive stroma. We can kill the cancer cells at the standard rate (180 cGy/fraction), but we have found the larger fractions specifically inhibit wound healing mechanisms by inactivating stromal fibroblasts. The long term goal would be to reduce recurrence rates for early stage breast cancer by treating postsurgical regions most likely to harbor residual tumor cells. Ionizing radiation stress and its effect on ECM mediated cellular functions continues to be an evolving area of research. This study is an initial step in my career plans to study stromal modulation of epithelial tumors. It is also my career goal to integrate basic science experiments and engineering tools into clinical practice.

To Radiya, my daughter, like this thesis you are a dream come true.

ACKNOWLEDGEMENTS

I would like to express my deep gratitude to, Dr. Michael F. Insana, for his advice, his support and for consistently challenging me with his exceptional high standards to reach my optimal potential. I would also like to thank the members of my committee Dr. W. O'Brien, Dr. Y. Wang, Dr. M. Garada and especially Dr. Ann Nardulli for sharing with me her advice and expertise in the time leading up to my defense.

The Chemical Imaging and Structures Laboratory under Dr. Rohit Bhargava have been instrumental in the successful completion of this work. I would like to acknowledge Jin Tae Kwak, for his scientific input to my research and collaboration in solving the difficult challenges that arose in the course of my research. Without their support and input this dissertation could not have been completed.

To Dr. Masab Garada and Provena Covenant Medical Center for allowing me to use their resources in pursuit of this research, without it my hypothesis for this project might not have developed. I would like to specially acknowledge Dr. Garada for his clinical input and guidance throughout my time on this project. I would not have been able to reach this conclusion without his support, for that I am sincerely grateful.

Additional thanks go to my colleagues in the lab: Dr. S. Kalyanam, Dr. K. S. Toohey, Dr. M. Orescanin, Jing Xu, and Yue Wang. They have all contributed to this project in various ways, which is stronger for all of their assistance.

Finally to my family, my Dad, Abdul Qayyum and my Mom, Saleha, for their never-ending faith in me; to my siblings Azeem, Khaled and Zaineb, who are always there for me when I need them, I am

extremely grateful for the support and love that has never wavered through the years of struggle and

sacrifice that it took for me to complete this work. And to my wife Naima, who helped make sure I

sound good. I love you all and I am so grateful to have you in my life.

TABLE OF CONTENTS

LIST OF TABLES AND FIGURES

LIST OF ABBREVIATIONS

α-SMA	alpha-smooth muscle actin
ANOVA	Three-way analysis of variance
BCS	Breast Conserving Surgery
BCT	Breast Conserving Therapy
CAFs	Cancer-Activated Fibroblasts
cGy	centiGray
ECM	Extracellular Matrix
IF	Immunofluorescence staining
IR	Ionizing Radiation
MCF-7	Michigan Cancer Foudation 7, malignantly transformed epithelial cells
MRC-5	Normal Human Lung Fibroblast
MTT	3-(4, 5-dimethylthiazol-2-yl)-2, 5-diphenyltetrazolium bromide
ROS	Reactive Oxygen Species
RT	Radiation Therapy
TGF-β1	Transforming Growth Factor beta 1
TR	Therapeutic Ratio

CHAPTER 1

INTRODUCTION

1.1 Challenges in Fractionated Radiotherapy for Breast Cancer

Breast conserving surgery (BCS) or lumpectomy for early stage breast cancer has revolutionized patient care over the last two decades. Early stage breast cancers with small primary lesions have been diagnosed through increased use of diagnostic mammography; thus making BCS the new gold standard over mastectomy (Veronesi et al. 2002; Goh & Yong 2004). An improved cosmetic outcome and overall quality of life stemming from the less invasive surgery is a significant benefit at the expense of a potential increased risk in local recurrence (Fisher et al. 2002). Clinical observations coupled with the notion that surgery modifies the growth kinetics of breast cancer micrometastasis (Demicheli et al. 2001; Baum et al. 2005), support the hypothesis that surgery itself presents a perturbing factor for metastasis development in humans. The effect of wound healing on tumor growth has been shown in studies of mice (Baker et al. 1989), which assessed the number of cells from three different tumor models needed to induce tumors at 50% of the injected sites (TD/50) when introduced into surgically wounded tissue compared with non-wounded tissue. The studies found there was a greater likelihood of recurrence in wounded tissues compared to non-wounded tissues. The difference was interpreted as the result of the presence of growth factors derived from the traumatized tissue and the inflammatory cells at the wound site. Also, studies by (Kaplan et al. 2005) and (Tsuchiya et al. 2003) found that tumor derived growth factors were able to create the formation of specific cellular cluster sites or premetastatic niches where tumor cells could successfully metastasize and develop into viable tumors.

The premetastatic niche could be thought of as a base for cancer cells to adhere and proliferate, or a budding version of the reactive stroma.

The complex cellular behavior in forming these pre-metastatic niches is paralleled in some respects to the events that occur during normal wound healing. The healing process conveys motility to the surrounding cells on the periphery of the cavity to become invasive and move towards the core of the wound to heal the breast after surgical removal of the tumor. During this phase any residual neoplastic cells at the excision site are also exposed to the physiological signaling associated with inflammation and wound repair. This effect has previously been related to growth factors produced by stromal cells during the wound healing process (Belletti et al. 2008). This indicates that growth factors in the microenvironment stimulate mammary cells, leading to residual disease locally following BCS. Ultimately this contributes to recurrences of breast cancer.

Possible explanations of residual disease include: (1) incomplete removal of the tumor, possibly due to breast duct anatomy and extensive intraductal components (Mannino & Yarnold 2009); (2) stimulation of migration and growth of residual occult tumor cells in response to the surgical wound healing (Tagliabue et al. 2003; Hockel & Dornhofer 2005; Belletti et al. 2008). However, the combined modalities of chemo and radiotherapy (RT) with BCS have proven in many trials to give similar local recurrence rates as that of mastectomy alone (Fisher et al. 2002; Veronesi et al. 2002). The ability of radiation to eradicate the microscopic foci of malignant cells remaining after a breast tumor mass is surgically removed, ultimately led to breast-conserving therapy (BCT) as an option for many breast cancer patients. This study focuses primarily on radiotherapy. Current clinical trials suggest radiation dose escalation to the tumor bed region may decrease the probability of recurrences at the surgical scar site and eradication of residual disease, if it's tolerated by patients. Ultimately, dose escalation is limited by the volume of breast irradiated or the amount of absorbed dose received by adjacent critical

2

normal tissues (ribs, lung, heart, etc.). Larger irradiation fractions may be used to sterilize residual

tumor, reactive stroma and inhibit activation of intracellular transduction pathways that initiate wound-

healing mechanisms characterized by angiogenesis, fibroplasia, collagen production and granulation

tissue formation. Important to the treatment of any disease is a simple relationship between treatment

and effect. In fact, the Standardization of Breast Radiotherapy Trails (START), have looked at late

adverse effects and tumor control, which strengthen evidence in favor of alternative fractionation

schemes, e.g., hypofractionated regimens, with potential for fewer adverse effects to normal breast

tissues (Abram et al. 2008). Hypofractionation is a radiation therapy schedule that delivers a larger dose

per fraction but a lower total dose than the conventional 25 fractions of 180 cGy (centigray) each for a

total dose of 4500 cGy.

Improvements in treatment planning and radiation delivery techniques have allowed for the

inclusion of radiobiological aspects, such as cell sensitivity, activation, proliferation or cell viability to

enhance treatment optimization (Fowler 2001; Muriel 2002; Yang & Xing 2005) parameters which we

have explored in our studies. We initially looked at the isolated stromal component response to IR. We

then developed a residual disease model to represent the incomplete removal of the tumor or the

stimulation of residual occult tumor cells in response to the surgical wound healing and then under IR.

1.2 Breast Conserving Therapy (BCT)

Breast-conserving surgery followed by external radiotherapy is the current standard of

treatment for localized cancer of the breast (Belletti et al. 2008). The common understanding is that RT

sterilizes the tumor bed of residual tumor cells. However, the absolute effect of radiotherapy on the

microenviroment of the post-surgical region is still unclear. There is a need to study the factors that play

a vital role in the elimination of tumor cells and suppression of reactive stroma following surgical

procedures.

Although the primary objective of ionizing radiation (IR) exposure is to control growth of cancerous epithelial cells (cancer cells), IR-induced gene expression in cells of adjacent stroma also modulates conditions that affect tumor growth (Barcellos-Hoff 2008, 2010). Stroma includes fibroblast, macrophage, lymphocyte, and endothelial cells; however, the focus of this study is the influence of cancerous epithelial and fibroblasts interaction on the mechanical environment that modulates the activity of signaling networks directing cell functions, including those of cancer cells.

We hypothesized that radiotherapy may not only decrease breast cancer cell survival but influence tumor microenvironment by changing the cell phenotype leading to tissue stiffness and cell signaling that promotes tumorigenesis and metastasis (Vaidya et al. 2004; Barcellos-Hoff et al. 2005), all of which alter patient prognosis. RT also impacts the post-surgical healing process. Wound healing processes are mechanically regulated (Grinnell 1994; Hinz et al. 2001; Tomasek et al. 2002; Wipff & Hinz 2009). Wound repair is known to eliminate injured cells and tissue; there is great deal of interest in examining it as a possible factor affecting the incidence of residual carcinoma following an incomplete excision of the tumor. Wound healing involves multiple stages including hemostasis, inflammation, tissue regeneration and matrix remodeling (Hockel & Dornhofer 2005). Under matrix remodeling, the extracellular matrix (ECM) stiffness and tissue strength increases from collagen upregulation and cross-linking to form scar tissue (Thibeault et al. 2002). The fibroblasts exert force to close the wound (Amadeu et al. 2003). It has long been recognized that wound healing is an important element during treatment and we would like to use our model to focus on the stromal components and their interaction to growth factors and IR. Investigators have noted that a stimulatory effect of wound healing on post-surgical residual disease contributes to the poor prognostic value of standard radiotherapy fractionation schemes. We investigated the altered fractionation schemes to evaluate the microenvironments response under RT.

1.3 Need for physical modeling in cancer treatment

Treatment regimens are conventionally designed through a range of controlled clinical trials. Clinical trials are vital prerequisites to establishing therapeutic principles. However, trials are lengthy processes which involve optimization of many coupled parameters for their success. In-vitro models simulate a less complex environment to isolate a specific set of tissue components for study. They allow us to overcome some of the limitations encountered by clinical trials. Beside animal models and single cell experiments, which are often used for pre-clinical studies, we propose models encompassing physical and engineering concepts that represent the systems biology approach.

Physical models used in cancer research provide simplified tools that reproduce isolated aspects of the tissue system. They do not reflect accurately the fine details of the real system. To compensate for some of its deficiencies, we propose a co-culture model which blends the cancer cell model and wound healing, as opposed to one cell type model. This process holds significant promise for providing new understanding of RT fractionation protocols on residual disease. Thus, we wish to model and examine the effects of irradiation delivered to cell cultures that represent a subset of the conditions of adjuvant patient treatments following BCS.

There is a large amount of cross-talk between tumor cells and surrounding stromal cells, which aids in post-surgical wound healing and metastatic invasion from residual disease. The tumor-cell microenvironment is recognized as an important determinant in the development and invasive potential of breast cancer (Bissell et al. 2002; Allinen et al. 2004). Cells are very sensitive to chemical and mechanical changes in their microenvironment, which can provide cues for developmental and other intracellular programs (Paszek et al. 2005; Engler et al. 2006). Culturing epithelial cells in 3D matrices leads to a difference in receptor expression, localization, and sensitivity to treatments when compared with a 2D culture. 2D cell cultures have considerable difference in morphology, cell-cell, and cell-matrix

interactions, and differentiation when compared to the more physiological 3D environments (Cukierman et al. 2001; Yamada & Cukierman 2007). Similarly, tumor cells interact with the microenvironment, which is known to be a key regulatory step for cancer progression. Innovative work in this field has shown that cancerous phenotypes can be stimulated (Olumi et al. 1999; Park et al. 2000) or suppressed (Weaver et al. 1997) simply by altering the tumor microenvironment. The tumor microenvironment, or stroma, in ductal carcinoma consists of ECM proteins, such as collagen and a variety of cells including fibroblasts and macrophages. Reactive stroma, characterized by the presence of cancer-activated fibroblasts (CAFs) that express α-smooth muscle (α-SMA) protein which cause ECM stiffness (Qayyum & Insana 2012b) is associated with poor prognosis in breast cancer (Bergamaschi et al. 2008).

Fibroblasts have been widely studied in 3D, most frequently in a collagen matrix, which is more representative of their natural environment (Grinnell 2003). Collagen was chosen because it resembles the ECM milieu of invasive breast carcinoma better than Matrigel, which may not simulate the ECM of normal breast tissues (Su et al. 2007). Many studies have shown that fibroblasts play a major role in the initiation and progression of carcinoma cells (Desmouliere et al. 2004; Orimo et al. 2005; Kalluri & Zeisberg 2006). Although current 3D models of breast cancer are a considerable improvement on 2D systems, they are limited in their focus on the behavior of cancer cells only. The complex nature of the stromal component in the breast means that the study of these cell types alone is unlikely to recapitulate what is seen in the in-vivo environment after BCS. A convenient way to study the complex mechanisms underlying epithelial–mesenchymal interactions in-vitro is through the reconstitution of cellular behavior in a 3D environment obtained by growing epithelial cells and stromal fibroblasts within collagen matrices. 3D cultures are composed of proliferating cells, non-proliferating viable cells, and activated cells resembling the multiple phenotypes found in the post-surgical microenvironment. Thus we propose a progressive culture model approach for investigating stromal-epithelial interactions in the microenvironment of the residual disease after BCS under RT.

6

Understanding how cell and molecular responses to IR produce organism reactions may be difficult in a reductionist model that emphasizes components and pathways, rather than on network interconnectivity and tissue context. Cells receive information about how they should behave from their microenvironment, which normally consists of other cells, insoluble ECM proteins, soluble hormones and cytokines. Thus, the cell-centric view in radiobiology has begun to shift toward achieving a broad understanding of cell systems. This view is paralleled in current cancer research with a new appreciation for the complicity of normal cells in processes involved during the formation of tumors (Barcellos-Hoff & Costes 2006).

1.4 Specific Aims and Research Conducted

The findings of Herskind & Rodemann (2000) show IR prompts the release of transforming growth factor beta 1 (TGF-β1) that directs the differentiation of fibroblast cells to further increase growth factor expression in a positive feedback manner. This process stiffens the peri-epithelial ECM that encourages cancer cell growth through integrin signaling (Levental et al. 2009; Shieh 2011).   While the balance of pro- and anti-tumorigenic IR responses favors the latter, the margin between cancer and noncancer cell effects are small at patient doses that can be tolerated. Consequently, optimal IR fractionation in adjuvant applications involves a careful balance among competing factors.

Given the complex multifactorial nature of tissue responses to various treatment strategies, it is essential to explore the therapeutic responses of the fibroblasts cells that interact with cancerous epithelia. We begin this process by investigating the effects of photon RT from the perspective of isolated stromal-cell radiobiology. While others have looked at the stromal environment from a cell centric view, we have looked at cell function in the context of the mechanical properties of the stromal microenvironment. Breast tumor growth depends on the cellular microenvironment and tissue mechanical properties. By studying the stromal environment, we can explore their interactions with IR

to modify the mechano-environment influencing the cancer cell-to-noncancer cell therapeutic ratio during fractionated RT.

The general accomplishments of this dissertation are:

- **Parametric description of isolated 3D stromal cell culture responses to fractionated radiotherapy**. The effects of fractionation schemes on collagen matrix stiffness and fibroblast activation were studied using this culture model.

- **Establishing a 3-D cell co-culture model.** Incorporating more breast tissue components such as cancerous mammary cell lines into fibroblast-collagen gel to mimic more natural signaling conditions. The goal was to produce co-cultures that will be used to deliver fractionated courses of radiation prescriptions that enable measurements of the cellular microenvironment.

- **Exposing the co-culture models to altered fractionation schemes to process optimized dose per fraction for eradication of residual disease**. We tracked a feature space that includes collagen matrix stiffness, fibroblast activation and epithelial cell proliferation.

  Table 1 provides a glossary of each experiment and its corresponding section within this paper.

Table 1 Model evolution of the experiment conducted for this thesis.

	With/with Out Radiation	Section in Paper
Collagen only	Base material	3.3.2
Collagen + MRC 5 Fibroblast	Stroma Cell Culture	3.3.3
Collagen + MRC-5 Fibroblast +/- TGF-β1	Reactive Stroma Cell Culture	3.3.4
Collagen + Fibroblast + MCF-7 cancer cells	Co-culture	4.2
Collagen + Fibroblast + MCF-7 cancer cells +/- TGF-β1	Residual disease in wound healing environment	4.3

By using the co-culture model for residual breast cancer following lumpectomy, we can begin to interrogate the link between cancer and wound healing. Cancer is referred to as a wound that does not

heal; the reactive stroma does not dissipate as it does following wound healing. The cell-culture model serves as a tool to evaluate fractionation schemes based on a new understanding of the radiobiology of the response of cells in culture to IR. ***We tracked cell proliferation, differentiation, and ECM stiffening in 3-D collagen co-cultures that were stimulated by growth-factor and irradiation. This is an important step in acquiring a systems-radiobiology perspective for optimizing breast cancer RT***.

Our initial study found IR fraction size affects the matrix stiffness and fibroblast activation of a reactive stroma differently. If it is more important to reduce fibroblast activation than matrix stiffness, then larger fractions are recommended. However large radiation dose fractions will quickly cross link the collagen to stiffen the matrix. If stiffening is the dominant factor in the reactive stroma promoting cancer cell progression, then smaller fractions are recommended.   Therefore, our observations would imply that staging the reactive stroma, might be an important step in assertively selecting fractionation dose schemes. Irradiation of the co-culture model was expected to target the microscopic spread of disease and inhibit signaling from the wound healing response, thus reducing the probability of recurrence. We would predict that treating the excised tumor area with an optimum dose of radiation not only kills residual cancer cells within the vicinity, but also inhibits the wound healing by inactivating stromal fibroblasts. The long term goal would be to reduce the recurrence rates for early stage breast cancer by treating regions most likely to harbor residual tumor cells.

1.5 Outline of this Dissertation

Optimum fractionation in radiotherapy occurs when tumor control is improved without enhancing adverse reactions in the surrounding tissue. It depends on the proliferative state of the tumor cells relative to that of the normal tissue at risk. This is where biological understanding and clinical radiation oncology meet. The initial study was undertaken on stromal component responses to altered fractionation schemes. In order to build a more relevant in-vitro model, we incorporated more

components to represent a subset of the conditions of adjuvant patient treatments following BCS.

Chapter 2 is a study on the research design of building the physical model of the cancer

microenvironment after BCS as well as discussing radiobiological fractionation protocols in the clinic.

The response of stromal components to fractionated radiotherapy is explored in Chapter 3, which is

modified from a paper published in the International Journal of Radiation Biology (Qayyum & Insana

2012a). As an extension of Chapter 3, Chapter 4 examines stromal-epithelial cell interactions following

fractionated radiotherapy. Finally, Chapter 5 describes the general conclusions about the developments

presented in previous chapters, and provides an outline of possible future directions derived from this

dissertation work.

CHAPTER 2

MODELING IN RADIOTHERAPY

2.1 Physical modeling in radiotherapy cancer treatment

The biological requirements integral to the survival of a cancer cell are likely very different when it is embedded within a mature tumor microenvironment, which is composed of stromal fibroblasts, myofibroblasts, and mature matrix – than it is during the initial stages of tumor formation or near the tumor margins. Cancer cells within a mature tumor microenvironment are more likely to be resistant to adjuvant therapies for multiple reasons. One reason is cancer therapies are not likely to reach cancer cells within dense primary tumor stroma as easily as they would if those cells were within emerging tumor microenvironments. The inadequate response of primary solid tumors to chemotherapy is the poor penetration and distribution of such agents in the tumor tissue due to interstitial hypertension, which is a universal characteristic of solid tumors (Camara et al. 2007).   Within the tumor cell microenvironment, RT effectiveness is closely dependent on oxygen availability at the time of treatment. Hypoxic cells are 2 to 3 times less radiosensitive than well-oxygenated cells. The hypoxic cell fraction in solid tumors ranges from less than 1% to more than 50%. Hypoxia in the tumor microenvironment may be a result of increased interstitial pressure, which leads to vascular collapse with resulting areas of transient or persistent hypo- perfusion, local hypoxia, and acidosis (Wachsberger et al. 2003). Many patients with cancer are anemic; a factor that may also contribute to localized hypoxia and that has an adverse effect on curability of a tumor by RT (Gunderson & Tepper 2007). Therefore, studying alternative fractionation (e.g. hypofractionation) schemes may improve the ability to eradicate resistant residual cancer cells and reactive stroma.

Breast cancer is a complex and heterogeneous disease. In the laboratory, breast cancer is often modeled using established cell lines. A variety of models for in-vitro cancer growth and treatment have made significant advances toward mimicking in-vivo tumor architecture and growth behavior as compared to cells grown on 2D tissue culture substrates. We developed an in-vitro system using immortalized and widely available cell lines that would serve as a model for the study of the paracrine interactions in breast cancer post-surgery.

The ECM is a heterogeneous composition of proteoglycans, proteins, and signaling molecules that was originally known for its role in providing structural support to cells and as a milieu for cell migration. The ECM influences cell differentiation, proliferation, survival, and migration through both biochemical interactions (cell adhesion and presentation of growth factors) and mechanical cues (stiffness and deformability). For example, expression levels of the ECM protein lysyl oxidase (LOX), which is responsible for collagen cross-linking, is elevated in cancer patients and associated with metastasis and reduced patient survival (Erler et al., 2006). In figure 1 is a cartoon depicting the stages of breast tumorigenesis (A) from left to right; normal ducts, ductal carcinoma in situ and invasive phenotype, highlighting key changes within the tissue stroma. (B) Force-dependent focal adhesion maturation mediated by elevated tumor matrix stiffness. Integrins are bidirectional mechanosensors that integrate biochemical and biophysical cues from the matrix and the actin cytoskeleton and transduce cell-generated force to the surrounding microenvironment. Activated integrins bind to ECM proteins via cooperative interactions between their alpha and beta extracellular domains and form nascent highly dynamic adhesion signaling complexes. In response to external mechanical force or elevated cell-generated contractility integrin clustering is enhanced and the recruitment of multiple integrin adhesion plaque proteins including talin and vinculin is favored. These, in turn, associate with the actin cytoskeleton and multiple signaling proteins including focal adhesion kinase (FAK), Src family kinases, and integrin-linked kinase, to promote cell growth, survival, migration and differentiation (Yu et

12

al. 2011). Matrix stiffening, which reflects elevated matrix deposition, linearization and cross-linking, can co-operate with oncogenic signaling to enhance cell-generated contractility to foster integrin associations and focal adhesion maturation. Maturation of focal adhesions promotes cell generated forces by enhancing Rho GTPase and ERK-mediated acto-myosin contractility—which feed forward to further promote integrin clustering and focal adhesion assembly and transmit acto-myosin-generated cellular forces to the ECM (Dobaczewski et al. 2010)
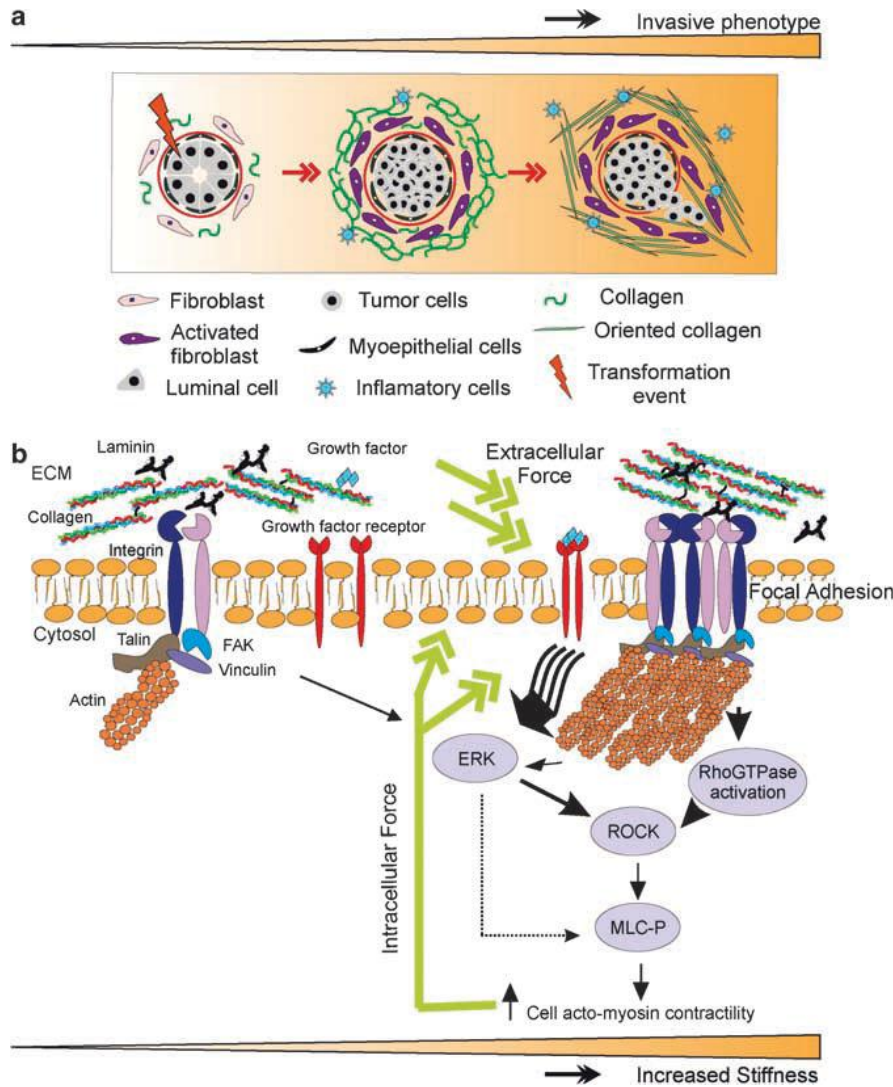
Figure 1 Malignant transformation of mammary epithelial cells is regulated by matrix stiffness. Breast transformation ensues through progressive of genetic alterations in the epithelial cells residing within the mammary ducts. The tissue stroma responds to these epithelial alterations by initiating a desmoplastic response that is characterized by activation and differentiation of fibroblasts, infiltration of immune cells, increased secretion of growth factors and cytokines, and elevated matrix synthesis and remodeling that manifests as matrix stiffening. (a) Cartoon depicting the stages of breast tumorigenesis (from left to right;normal ducts, ductal carcinoma in situ and invasive phenotype), highlighting key changes within the tissue stroma. (b) Force dependent focal adhesion maturation mediated by elevated tumor matrix stiffness. Integrins are bidirectional mechanosensors that integrate biochemical and biophysical cues from the matrix and the actin cytoskeleton and transduce cell-generated force to the surrounding microenvironment. Activated integrins bind to ECM proteins via cooperative interactions between their alpha and beta extracellular domains and form nascent highly dynamic adhesion signaling complexes. In response to external mechanical force or elevated cell-generated contractility integrin clustering is enhanced and the recruitment of multiple integrin adhesion plaque proteins including talin and vinculin is favored. These, in turn, associate with the actin cytoskeleton and multiple signaling proteins including focal adhesion kinase (FAK), Src family kinases, and integrin-linked kinase, to promote cell growth, survival, migration and differentiation. Matrix stiffening, which reflects elevated matrix deposition, linearization and cross-linking, can co-operate with oncogenic signaling to enhance cell-generated contractility to foster integrin associations and focal adhesion maturation. Maturation of focal adhesions promotes cell generated forces by enhancing Rho GTPase and ERK-mediated acto-myosin contractility–which feed forward to further promote integrin clustering and focal adhesion assembly and transmit acto-myosin-generated cellular forces to the ECM. (Reprinted from Mammary epithelial cell: Influence of extracellular matrix composition and organization during

14

In a wound response, platelets not only release the clotting factors needed to control the bleeding and loss of fluid and electrolytes but they also provide a cascade of chemical signals, known as cytokines or growth factors, that initiate the healing response (Guo & Dipietro 2010). The two most important signals are platelet-derived growth factor (PDGF) and TGF-β1. TGF-β1 adds an important signal for the initiation of the healing cascade by attracting macrophages and stimulates them to secrete additional cytokines including FGF (fibroblast growth factor), PDGF, TNFa (tumor necrosis alpha) and IL-1 (interleukin-1). In addition, TGF-β1 further enhances fibroblast and smooth muscle cell chemotaxis and modulates collagen and collagenase expression (Diegelmann & Evans 2004). TGF-β1 regulates ECM tension and stiffness through increasing the expression of ECM proteins by tumor cells or CAFs and thereby increase the oncogenic activities (e.g. proliferation) of cancer cells (Ungefroren et al. 2011). TGF-β1 in the cancer model is produced by cancerous epithelia and CAFs. Cancer cells in advanced tumors are unresponsive to the growth inhibitory effects of TGF-β1, but instead increase cancer cell growth, survival, motility and invasion (Bagely 2010). Paracrine interactions between tumor cells and fibroblasts then become important determinants of cell proliferation, angiogenesis, and metastasis (Ronnov-Jessen et al. 1996).

We introduced a 3D co-culture model using cancer cells and normal fibroblasts in a collagen matrix. 3D cell cultures of standard cell lines provide biologically representative samples of cell-ECM systems for mechanobiology studies that can be assayed with standard phase contrast and confocal fluorescence microscopy. These samples are homogeneous with a controlled geometry that allows for accurate mechanical measurements. 3D cell cultures lack perfusion and tissue organization, but they model the mechanical dynamics of ECM and interstitial fluids moving through a cell-matrix system that are the primary components of elasticity.

The fibroblast-to-myofibroblast cellular transformation is well maintained in the tumor stroma of many cancers, as well as during wound healing, but the process is poorly understood (Carlson & Longaker 2004) and can only be characterized by the cellular marker α-SMA (Wang et al. 2005). The fibroblast-populated collagen matrix has been utilized as an in-vitro model of wound healing for more than 2 decades (Carlson & Longaker 2004). Studies of both tumor development and the process of wound healing have suggested a critical role for ECM components that are produced by fibroblasts. The development of fibrosis appears to mimic the same cellular processes as wound healing, a major difference being the sustained overproduction of ECM components in fibrosis (Grinnell 2003; Holliday et al. 2009).

Carcinoma-associated fibroblasts (CAFs) also known as myofibroblasts are normally induced transiently during wound healing, but inappropriate induction of myofibroblasts causes organ fibrosis, which greatly enhances the risk of subsequent cancer development. As our previous studies showed, myofibroblasts are found in the reactive tumor stroma, the processes involved in their development and activation are central to our investigation.

MRC-5 human lung fibroblasts have been used extensively with both epithelial lines and respond predictably to biochemical and mechanical stimuli. These cell lines represent polyclonal populations of cells that have adapted to tissue culture conditions but retain many of their phenotypic and genotypic properties over many passages.(Lacroix & Leclercq 2004; Stuelten et al. 2005; Fillmore & Kuperwasser 2008) This suggests that, despite their acquired ability to grow in vitro, cell lines continue to share many of the molecular and genetic features of the primary breast cancers from which they were derived. With the role of the stroma regulating breast cancer behavior receiving more attention, many investigators are incorporating stromal cells, such as fibroblasts, into these cultures.

To generate a tumor-like mechanobiological environment, the matrix is seeded with malignantly transformed epithelial cells (Michigan Cancer Foudation, MCF-7) cells. This cell line was chosen because these cells over express integrins and create focal adhesions points leading to contraction. MCF-7 cells are well-respected as a model for in-vitro study of neoplastic mammary cells (Rossi et al. 2000). Integrin's, which are trans-membrane adhesive receptors, are responsible for perceiving and responding to changes in both the extracellular microenvironment and the inner cell by linking the ECM to the cytoskeleton. For example, beta-1 integrins, among others, have been associated in the regulation of protein Kinase B (PKB) also known as Akt, which plays a crucial role in regulating breast cancer cell invasion. Furthermore, inhibition of beta-1 integrin has been shown to result in a change of invasive strategy (Castelló-Cros et al. 2009).

In our model the fibroblasts were co-cultured with tumorigenic breast epithelial cells, MCF-7, and stimulated with TGFβ1, a growth factor known to induce the fibroblast-to-myofibroblast phenotypic change. Others have investigated 3-D cell co-cultures to study irradiated mammary cell lines (Rossi et al. 2000). Those studies have guided our proposed approach (MRC-5 fibroblasts with MCF-7 epithelial). Our initial work in this study has resulted in finding co-culture with MCF-7 cells induced transformation in fibroblasts-to-myofibroblast. Cancerous epithelial cell secrete TGF-β1 to cause differentiation of the fibroblast-to-myofibroblast. This would be true for a tumor forming model, but since our model has been designed to represent the wound healing process after lumpectomy of early stage breast cancer, we incorporated a sparse distribution of MCF-7 cells and denser amounts of fibroblast cells. We then stimulated the fibroblast exogenously with TGF-β1 to mimic the wound environment. Literature indicates that the doubling time for sparse cancer cells is about 2 weeks (Rossi et al. 2000; Shen et al. 2006). Patients are treated anywhere from 2- 4 weeks post-surgery at the discretion of the physician. Our model was built to mimic the residual disease at this point in time and consisted of a 3:1 (MRC-5 fibroblast to MCF-7 cancerous epithelial) ratio.

We believe the responses of fibroblasts that mimic successive stages of tumor-induced stroma progression can be used in 3D cultures with epithelial cells in order to study tumor-associated ECM induced responses such as growth and cell morphology. ***By classifying cultures as having an activated or a quiescent reactive stroma, using the mechanobiology profile (stiffness, activation, differentiation, and proliferation) we may be able to discriminate between effectiveness of fractionation schemes***.

Our general approach was to first analyze the initial stromal components of the stimulated 3D cultures alone; thus we found this model to be viable to test mechno-environmental changes. We then experimented with 3D co-culture to model residual disease. This study yields a reproducible system developed to co-culture malignant epithelial cells and fibroblast populations in an ECM, thus providing a physiologically relevant in-vitro model system to study the role of the microenvironment under breast conserving treatment. This is an important step in acquiring a systems-radiobiology perspective for optimizing breast cancer radiation therapy.

2.2 Radiobiology

All cancer therapies try to target characteristics that are unique to cancer cells that also minimize damage to normal cells. There are several factors that may affect both normal and cancer cells that survive radiation. Normal cells can repair some of the damage caused by the radiation and survive. In addition cells going through mitosis are more sensitive and will be more readily killed than those in the synthetic phase of the cell cycle (Figure 2) (Schulz 2005). Cancer cells, being highly proliferative, are more likely to be undergoing mitosis, and thus they are more radiosensitive than normal cells.

Cell cycle and cell death are defined by mitosis (M) where division takes place and synthesis (S), the period of DNA synthesis. The M and S phases are separated by two periods G1 and G2 during which DNA is not synthesized but other metabolic processes take place. In general, cells are most radiosensitive in the M phase and G2 phase and most resistant in the late S phase (Hall 1994).

When cells are exposed to IR, bond breaking occurs in one of two ways; directly, by ionization of the biomolecule, or indirectly, through the ionization of water and formation of damaging reactive radicals. It is known that the most radiation-sensitive biomolecule in living tissue is DNA (Hall 1994). When IR impinges upon an aqueous environment, O-H bonds within water molecules break to form the highly reactive •OH. •OH disrupts DNA primarily by abstracting H• at various places on the helix. This process leaves behind radical lesions which can form various oxyl and peroxyl radicals by reacting with O_2 or SO; the resultant peroxides can undergo Fenton type reactions (Bloomer & Adelstein 1982). Fenton reagent is a hydrogen peroxide which is used to oxidize contaminants. IR can induce cell-cycle arrest. Normal cells react to DNA damage during drug or radiation therapy by checkpoint activation, with cell cycle arrest and resume proliferation (if at all) only after DNA repair is completed. Because of defective checkpoint control, cancer cells proceed through mitosis and G1 irrespective of DNA damage. This can lead to mitotic catastrophes, mitotic arrest, or to persistent double-strand breaks that elicit apoptosis during the next round of replication. However, while most cancer cells die or arrest, a few may escape with severely damaged genomes and increased genomic instability. These are responsible for remissions and are usually resistant to treatment. Checkpoint mechanisms are major determinants of the cellular response to radiation.
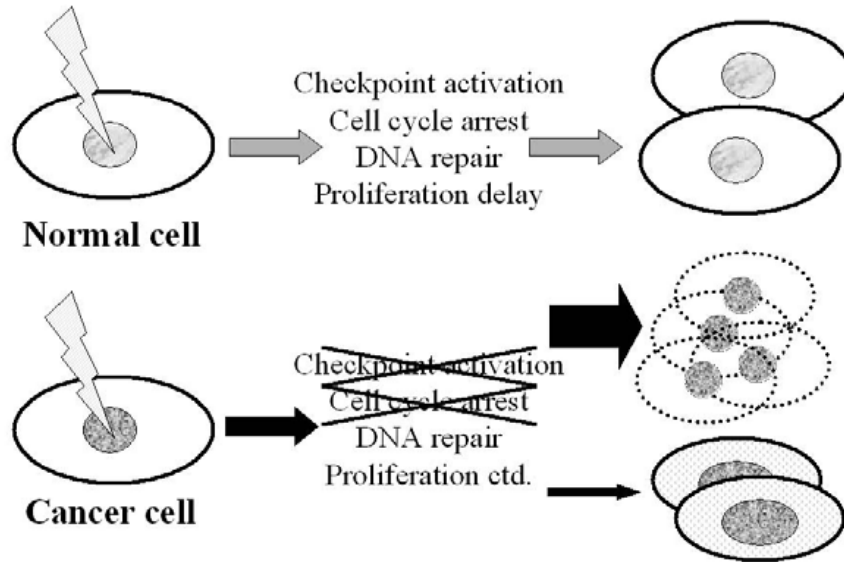
Figure 2 Normal cells react to DNA damage during drug or radiation therapy by checkpoint activation, with cell cycle arrest and resume proliferation (if at all) only after DNA repair is completed. Because of defective checkpoint control, cancer cells proceed through mitosis and G1 irrespective of DNA damage. This can lead to mitotic catastrophes, mitotic arrest, or to persistent double-strand breaks that elicit apoptosis during the next round of replication. However, while most cancer cells die or arrest, a few may escape with severely damaged genomes and increased genomic instability (bottom right). These are responsible for remissions and are usually resistant to treatment.

G2 checkpoint protein(s) play a major role in recognizing radiation-induced DNA damage and initiating repair responses in the cell. Thus, loss of the G2 DNA damage checkpoint renders lymphoma and carcinoma cells more sensitive to the cytotoxic actions of radiation and chemotherapeutic agents. DNA damaged cells rapidly enter into mitosis, resulting in further chromosomal damage, chromosome loss, and cell death. Radiation damage of DNA is a consequence of cells being radiated. Cells with radiation damaged DNA can try to repair the damage so it is viable once again, however if the repair fails, a mutation can lead to cancer. In some cases the DNA damaged cell does not repair and dies (Qin & Li 2003).

Cancer radiobiology is usually the study of damage and repair of clonogenic cancer cells. Yet IR is known to also remodel stroma through production of chemically-reactive oxygen species (ROS) that increase ECM cross linking and promote enhanced release of growth factors. ROS are free-radical

molecules (unpaired valence electrons) generated from ionized water that damage cell components as they migrate. ROS are formed slowly during metabolism at a rate that can be scavenged naturally in cells by the production of catalase, vitamins, and enzymes, e.g., superoxide dismutase (Rao et al. 2008), to mitigate cell damage and genomic mutations. When ROS is produced in large concentrations by IR, however, the antioxidant defenses of cells are overwhelmed, placing them in oxidative stress and making them susceptible to extensive damage. IR can break apart DNA strands directly through charged particle ionization, but more common for low Linear Energy Transfer (LET) radiation is ROS damage. ROS also stimulates TGF-β1 release to induce CAF transitions (Nguyen et al. 2005). Cell proliferation occurs through integrin receptor-tyrosine-kinase signaling. Simultaneously, TGF-β1 reduces cell adhesions and the anchorage-dependent cell growth requirement (Chiarugi et al. 2003). Interactions between the reactive stroma and surviving cancer cells during fractionated IR exposure are important understudied factors for RT planning.

2.3 Radiotherapy treatment fractionation

The aim of radiotherapy is to deliver enough radiation to the tumor to destroy cancer cells while damaging normal tissue as little as possible. Figure 3 presents the area of optimal dose where the tumor receives the greater effect of radiation while the healthy tissue is spared from the lethal effects. This is the narrow margin which clinicians need to work with to deliver a safe and successful treatment. Though it is difficult to change the sensitivity or resistance of cells, fractionation is employed to achieve optimal dosage.
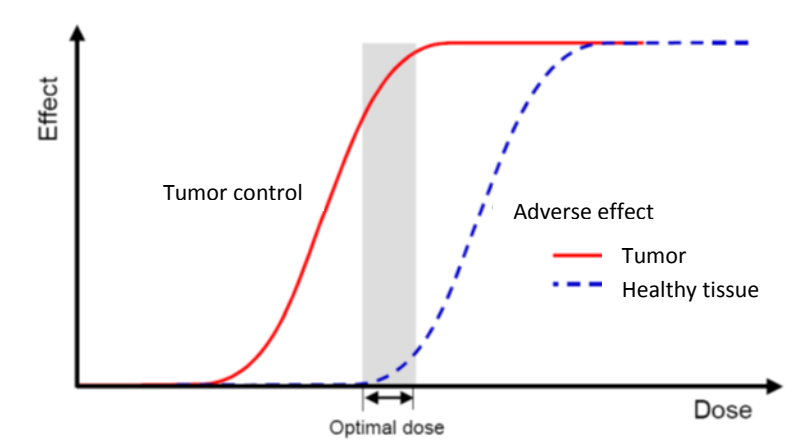
Figure 3 The tumor tissue suffers from the radiation dose which is still tolerated by the healthy tissue. The width of the window sets the upper and the lower limit for the dose that is applied to the target volume. Image adapted from (Gunderson & Tepper 2007).

Most clinical radiotherapy treatments are not given at one time. In fact, dose fractionation is used to deposit a total tumor dose in a number of small fractional doses. This is done to reduce late effects to normal tissues while efficient killing tumor cells.

The basis for fractionation in radiotherapy can be demonstrated through the four R's of radiobiology: repair, re-assortment, repopulation and re-oxygenation (Hall 1994). Repair is simply the restoration of the integrity of damaged macromolecules. Re-assortment is the return of cells towards a natural distribution within the cell cycle following the selective killing within certain phases of the cycle. Repopulation is the proliferation of clonogenic cells, and reoxygenation is the process by which surviving hypoxic clonogenic cells become better oxygenated during the period after irradiation. Fractionation helps spare normal tissues through repair and repopulation and increases tumor cell kill due to reassortment and reoxygenation (Van Dyk 1999). Therefore, optimizing the dose fractionation schedule to accommodate the various effects becomes an important clinical concern.

Due to differences in radiosensitivity and sublethal-damage repair rates between cancerous and noncancerous cells, dose fractionation parameters are important for maximizing the Therapeutic Ratio

(TR), where the limiting factor is the response of noncancerous tissues (patient tolerance). Fractionation schedules are selected to allow time for normal cells to repair radiation damage; cancer cells are less efficient at repair (Hall 1994). The current standard for breast treatment considers patients presenting in two stages, T1 and T2. T1 tumors are 2 cm or less in size and T2 tumors are between 2-5 cm and candidates for breast conserving therapy (Kantarjian 2006).   After lumpectomy and lymph node sampling, whole breast RT is administered to patients with early invasive breast cancer to decrease recurrence rate (Hall 2003). A common schedule for T1 and T2 lesions is 4500 cGy dose delivered over 25 fractions at a dose per fraction of 180 cGy (Gunderson & Tepper 2007). More invasive carcinomas may receive a boost dose of an additional 1600 cGy over 8 fractions to the primary site (Holloway et al. 2010). Failure of RT to control residual cancer-cell progression in some patients is still a major clinical problem (Pinsky et al. 2007).   Our focus is on the response of the cancer cells and the microenvironment (reactive stroma) to different fractionation schedules.

Fractionation schedules are established from dose-survival curve observations (Muriel 2002). Treatment parameters (dose per fraction, time between fractions, and total dose) are selected to yield the highest patient-tolerated TR. As we discover more about microenvironmental influences in cancer cell biology and as molecular imaging improves our ability to track relevant cellular biomarkers, the systems approach to treatment design becomes more realistic.

Thus breast tumor growth depends on the behavior of cancer cells in their microenvironment, and both components are affected by IR fractionation parameters. Our study reports on the use of 3D cell culture model to examine fibroblast cell responses to growth factor stimulation and IR at various fraction sizes. The goal is to characterize how the microenvironment changes with and without IR fractions.

CHAPTER 3

STROMAL RESPONSES TO FRACTIONATED RADIOTHERAPY

3.1 Introduction

The search for optimal radiotherapy fractionation schedules for treating breast cancer, viz., ones that minimize breast tumor recurrence following conservation surgery (Marcu 2010), must include the influences of the mammary-cell microenvironment that plays a complex and central role in regulating tumor growth (Polyak & Kalluri 2010). Although the primary objective of ionizing radiation (IR) exposure is to control growth of cancerous epithelial cells (cancer cells), IR-induced gene expression in cells of adjacent stroma also modulates conditions that affect cell growth (Barcellos-Hoff 2008, 2010).   Stroma includes fibroblast, macrophage, lymphocyte, and endothelial cells, although fibroblasts are the most abundant and active during malignant tumor growth. IR prompts release of TGF-β1 that directs the differentiation of fibroblast cells to further increase growth factor expression in a positive feedback manner (Herskind & Rodemann 2000). This process stiffens the peri-epithelial ECM that encourages cancer cell growth (Levental et al. 2009; Shieh 2011). While the balance of pro- and anti-tumorigenic IR responses favors the latter, the margin is small such that optimal IR fractionation in adjuvant applications involves a careful balance among several competing factors.

Normal adult female glandular breast tissues are remodeled cyclically in response to systemic, paracrine, and autocrine cell signaling (Bissell 2006). Homeostasis depends in part on the ability of stromal cells to sense their microenvironment and respond by producing soluble and insoluble proteins. Fibroblast cells excrete insoluble proteins including collagen and glycoproteins that constitute the ECM. The ECM is the substrate that gives glandular tissues their mechanical properties and enables cell

movement. Integrin receptors found in cell membranes coalesce to form focal adhesion points that, once attached to ECM glycoproteins, enable cells to move while sensing the stiffness of their local matrix. Cells move by adjusting cytoskeletal tension in proportion to forces sensed by their integrin receptors.

Cancer cells in a stiff matrix display malignant features; e.g., disrupted adheren junctions, lost polarity, and enhanced proliferation rates (Paszek et al. 2005). They release growth factors that activate the differentiation of adjacent fibroblasts into cancer associated fibroblasts (CAF), or myofibroblasts, through wound healing mechanisms (Eck et al. 2009). The enhanced α-SMA increases the ability of CAFs to generate large contractile forces, further stiffening the matrix and promoting further expression and release of TGF β1. Cancerous epithelial cells can themselves transition into mesenchymal cells through epithelial-mesenchymal transition (EMT), including CAFs, as a result of growth factor signaling (Petersen et al. 2001). Thus CAFs alter the chemo-mechano-environment of surrounding cells to favor pro-tumorigenic conditions.

Primary malignancies grow quickly once epithelial cells from in situ disease invade the peri-ductal stroma and are able to communicate directly with mesenchymal cells. Responding to limited resource challenges, cancer cells cooperate with mesenchymal cells to remodel the stromal microenvironment, in part, to build the vascular infrastructure necessary to sustain tumor growth (Weinberg 2007). Heterotypic signaling results in a *reactive stroma* characterized by inflammatory responses that stimulate fibrosis, neoplasia, edema, desmoplasia, as well as angiogenesis; each response increases tumor mass stiffness as cancer cells in the reactive stroma proliferate. At the heart of cancer progression is growth factor signaling of fibroblasts, their differentiation to CAFs and concentration at the margins of the developing solid tumor. TGF-β1, a product of both CAFs and cancer cells, plays an important dual role during carcinogenesis. In normal breast tissues and during the early

stages of tumor development, TGF-β1 suppresses growth. During later stages, however, it favors pro-tumorigenic and metastatic activities (Kalluri & Zeisberg 2006). TGF-β1 is a powerful stimulant of stromal tissue responses that lead to changes in the cellular mechanoenvironment.

Despite considerable advancement in tumor biology, the primary curative treatments for breast cancer continue to be surgery, chemotherapy, and radiation therapy (RT) (Nemade 2008). Combinations of these three, which increasingly include endocrine and/or growth-factor inhibition adjuvants, have been found to significantly extend progression-free survival (Johnston 2009). We are investigating photon RT applied as an adjuvant treatment following breast-conserving surgery and in the context of stromal-cell biology. We are using a fibroblast-cell culture model to understand the interactions between IR and stroma in creating mechano-environments that can affect the cancer cell-to-noncancer cell therapeutic ratio (TR) during fractionated RT.

Thus breast tumor growth depends on the behavior of cancer cells in their microenvironment, and both components are affected by IR fractionation parameters. Our study reports on the use of 3-D cell culture model to examine fibroblast-cell responses to growth factor stimulation and IR at various fraction sizes. The goal is to characterize how the mechanical environment changes as MRC-5 fibroblasts become activated by TGF β1 with and without IR.

3.2 Materials and Methods

Three-dimensional collagen matrices are frequently used to isolate and model the behavior of various mammary cell types (Olsen et al. 2010). We adopted a system composed of human fibroblast cells embedded within a collagen I matrix to study two effects of varying fractionation size on the cellular microenvironment – fibroblast activation (i.e., transformation to myofibroblast cells) and matrix stiffness. This section describes our measurements of collagen-matrix stiffness and fibroblast-cell

26

differentiation ratios in 3-D culture samples undergoing TGF-β1 stimulation following various IR exposures.

3.2.1 Cell cultures

Human lung fibroblast cells (MRC-5) purchased from American Type Culture Collection (ATCC, Rockville, MD, USA) were cultured in 75 cm^2 tissue culture flasks with Minimum Essential Medium Eagle (MEME, Invitrogen, Carlsbad, CA) to which 10% fetal bovine serum (FBS, Sigma, St. Louis, MO, USA) and 1% pen/strep (Sigma) were added. Cells were incubated at 37°C, 5% CO_2, propagated to 80-90% confluence, and harvested with 0.25% trypsin/1mM EDTA (disodium ethylenediamine tetraacetic acid, GIBCO, Carlsbad, CA, USA) that was neutralized with 10% FBS MEME. Cell passage numbers were between 5 and 12.

Culture matrices were prepared from a commercial type I collagen stock solution (10 mg/ml, rat tail, BD Biosciences, Bedford, MA, USA). Collagen solutions were diluted and neutralized with medium and 1N sodium hydroxide to 2.0 mg/ml. If cells were introduced to a particular sample, it occurred at this time. 600 μl volumes of collagen solution were dispensed to a 48-well plate and incubated at 37°C as the collagen polymerized over 30 min. After polymerization, 300 μl of complete MEM was applied to the top of the gelled samples. With or without cells, the total fluid volume added to each sample was 600 μl so that matrix stiffness was not influence by medium volume.

To select a cell density for the 3-D collagen-culture samples, an initial study was performed in which fibroblasts were added to the collagen solution at five different densities: 10,000, 50,000, 100,000, 250,000, and 500,000 cells/ml. At low densities (10,000 and 50,000 cells/ml), cells did not thrive. At high densities (250,000 and 500,000 cells/ml), many gel samples shrunk substantially as growth-factor stimulated cells to contract until the gel was pulled from the walls of the well. We used

200,000 cells/ml throughout the study, because at this density cells thrived without gel samples changing shape or collapsing.

Within the collagen matrix, fibroblast activation (differentiation to myofibroblasts) was intentionally promoted by first incubating samples as described above for 24 hours, then replacing the growth medium with low serum-media to starve cells overnight, and finally replacing the low-serum medium with 10 ng/ml TGF-β1(Sigma) in 0.5% FBS/MEM. TGF-β1 was applied in a single treatment application prior to the irradiation. Because the density of collagen-matrix cross links increase over time even without cells or irradiation, and since matrix tension develops as embedded cells contract, the stiffness of all samples increased over time. Matrix stiffness increased further depending on cell number and on processes that modify matrix cross linking or fibroblast differentiation; both are in flux following TGF-β1 introduction or sample irradiation. We experimented with different TGF-β1 concentrations in the range of 0.10–10 ng/ml and measured the cell activation that resulted (Xu 2010). From the activation data in Figure 4, we chose to apply a TGF-β1 concentration of 10 ng/ml to all samples in this study. This concentration consistently induced a repeatable and measurable range of cell activation ratios within 24 to 72 hours.
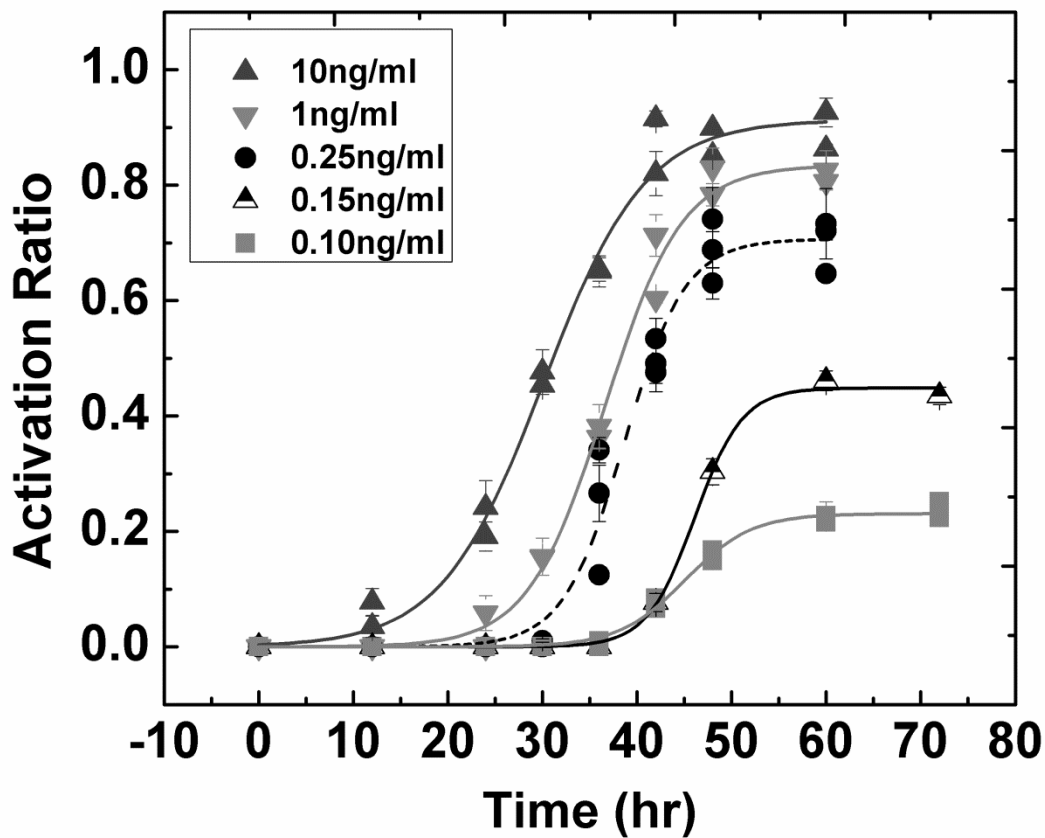
Figure 4 MRC-5 fibroblast cell activation ratio is plotted as a function of time for TGF-β1 concentrations between 0.1 – 10.0 ng/ml. A ratio of one means all cells are activated in a sample. Activation is determined from the mean fluorescence intensity of α-SMA of three sample regions within several sample layers using confocal microscopy. Error bars indicate ±1 standard error. Experimental data are fitted to a three-parameter logistic function assuming activation over time for a fixed amount of growth factor is modeled as population growth. The three parameters are maximum activation ratio, activation rate, and carrying capacity. Reprinted with appropriate permission obtained from (Xu 2010).

3.2.2 Sample groups

Our current study consists of 6 groups of samples: collagen-only gel control (Group 1), irradiated collagen-only gel (Group 2), collagen plus MRC-5 fibroblast cells (Group 3), irradiated collagen with MRC-5 cells (Group 4), collagen plus MRC-5 cells stimulated by TGF-β1 (Group 5), and irradiated collagen with MRC-5 cells stimulated by TGF-β1 (Group 6). Although the initial cell density in each sample was

200,000 cells/ml, the density of living cells changed over the experiment time depended on the group as described in Figures 11 and 12.

3.2.3 Sample irradiation

Samples were irradiated by placing them in a 6 MV (million electron volt) photon field generated by a linear accelerator (Varian Medical System, Palo Alto, CA, USA). A uniform dose was delivered with the gantry set to 0 degrees and with a 100 cm source-to-axis distance. An 8 x 8 cm^2 field size was selected to ensure cell culture samples were uniformly irradiated (Figure 5). Dosimetric-quality solid water was placed above and below the well plates to provide proper build-up dose. All samples were taken from the incubator and placed in a thermally isolating container for transportation to the clinic. Once removed from the container, samples were exposed to IR at room temperature in a single dose and returned to the incubator within 30 minutes.   The standard clinical dose fraction for breast treatment of 180 cGy was delivered to samples at a rate of 400 cGy/min. Other samples were exposed at the same dose rate but at a reduced fraction of 90 cGy or an accelerated fraction of 360 cGy. All sample irradiations were delivered in three fractions, once each 24 hours over three consecutive days, so the total dose was 270, 540, or 1080 cGy. This dose was experimentally verified using an ionization chamber (Exradin Model A12). Experimental setup was scanned using computed tomography unit (Brilliance CT, Philips) (Figure 6) and imported into Radiation Treatment planning software system (Philips Pinnacle3 System, Madison, WI) for dose delivery verification (Figure 7).
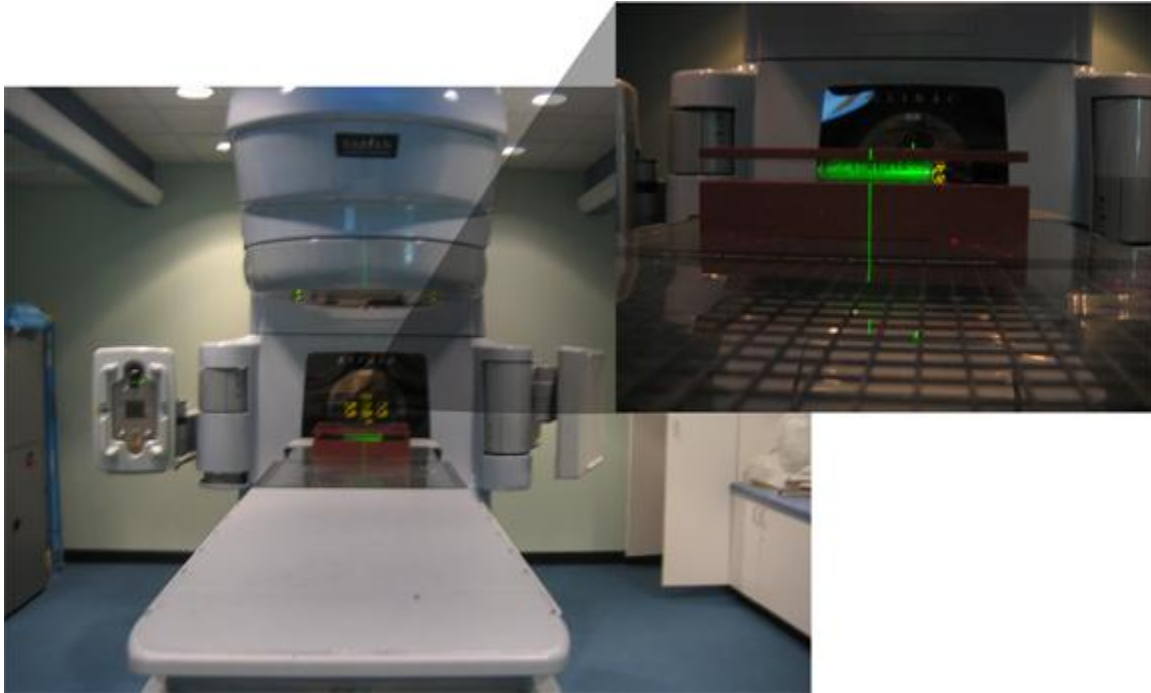
Figure 5 Varian Clinac with our experimental setup. (Inlet): The 48 well plate was placed on a 5 cm tissue equivalent material (TEM). Above the well plate was a 1cm bolus plus a 1 cm of TEM to provide proper build-up dose. Samples were irradiated by placing them in a 6 MV photon field generated by accelerator. A uniform dose was delivered with the gantry set to 0 degrees and with a 100 cm source-to-axis distance. An 8 x 8 cm^2 field size was selected to ensure cell culture samples were uniformly irradiated.

Figure 6 Experimental set-up was scanned using a Philips Big Bore CT to be imported into treatment planning system for dose computation.

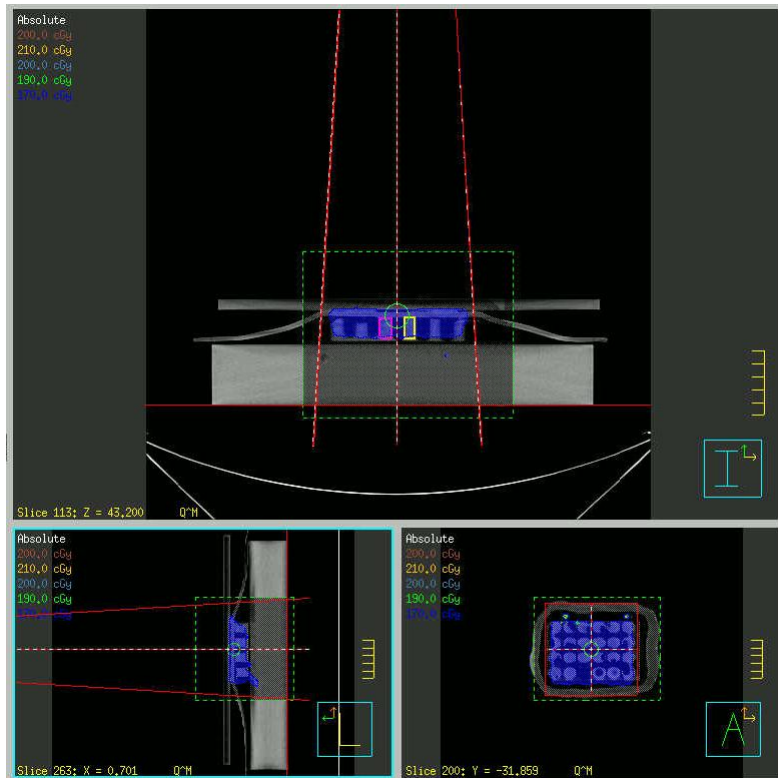**Figure 7 CT scan imported into Philips ADAC Treatment planning system to verification dose distribution for fractionated studies. The software simulated the set on the Clinac to deliver the prescribed fraction to be delivered at a rate of 4 Gy/min (Please reference Appendix B for details on designing a treatment plan).**

3.2.4 Mechanical testing

Within 1 hour following delivery of the last fraction, samples were mechanically tested using a TA.XT Plus Texture Analyzer System with a 1 kg load cell (Texture Technologies Corp., Scarsdale, NY, USA) and a compressive indentation procedure. The experimental protocol is the same as that used in our lab's earlier studies on gelatin hydrogels (Kalyanam et al. 2009). The fluid medium was removed from the top of the sample before testing with a 5-mm-diameter spherical indenter. The indenter was pressed into the sample surface at low velocity, 10^{-1} mm/min and to a depth of 2.5 mm (Figure 8). Force (F) and displacement (d) were recorded by the instrument to estimate sample stiffness.

An indentation rate of 10^{-1}mm/min was used to minimize poroelastic responses due to fluid flow within samples.   Though indentations were performed to depths up to 2.5 mm, the mechanical stiffness was measured from the slope of the force-displacement curve in the range 0 < d < 0.5 mm where the curve is approximately linear. The slope was converted to stiffness k measured in Newtons/meter (N/m) as shown schematically in Figure 8. Although k is not an intrinsic property of the material, it may be considered as a relative stiffness modulus since the geometry of all samples in the study is identical. One stiffness measurement was made for each sample during the first force-displacement cycle. The stiffness values shown in the results below are an average of measurements from 4 or 6 samples, as indicated in the figure captions.
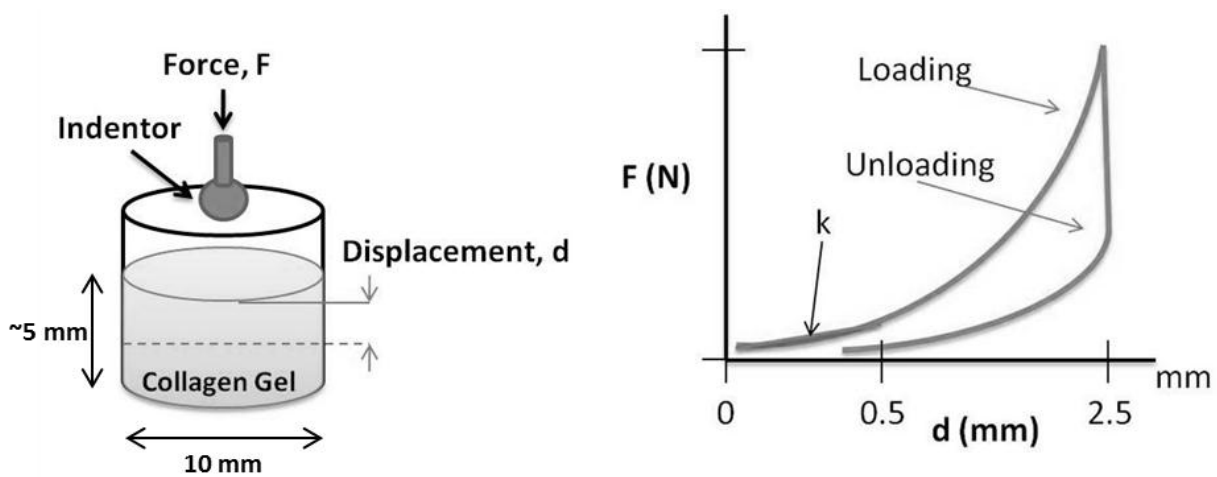
Figure 8 (left) Indentation measurement of the mechanical stiffness of 3-D collagen-matrix cell cultures is illustrated. (right) Force-displacement plots show how the force F sensed by the indenter varied with indenter depth d during loading and unloading phases. Stiffness k is defined by the slope F(d)/d near d=0. Reprinted with appropriate permission obtained from Informa Healthcare.

3.2.5 Immunofluorescence staining

Activated cells were identified based on their appearance following alpha-smooth muscle actin (α-SMA) targeted immunofluorescence staining. The total number of cells in the field was determined based on TO-PRO 3 (TO-PRO®-3 iodide (642/661)* 1 mM solution in DMSO (dimethylsulfoxide,

Molecular Probes, Inc., Eugene, OR, USA) nuclear staining. The fraction of activated cells was determined from the number expressing high levels of α-SMA divided by the total number of cells. Following mechanical testing, collagen samples were fixed as follows. Samples were washed with Phosphate-Buffered Saline (PBS, Lonza, Wackersville, MD, USA) before being fixed with 4% paraformaldehyde at 4°C overnight. Samples were then washed and permeabilized in 0.02% Triton X-100 in PBS for 15 mins followed by 5% non-fat milk blocking for 2 hours. Gels were then incubated with primary antibody, consisting of Bovine Serum Albumin (BSA, Sigma), PBS and Tween 20 (T, Sigma), (1:100 in 1% BSA/PBS/T) overnight at 4°C and secondary antibody (1:200 in 1% BSA/PBS/T) at room temperature for 2 hours. Cell nuclei were stained with TO-PRO 3 (1:1000 in PBS) for 20 mins. Sections were mounted between two glass coverslips with anti-photobleaching reagent.

3.2.6 Confocal microscopy

Immunofluorescence-stained samples were examined with a Leica SP2 laser scanning confocal microscope (Leica, Heidelberg, Germany) with Hg lamp and helium/neon laser and the associated software (Leica Confocal Software Version 2.00). A 488 nm excitation wavelength was applied for Fluorescein isothiocyanate (FITC) mapping, and a 633 nm excitation wavelength was used to find nuclei via TO-PRO 3 mapping. For each sample, a 20X objective captured a series of images along the z-coordinate (sample depth) at 3-5 μm increments. For confocal microscopy, an imaging system was employed (Microradiance; Bio-Rad, Philadelphia, PA, USA) consisting of a 25-mW argon ion laser emitting at 488 and 514 nm and a 1-mW green helium–neon laser emitting at 546 nm attached to a BX-50 microscope (Olympus Imaging America, Inc., Center Valley, PA, USA).
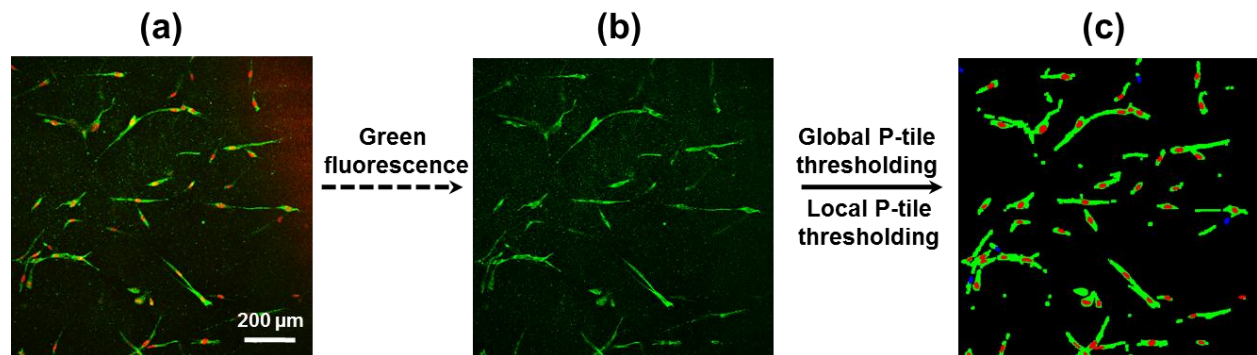
3.2.7 Automated cell counting

Activated fibroblasts are characterized as cells expressing large amounts of intracellular α-SMA as visualized using immunofluorescence imaging techniques. Confocal imaging yielded 40 images from

adjacent planes of each sample from which cells were counted to determine activation fractions. An automated segmentation method was developed to identify and count activated cell bodies and all cell nuclei from each confocal image. Counted cells had intensity and shape information at or above threshold values as specified in an image analysis program.

The threshold values adopted were those providing consistent cell counts that correlate with visual counting tests on the same images. We visually counted nuclei and cell bodies in many images several times, e.g., see Figure 9, and found it was straightforward to consistently identify the number of activated cells based on the appearance of green-fluorescent cell bodies showing large levels of α-SMA.

The intensity level of the cell-counting algorithm was adjusted to be consistent with estimates made by visual counting.   Similarly, the algorithm threshold was adjusted for the red-fluorescent nucleus so that the algorithms gave mean counts consistent with visual counts. To avoid double counting activated cell bodies in images from adjacent confocal planes, we only counted as active MRC-5 fibroblasts those cells where a green-fluorescent (GF) cell body and red nucleus (RN) were both super-threshold and spatially coincident (cf. Figure 8c). Please see Appendix A section 1 for a detailed description of how this was done.

(a) **(b)** **(c)**

Green fluorescence

Global P-tile thresholding

Local P-tile thresholding

200 µm

Figure 9 Automated cell counting using fluorescent images of fibroblasts is outlined.   (a) Confocal fluorescence microscopy images (20×) indicate the α-SMA content of individual fibroblasts (green) and associated cell nuclei (red). Green cell bodies (b) that m meet intensity threshold criteria (c) are counted as activated. A similar method was used to identify cell nuclei from red fluorescence images (not shown). The number of supra-threshold red nuclei indicates the total number of cells (activated and not activated) in the confocal plane. The number of red nuclei found within a green fluorescent cell body,

3.2.8 Statistical analysis

Three-way analysis of variance (ANOVA) was performed using R software to determine the significance of differences at a α = 0.05 level among mean stiffness and activation measured for the various collagen samples. The input parameters were (a) culture condition (collagen matrix alone, collagen with MRC-5 fibroblast cells, and collagen with TGF-β1 activated MRC-5 fibroblasts), (b) culture age, and (c) ionizing radiation dose. Observed differences among mean sample stiffness for sample groups were evaluated with post-hoc analysis, including Tukey HSD (honestly significant difference) (Calinski 1981).

3.3 Results

In the results presented below, the stiffness of the collagen matrix, the total number of MRC-5 fibroblast cells in a 1 ml collagen sample, and the fraction of activated MRC-5 fibroblasts are reported as functions of culture condition (matrix only, matrix with cells, and matrix with cells stimulated by growth factor), culture age, and radiation fraction size. The results are focused on differences between different classes of samples to demonstrate responses. Therefore, it's important to discuss statistical analysis to state significance.

3.3.1 Statistics Result

For stiffness we found that culture condition, culture age and radiation dose each had a significant effect on matrix stiffness (p-value < 0.01). We also found a significant interaction between culture condition and radiation dose, culture condition and culture age, and culture condition, radiation dose and culture age (p-value < 0.01). However, no significant interaction was detected between

radiation dose and culture age (p-value > 0.05). Significant interaction indicates the groups together had

an impact on stiffness.

For activation we found that culture condition, culture age and radiation dose has a significant

effect on activation of fibroblasts (p-value < 0.01). We also found a significant interaction between

culture condition and radiation dose, culture condition and culture age, radiation dose and culture age

and culture condition, radiation dose and culture age (p-value < 0.01).

3.3.2 Irradiation of collagen matrix

During the first study, we measured the stiffness of collagen samples made without cells for the

matrix-only control Group 1. We also measured the stiffness of irradiated matrix-only samples, Group 2.

These data are reported in Figure 10. The goal was to observe the effects of age and dose fraction on

the matrix stiffness without the influence of fibroblast cells. Without irradiation, Group 1 samples

stiffened measurably over three days. After irradiation, Group 2 samples showed the same pattern of

time-dependent matrix stiffening, while the overall stiffness scaled with radiation dose.
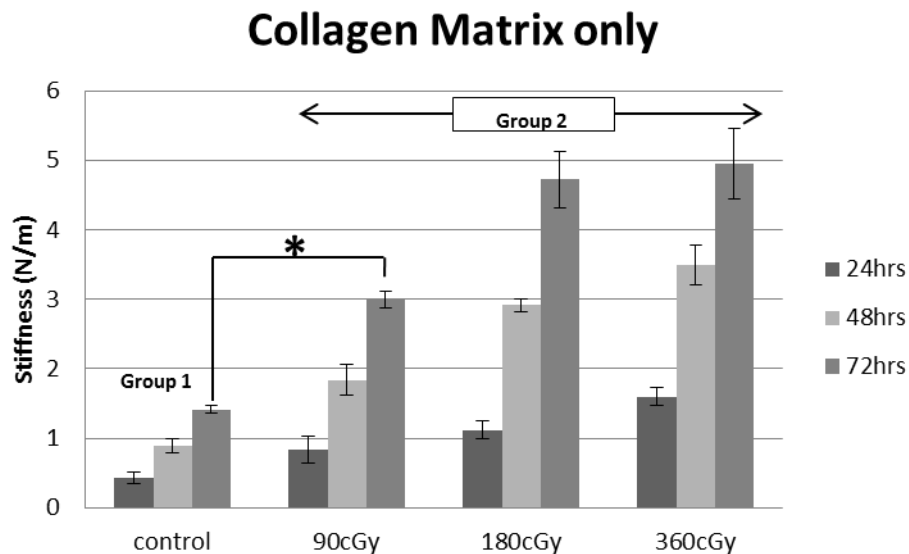

Figure 10 Measured stiffness of collagen gel samples (Groups 1 and 2) formed without cells are shown as a function of three daily IR fractions of 6 MV photons and at the three times indicated. Each data bar results from measurements on N=6

38

The observed sensitivity of matrix-only samples to radiation is expected, given that IR produces reactive oxygen species (ROS) that chemically react with collagen molecules to cross link and stiffen matrices. It was proposed that cross linking occurs through energy absorption by aromatic groups within the collagen molecules (Gouk et al. 2008). Although x-rays also degrade collagen through peptide-bond cleavage, increased collagen cross linking dominates because the high water content of samples generates a large concentration of free radicals (Barcellos-Hoff & Dix 1996; Nguyen et al. 2005). The initial production of radicals and their reaction with surrounding molecules stiffens the matrix instantaneously following irradiation.

3.3.3 Irradiation of MRC-5 fibroblasts in collagen matrix

During the second study, summarized in Figure 10, we measured cell activation and stiffness for sample Groups 3 and 4. These samples were also 3-D collagen matrices but with cells embedded and no added growth factors. They were irradiated over time in the same manner as Groups 1 and 2. The presence of cells initially softened the matrix by approximately 40% (Group 3 in Figure 11a) as compared with matrix-only samples (Group 1 in Figure 9), but matrix stiffness rose to recover after 72 hours. Cell numbers nearly doubled in samples over 72 hrs (Group 3 in Figure 11b), but few of the cells (< 10%) were activated (Group 3 in Figure 11c). Thus we attribute Group 3 sample stiffening seen in Figure 10a primarily to aging of the collagen matrix.

Irradiation at a 90 cGy fraction stiffened Group 4 (Figure 11a) samples significantly after one dose fraction at 24 hours, but there was no significant increase in stiffness after 48 hours (2 fractions) or 72 hours (3 fractions). The increase in stiffness mirrors the increase in cell density and activation ratio at 90 cGy, suggesting that larger numbers of activated fibroblasts are responsible. Increasing the IR fraction size to 180 or 360 cGy initially stiffened the matrix further as it activated larger fractions of

fibroblasts, but dose fractions delivered in subsequent days did not further stiffen samples as it did for

matrix-only samples. The presence of cells seems to buffer the time-varying effects of radiation. At

higher doses, cells are not proliferating and activation is decreasing over time as cells die off. Note that

nuclear staining identifies all cells present at the time of preparation, dead or alive, so cell number

cannot decrease over the 3-day observation time. The images inset in Figure 11c are examples of cell

culture imaged at 48 hours for a Group 3 sample and a Group 4 sample following two 180 cGy fractions.

Images show 8% and 18% activation, respectively. Figure 11 (cont. on next page).
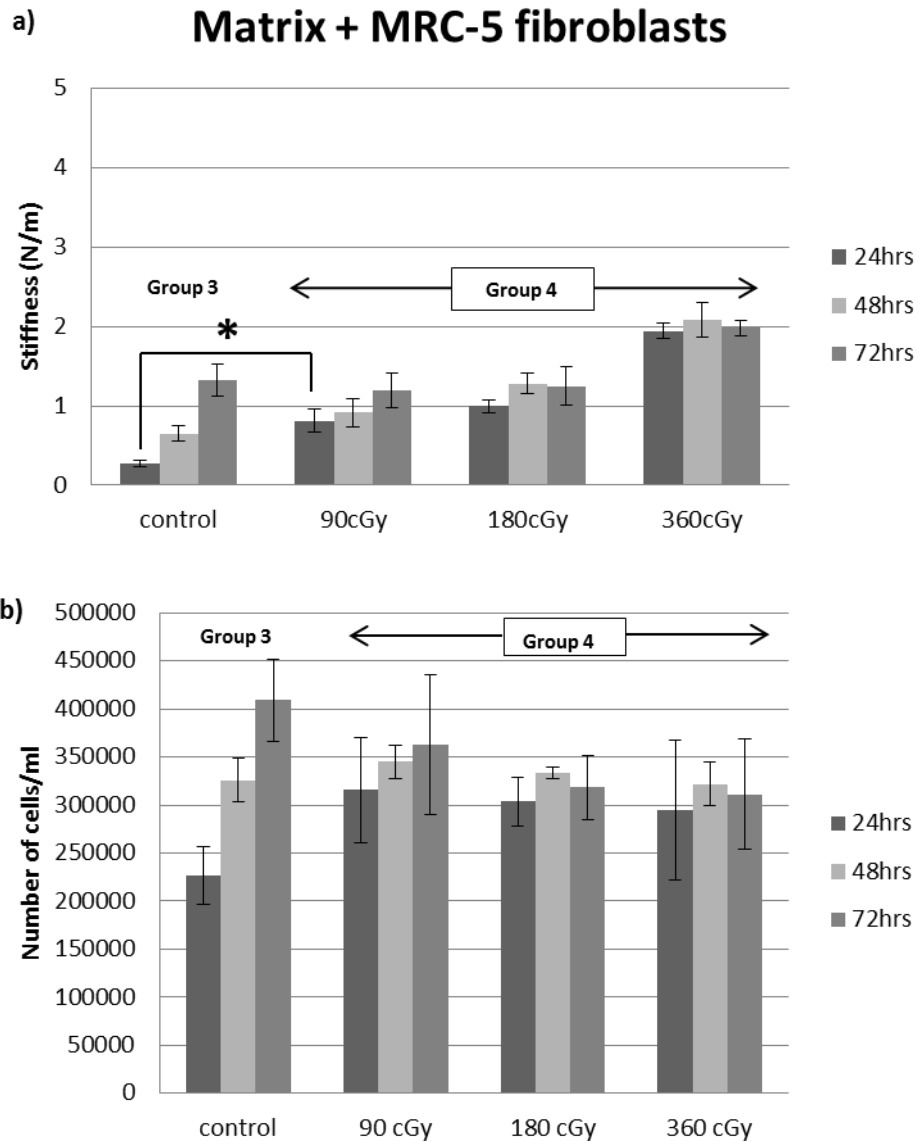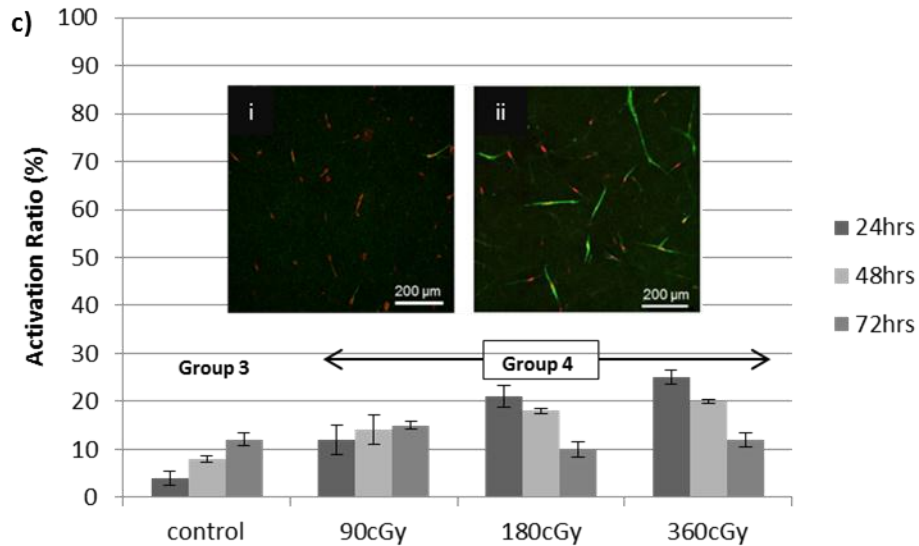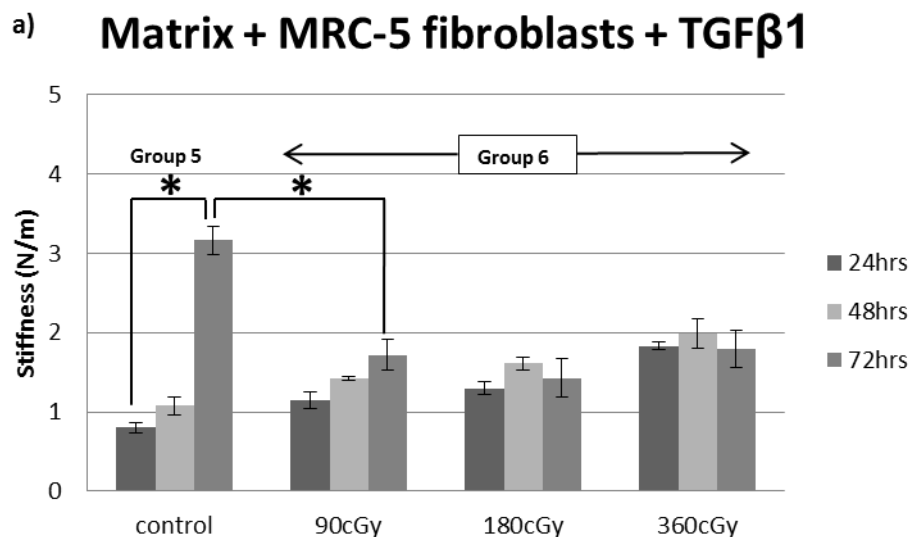
Figure 11 Measurements of sample stiffness (a), total cell number per sample (b), and cell activation ratio (c) for collagen gel samples (Groups 3 and 4) formed with fibroblast cells and without TFG-β1. Group 4 samples are given three daily IR fractions at the three times indicated. Each bar in the stiffness results is taken from measurements on N=6 samples (mean ± 1 SE). Cell numbers (b) and activation ratios (c) are for N=4 samples. No radiation was given to the control samples. * indicates statistical significance at the p < 0.05 level. INSET: IHC-stained confocal fluorescent images for (i) a non-irradiated sample and (ii) a sample irradiated with 2 fractions of 180 cGy. Both samples were imaged after 48 hours. Reprinted with appropriate permission obtained from Informa Healthcare.

Consistent with the findings of others (Herskind & Rodemann 2000), irradiation initially activated fibroblast differentiation to myofibroblasts. One mechanism might involve autocrine TGF-β loop signaling (Ronnov-Jessen et al. 1996). Others (Herskind & Rodemann 2000) found that the amount of TGF-β1 released per cell increased in radiated cultures. TGF-β1 may also increase through activation of latent TGF-β1 stored in serum. Thus TGF-β1 is a likely mediator of radiation-induced differentiation (Hakenjos et al. 2000). Dose-dependent activation of latent TGF-β1 has been observed at doses as low as 10 cGy and attributed to ROS activity (Barcellos-Hoff & Dix 1996; Rave-Frank et al. 2001). Radiation induced ROS production is known to have important effects on cell-cycle progression and differentiation (Storz 2005), which may factor into the changes in matrix stiffness seen in Figure 10 for different fraction sizes. This mechanism involves the activation of specific proteolytic enzymes from inactive proenzymes and is most likely dependent on the presence of ROS. Scavengers of radiation-induced free radicals or

ROS, such as amifostine, can inhibit ROS-induced activation of latent TGF-β (LTGFβ) as well as diminish the plasma level of TGF-β1(Rodemann & Blaese 2007).

3.3.4 Irradiation of MRC-5 fibroblasts stimulated by TGF-β1 in collagen matrix

During the third study summarized in Figure 12, we measured cell activation and stiffness for sample Groups 5 and 6. As in the previous study, samples were composed of a 3-D collagen matrix with interspersed fibroblasts, but these cells are activated by 10 ng/ml TGF-β1. As in the other studies, samples were irradiated over time at different dose fractions. TGF-β1 stimulated cells that were not irradiated (Group 5 in Figure 12) were almost fully activated (90%) in two days, producing a matrix nearly four-times stiffer after 72 hrs. However, irradiation reduced cell-generated matrix stiffness and fibroblast activation even as the cells continued to slowly proliferate over three days. We found that cell proliferation and activation decreased or remained the same with increasing fraction size, while sample stiffness increased marginally. Observed stiffness changes caused by fraction size were minimal. Despite a stiffening matrix, larger fraction sizes do not appear to significantly promote a reactive stroma, at least for these isolated model components. Figure 12 (cont. on next page).

a) **Matrix + MRC-5 fibroblasts + TGFβ1**
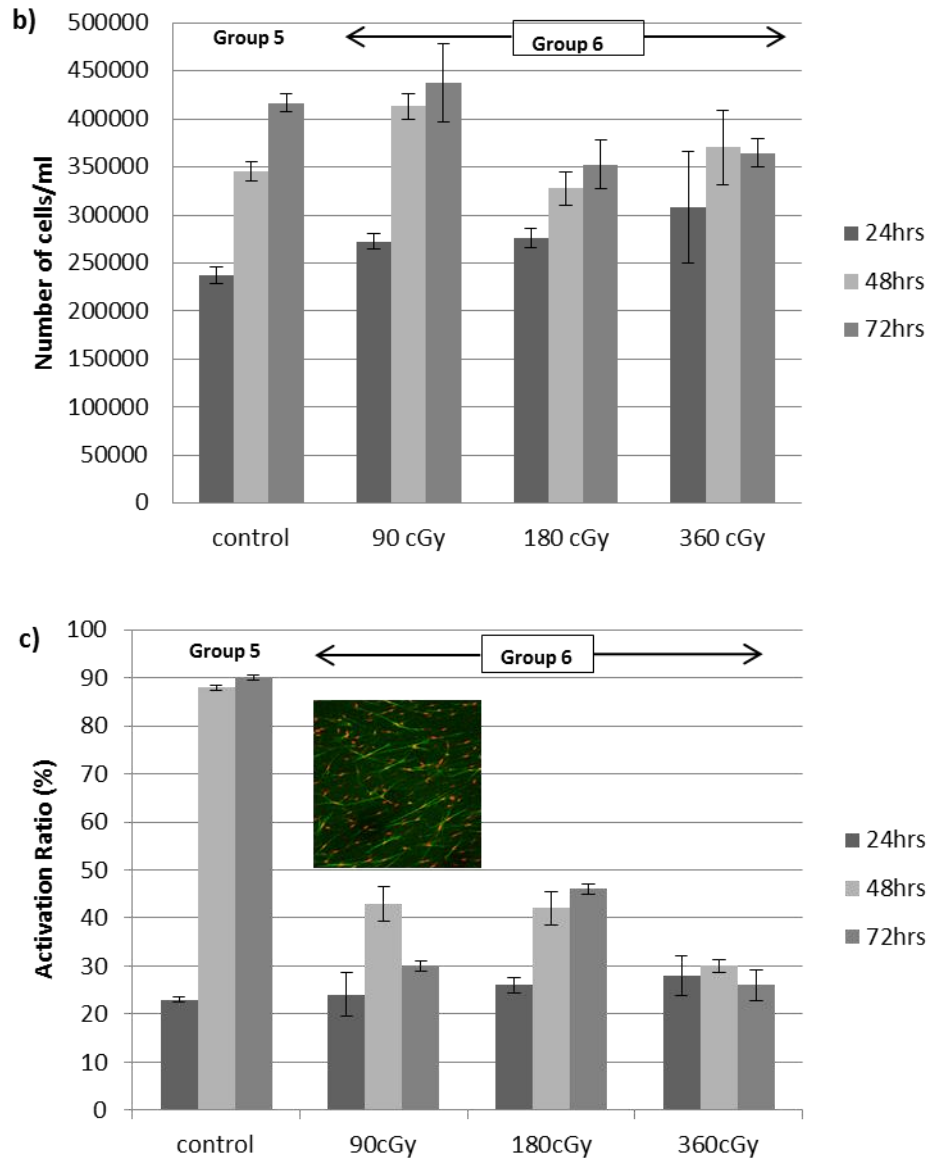
Figure 12 Measurements of sample stiffness (a), total cell number per sample (b), and cell activation ratio (c) for collagen gel samples (Groups 5 and 6) formed with fibroblast cells that were stimulated by 10 ng/ml TFG-β1. Group 6 samples were given three daily IR fractions at the three times indicated. Each bar in the stiffness results is taken from measurements on N=6 samples (mean ± 1 SE). Cell activation and number results are for N=4. No radiation was given to the control samples. * indicates statistical significance at the p < 0.05 level. INSET: IHC-stained confocal fluorescent image, showing α-SMA in green and nuclei in red, for a sample irradiated with one fraction of 90 cGy. The measured activation ratio is 43%. Image is at 20X magnification. Reprinted with appropriate permission obtained from Informa Healthcare.

3.4 Discussion

The results above describe the responses of isolated 3-D cultures of fibroblast cells stimulated

by a growth factor and ionizing radiation. We measured three output variables to describe the

environment that would surround cancer cells if they were present. However, this analysis was focused

on two variables, collagen matrix stiffness and fibroblast activation, since our interest is in the

mechanobiology of the breast tumor environment. The addition of TGF-β1 was meant to simulate one

important consequence of the heterotypic signaling that occurs between cancerous epithelial cells and

fibroblasts during tumorigenesis (Weinberg 2007). To discuss these multifactorial results, we recombine

the raw data from Figures 10-12 in Figures 13-15 so that we may draw attention to various elements.

Figure 13 displays results from all groups of samples, although we fixed two of the input

variables to show results after 72 hrs and for 180 cGy/fraction. Without irradiation (solid curve,

control), there were $4\text{x}10^5$ fibroblast cells per ml present. Yet they affected the matrix stiffness very

little because without growth factor stimulation only about 10% of cells were converted to

myofibroblasts. Simulated by TGF-β1, however, the same fibroblast density is 90% activated, which

triples the matrix stiffness as myofibroblast cells are able to attach to the matrix and contract. Since the

interaction between cancer cells and fibroblasts promotes the release of growth factors (Eck et al.

2009), fibroblast activation further increases growth factor production and matrix stiffening, which sets

up a positive feedback loop promoting tumor growth (Petersen et al. 2001).

However, irradiating the same sample types (Fig 13, dashed curve) shows a very different

stiffness pattern. Chemical cross linking in the cell-free matrix induced by three fractions of 180

cGy/fraction greatly stiffens the matrix. The presence of cells mitigates stiffening even if the cells are

stimulated by growth factor. Although 45% of the fibroblasts were activated by growth factor compared

to just 10% without growth factor, the radiation has either reduced the total cell population or

prevented viable cells from attaching to the matrix such that the matrix remains soft.
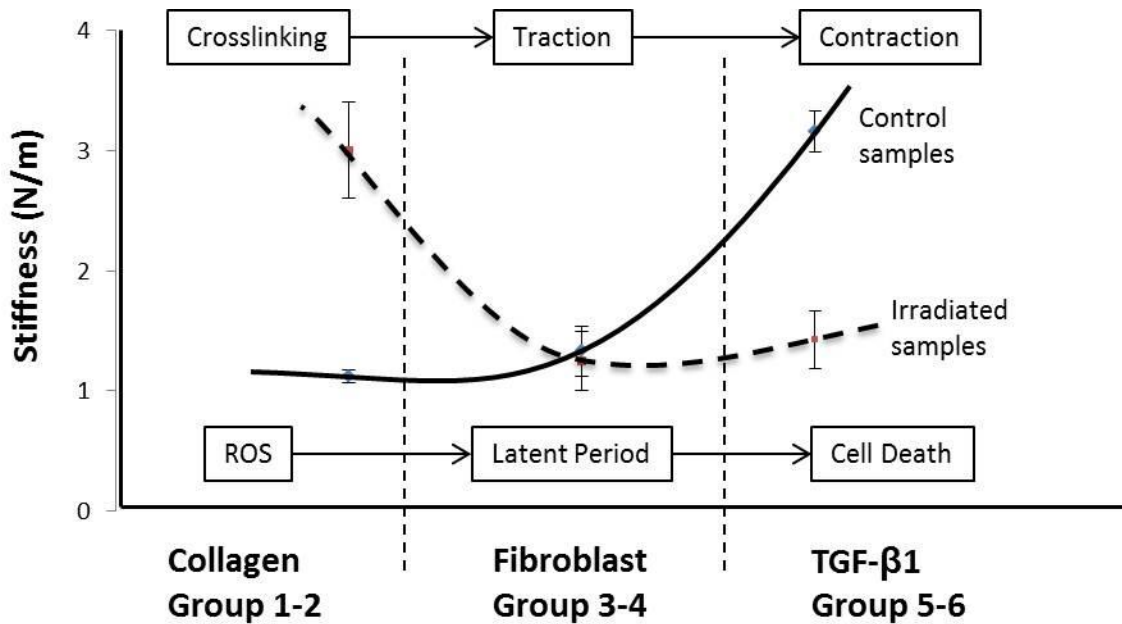
Figure 13 The behavior of all six study groups is shown for samples measured at 72 hrs and at 180 cGy/fraction. These data are replotted from Figs 9-11. Reprinted with appropriate permission obtained from Informa Healthcare.

If we focus just on activated fibroblast samples, we may observe the effects of irradiation in

Figure 14, where sample stiffness is plotted as a function of cumulative dose for Groups 5 and 6.

Without irradiation (control group), cells act to triple the stiffness of the matrix. With irradiation,

however, there is a modest increase in stiffness with dose. Larger fraction sizes double matrix stiffness

through a combination of collagen cross linking and enhanced fibroblast activation, but as dose

accumulates the net effect keeps the stiffness less than that occurring without irradiation.

Stiffness vs. Total Dose
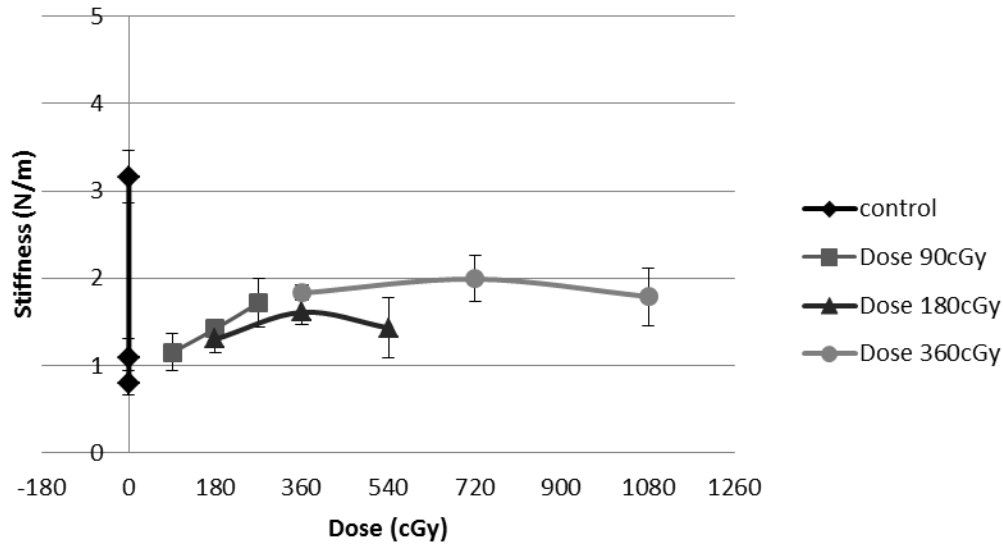
Figure 14 Matrix stiffness data from Groups 5 and 6, containing TGF-β1-stimulated fibroblasts, are plotted versus cumulative radiation dose over 72 hrs. Error bars indicate one standard error of the mean (SEM). Reprinted with appropriate permission obtained from Informa Healthcare.

So we see from Figures 12 and 13 that irradiating the matrix without cells will significantly increase stiffness. Allowing stimulated fibroblasts to grow also increases stiffness, and a stiff matrix in the presence of growth factor generates a reactive stroma that promotes tumor growth (Barcellos-Hoff 2010). However, combining these elements by irradiating stimulated fibroblasts, we find a moderate increase in matrix stiffening.

In Figure 15, we plot two of the output variables against each other, matrix stiffening and fibroblast activation, to show how radiation fraction size reduces the reactive stroma required for tumor progression. Curves are generated by plotting data obtained over three time points, although time is not explicitly indicated. The control group in this plot consists of non-irradiated samples with fibroblasts not stimulated with growth factor. This represents a normal-tissue condition, and we find that all of these data points reside in the lower left corner.
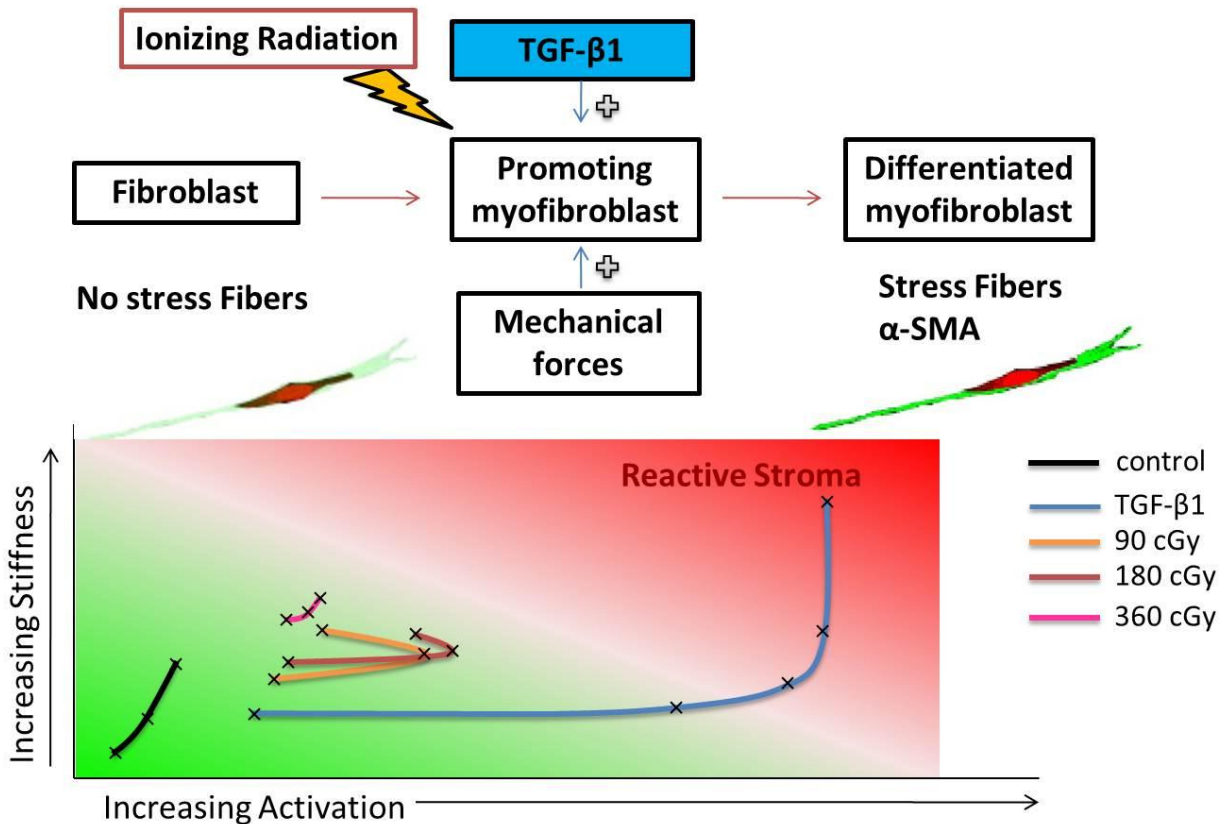
Figure 15 (top) Elements that contribute to a reactive stroma, which is an important for cancer cell proliferation and tumor growth. (bottom) Stiffness measurements and plotted versus activation ratio from the data of Figs 4-6, where the most reactive stroma is found for stiff matrix with highly activated fibroblasts. Reprinted with appropriate permission obtained from Informa Healthcare.

Stimulating the fibroblasts with growth factor without irradiation (labeled TGF-β1) shows that cells become almost entirely activated before contracting to stiffen the matrix. This curve represents the matrix condition in the presence of untreated cancer cells, which quickly generates features of a reactive stroma.

Finally irradiating stimulated cells with different fraction sizes prevents a reactive stroma but it influences the two output variables in different ways. The smaller fraction allows more fibroblasts to convert to myofibroblasts before a reduction in cell number ultimately reduces activation. Larger fraction sizes maintain a low activation ratio but quickly and significantly stiffen the matrix. So fraction size affects these two features of a reactive stroma differently. If it is more important to reduce

fibroblast activation than matrix stiffness, then larger fractions are recommended. However large radiation dose fractions will quickly cross link the collagen matrix to stiffen the matrix. If stiffening is the dominant factor in the reactive stroma promoting cancer cell progression, then smaller fractions are recommended.

Optimization of fractionation size differs for each tumor. A given radiation dose results in nonrepairable and repairable damage to tissue. The ratio of these two parameters differs by tumor type. If the ratio of non-repairable to repairable damage for a tumor is similar to or less than that of the surrounding normal tissue, then a larger dose per fraction (hypofractionation) to a lower total dose should be the most effective balance of benefits and harms. Recent clinical investigations indicate that this is true for breast cancers (Owen et al. 2006; Abram et al. 2008; Prosnitz et al. 2009). The Standardization of Breast Radiotherapy (START) Trials, which have looked at late adverse effects and tumor control, strengthen evidence in favor of alternative fractionation schemes, e.g, hypofractionated regimens, with potential for fewer adverse effects to normal breast tissues (Abram et al. 2008). A similar conclusion was drawn by a Cochrane review (James et al. 2010).

The data presented in this study have the advantage of being from a well-defined culture medium that includes essential stromal-cell elements that are involved in breast tumor development. Isolating tissue elements allows us to study their responses without the myriad other influences normally present in vivo. The disadvantages of isolated cell preparations are the same as for all cell culture studies: isolated elements do not recognize the full extent of systemic influences that lead to tumor formation and responses to therapy. Nevertheless, we see that through a series of cell culture and co-culture studies, with increasingly realistic elements that build systemic complexity, we and others can discover how to combine the input parameters available to radiation therapists to maximize the therapeutic ratio.

CHAPTER 4

STROMAL-EPITHELIAL DYNAMICS IN RESPONSE TO FRACTIONATED

RADIOTHERAPY

4.1 Introduction

One of the major challenges in the successful treatment of breast cancer is the effective application of adjuvant therapies. Unfortunately the heterogeneity of breast cancer results in a wide range of sensitivities and even resistance to existing therapies. Stromal cells in tumors were thought to be merely remnants of tissue among which the cancer cells grew. We now have evidence that heterotypic signaling exists in the tumor microenvironment, by which cells encourage or limit the growth of other types of cells in the area. Although the heterotypic interactions between fibroblasts, ECM, and cancerous epithelial cells are being studied by our group and others, it is unclear how the sum of these interactions determines the tumor outcome under therapies. Differences in radiosensitivity and sublethal-damage repair rates between cancerous and noncancerous cells, dose fractionation parameters are important for maximizing the TR, where the limiting factor is the response of noncancerous tissues (patient tolerance). Thus evaluating alternative radiotherapy techniques on a subset of residual disease conditions for early stage breast cancer has the potential for identifying more effective and less toxic treatments.

It is well-established that the tumor microenvironment plays a role in promoting or suppressing cancerous phenotypes in epithelial cancers. These thoughts have led to a paradigm shift in the way that researchers work with cell culture, moving towards studying cells in more physiologically-relevant 3D

environments. Co-culture with cell types present in the microenvironment, including cancer-activated

fibroblasts (CAFs), are known to change cancer cell behavior. Paracrine communication between CAFs

and neighboring cancer epithelial cells is a crucial factor for the continued growth of the tumor mass

(Sotgia et al. 2009). The tumor microenvironment also plays a role in resistance to radio/chemotherapy

(Andre et al. 2010).   This makes CAFs key player(s) in tumor progression, invasion, and metastasis

(Pavlides et al. 2012). With this understanding, we proposed that contact with CAFs also modulate the

behavior of cancerous epithelial cells. Although the system we use is that of the mammary gland, we

expect that general principles emerging from these results will apply to carcinomas from other tissue

types as well.

The reactive stroma contributes to tumor growth via multiple factors. This occurs at the level of

molecular cross-talk between epithelial cells and fibroblasts via the diffusion of soluble growth factors as

well as the epithelial cells that are responding to changes in mechanical forces due to CAFs stiffening the

matrix, upsetting tensional homeostasis. Apart from cell survival, other parameters such as metabolic

activity of surviving cells are relevant to assess the effectiveness of radiotherapy. We tested the

metabolic activities with the MTT assay of MCF-7 cancer cells, MRC-5 fibroblast and CAFs to improve our

understanding of the metabolic activity of these cells in terms of their radiobiological functions during

the course of radiotherapy.

MCF-7 cancer cells are a commonly used breast cancer epithelial cell line. They are Estrogen

receptor – α positive (ER +) and extensively used to model cancer in 3D cultures. They were derived

from a pleural effusion (that they were metastatic in the patient from whom they were derived);

however when injected into animals they do not metastasize, and they can be thought of having a

"milder" cancerous phenotype than other breast cancer cells lines. This property fits well with our

residual disease model for early stage breast cancer.

MRC-5 Fibroblasts, when exposed to cancerous stimuli either through treatment with TGF-β1 or contact with cancerous epithelial cells (Tsuchiya et al. 2003; Qayyum & Insana 2012b) become myofibroblast. This transition is also associated with a stiffening of the local microenvironment in 3D culture and in tissue. Thus, it is possible that CAFs, via alteration of their microenvironment, may regulate epithelial cell populations through mechanical forces. Mixtures of MCF-7 cancer cell and MRC-5 fibroblast will be incorporated into type I collagen gels, and mechanical indentation tests will be performed in order to determine the stiffness.

Fibroblasts are the predominant cell type that comprises the microenvironment of solid tumors; they regulate mechanical and chemical homeostasis. When exposed to factors secreted by cancer cells, they undergo a fibroblast-to-myofibroblast phenotypic change, characterized by elevated expression of α-SMA. CAFs have been shown to enhance cancerous phenotypes in the progression of disease models and are associated with poor prognosis in patients (Hellevik et al. 2012). Here we show that CAFs enhance epithelial proliferation by creating a pro-inflammatory (wound healing) environment.

Using 3D in-vitro models of the breast tumor microenvironments after lumpectomy, (1) we tracked the feature spaces of stiffness, activation and proliferation under fractionated radiotherapy. Sample stiffness defines the mechano-environment of the embedded cells that contributes to disease progression (Baker et al. 2010). (2) Test cellular differentiation and overall contractility of myofibroblasts which would indicate reactive stroma (Desmouliere et al. 2004). (3) Investigate cell proliferation rate via metabolic activity, which links aggressive and metastatic behaviors under radiotherapy (Martinez-Outschoorn et al. 2011).

To our knowledge, no systematic investigation has observed cancer cell behavior for different radiation fractionation schedules in a residual disease model. The effect of radiotherapy in blocking the release of stimulatory factors during wound healing might lead to the development of optimal post-

surgical fractionation schedules. We hypothesize that 3D co-cultures are predicative models for this investigation. Finally, in view of these postulated effects of radiotherapy on tumor-wound interactions, our ultimate goal is to deactivate cancer cells and their reactive stroma so the latter does not act as a promoter of the former. It seems possible that a fractionated treatment which allows for a more complete recession of residual disease might be found using these methods.

Post-operative radiotherapy has commonly been used for early stage breast cancer to treat residual disease. Due to differences in radiosensitivity and sublethal-damage repair rates between cancerous and noncancerous cells, dose fractionation parameters are important for maximizing the therapeutic ratio, where the limiting factor is the response of noncancerous tissues (patient tolerance). Fractionation schedules are selected to allow time for normal cells to repair radiation damage, while cancer cells are less efficient at repair (Hall 1994). Failure of RT to control residual cancer-cell progression is still a major clinical challenge (Pinsky et al. 2007). One method to overcome resistant residual disease of breast cancer is to change daily doses. In fact the Standardization of Breast Radiotherapy Trails (START), have looked at late adverse effects and tumor control, which strengthen evidence in favor of alternative fractionation schemes, e.g, hypofractionated regimens, with potential for fewer adverse effects to normal breast tissues (Abram et al. 2008). This study characterizes the fractionation schemes using stiffness, activation and proliferation to assess effectiveness in sterilizing residual disease in early stage breast cancer post-surgery.

4.2 Materials and Methods

4.2.1 Material

Collagen type I stock solution (10 mg/ml, rat tail) were purchased from BD Biosciences (Bedford, MA, USA); 3-(4,5-dimethylthiazol-2-yl)-2,5-diphenyltetrazolium bromide (MTT) was obtained from Sigma (St. Louis, MO); Cell culture media consisted of Dulbecco's Modified Eagles Essential Medium (DMEM,

Invitrogen, Carlsbad, CA) to which 10% fetal bovine serum (FBS, Sigma, St. Louis, MO, USA) and 1%

pen/strep (P/S, Sigma, St. Louis, MO, USA); Dimethylsulfoxide (DMSO) were purchased from ATCC

(Rockville, MD, USA); 48 and 96-well cell culture clusters and other plastic disposables were purchased

from Corning Inc. (Corning, NY).

4.2.2 Cell Lines cultures

The human mammary carcinoma cell lines MCF-7 and MRC-5 lung fibroblasts were obtained

from the ATCC (Rockville, MD, USA). Both MCF-7 and MRC-5 cells were maintained in DMEM

supplemented with 10% FBS and 1% P/S.

3D Co-culture

Type I collagen was used at a concentration of 10 mg/ml in accordance with our previous work

(Qayyum & Insana 2012b). Collagen was chosen because it resembles the extracellular matrix milieu of

invasive breast carcinoma better than other materials. Collagen solutions were diluted and neutralized

with medium and 1N sodium hydroxide to 2.0 mg/ml. Cells were introduced to a particular sample at

this time. 600 μl volumes of collagen solution were dispensed to a 48-well plate and incubated at 37°C

as the collagen polymerized over 30 min. After polymerization, 300 μl of complete DMEM was applied

to the top of the gelled samples. With or without cells, the total fluid volume added to each sample was

600 μl so that matrix stiffness was not influence by medium volume.

In co-cultures, 60,000 MCF-7 cells and 200,000 MRC-5 cells per 600 μl were used to mimic the

residual disease in-vivo ratio of epithelial cells to fibroblasts in the human breast post-surgery. The same

number of cells was seeded for each cell type cultured independently. Cultures were maintained for 5

days and the medium was changed every two to three days.

4.2.3 Sample irradiation

Samples were irradiated by placing them in a 6 MV photon field generated by a linear accelerator (Varian Medical System, Palo Alto, CA, USA)(Qayyum & Insana 2012b). Briefly, a uniform dose was delivered with the gantry set to 0 degrees and with a 100 cm source-to-axis distance. An 8 x 8 cm^2 field size was selected to ensure cell culture samples were uniformly irradiated. Dosimetric-quality solid water was placed above and below the well plates to provide proper build-up dose. All samples were taken from the incubator and placed in a thermally isolating container for transportation to the clinic. Once removed from the container, samples were exposed to IR at room temperature in a single dose and returned to the incubator within 30 minutes. The standard clinical dose fraction for breast treatment of 180 cGy was delivered to samples at a rate of 400 cGy/min. Other samples were exposed at the same dose rate but at a reduced fraction of 90 cGy or an accelerated fraction of 360 cGy. All sample irradiations were delivered in 5 fractions, once each 24 hours over 5 consecutive days, so the total dose was 450, 900, or 1800 cGy. Dose delivery verification was conducted following clinical standards.

4.2.4 MTT Assay

In order to measure the metabolic activity at the irradiated cell monolayer, the 3-(4, 5-dimethylthiazol-2-yl)-2, 5-diphenyltetrazolium bromide (MTT) assay was used. This is a sensitive, quantitative and reliable assay that measures the conversion of the yellow MTT substrate into a dark purple formazan salt by cellular dehydrogenase (Slater 1963). The MTT assesses cell metabolism based on the ability of the mitochondrial succinate-tetrazolium reductase system to convert the yellow compound to a purple formazan dye. Viable cells are able to reduce the water-soluble yellow colored MTT to a water-insoluble purple colored formazan product. The amount of colored formazan product formed, determined spectrophotometrically after dissolving the formazan crystals in DMSO, is proportional to the metabolic activity of the test sample. The general idea is that this metabolic activity

requires functional mitochondria. The MTT assay is a common tool in radiobiology to assess metabolic activity (Rossi et al. 2000).   We have applied it to cell cultures in-vitro for the assessment of growth characteristics and cell survival.

Cells were harvested from 75 cm^2 culture flasks by trypsinization. Cell were then resuspended in new medium (phenol free media), plated at different cell densities in 96-well culture plates and incubated at 37 °C in 5% CO_2 for the time-period indicated in the legends of the figures. The cell medium was replaced every 2-3 day. Unless stated otherwise, rows 1, 3, and 5 contained cells for each condition studied and row 11 was used for controlled conditions (Media, MTT assay, and DMSO). An example of a 96 well plate is shown in Figure 16. The cell monolayer is treated for 4 hours with MTT dissolved in PBS (concentration 5 mg/ml) at 37 °C and 5% CO_2. After incubation, the MTT solution is removed and 100 μl DMSO is added to each well of the 96-well plate to resolve the formazan crystals. Plates were shaken for 10 min on a plate shaker to ensure adequate solubilization. Assessment of metabolic activity was recorded as relative colorimetric changes measured at 570 nm. Samples were read in an Emax reader (Molecular Devices, Wokingham, UK) with software Softmax PRO version 4.3. Control wells for absorbance readings contained no cells or medium but MTT solution was added as per experimental wells, and removed after incubation, and DMSO was then added. All experiments were performed at least 3 times and the results were averaged.
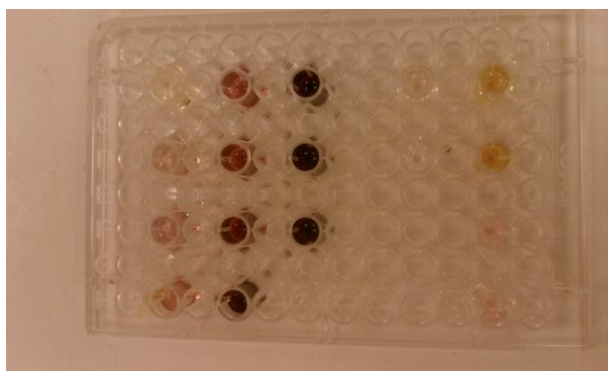
Figure 16 Costar 96 well plate with cell densities ranging from 50,000 to 120,000 in rows 1,3, and 5. MTT assay was added and the well was incubated for 4 hours. After removal of MTT, DMSO was added to resolve the formazan crystals, picture is the at this step. Increase in color intensity from top left to top right is due to increase cell number. Controls material in row 11.

4.2.4.1 Calculation of Absorbance rate:

Once a linear range was found from the standard curves, we chose the 20,000 cell concentration to observe for a 5 day period since in fell within linear range of 10,000 to 30,000 cells. The absorbance values at day 0, 3 and 5 were plotted and the slope taken to derive a rate of absorbance changes over the period of time (Figure 17). What is plotted in figure 16 for control and the 90cGy fraction dose conditions of the absorbance value at day 0 where 20,000 cells/µl initially and measured. Then the same density was tracked over 3 days and measured then 5 days and measured. A linear response was found over the 5 day period. The slope of the lines is what we report as the change rate of absorbance (**metabolic activity**) over the 5 days.
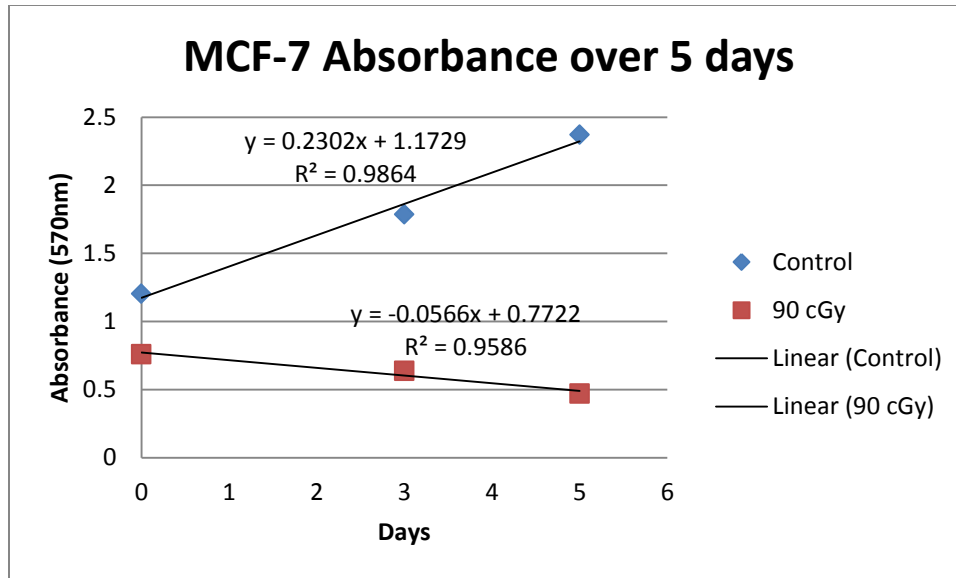
MCF-7 Absorbance over 5 days

$y = 0.2302x + 1.1729$
$R^2 = 0.9864$

$y = -0.0566x + 0.7722$
$R^2 = 0.9586$

Control

90 cGy

Linear (Control)

Linear (90 cGy)

Absorbance (570nm)

Days

Figure 17 The MTT assay done on the well plate containing an initial value of 20,000 cells/μl observed at day 0, 3 and 5 days.

4.2.5 Immunofluorescence staining (IF)

MRC-5 and MCF-7 cells were mixed at a ratio of 3:1 in collagen type I gel at a final collagen concentration of 2 mg/ml. Collagen gel co-culture was maintained in DMEM containing 10% FBS and 1% P/S at 37 °C in a humidified atmosphere containing 5% CO_2. To quantify the cell growth in collagen gel following mechanical testing, collagen samples were fixed as follows. Samples were washed with Phosphate-Buffered Saline (PBS, Lonza, Wackersville, MD, USA) before being fixed with 4% paraformaldehyde at 4°C overnight. Samples were then washed and permeabilized in 0.02% Triton X-100 in PBS for 15 mins followed by 5% non-fat milk blocking for 2 hours. Gels were then incubated with primary antibody, consisting of Bovine Serum Albumin (BSA, Sigma), PBS and Tween 20 (T, Sigma), (1:100 in 1% BSA/PBS/T) overnight at 4°C and secondary antibody (1:200 in 1% BSA/PBS/T) at room temperature for 2 hours. Cell nuclei were stained with TO-PRO 3 (1:1000 in PBS) for 20 mins. Sections were mounted between two glass coverslips with anti-photobleaching reagent.

4.2.6 Confocal microscopy

Immunofluorescence-stained samples were examined with a Leica SP2 laser scanning confocal microscope (Leica, Heidelberg, Germany) with Hg lamp and helium/neon laser and the associated software (Leica Confocal Software Version 2.00). A 488 nm excitation wavelength was applied for Fluorescein isothiocyanate (FITC) mapping, and a 633 nm excitation wavelength was used to find nuclei via TO-PRO 3 mapping. For each sample, a 20X objective captured a series of images along the z-coordinate (sample depth) at 3-5 μm increments. For confocal microscopy, an imaging system was employed (Microradiance; Bio-Rad, Philadelphia, PA, USA) consisting of a 25-Mw argon ion laser emitting at 488 and 514 nm and a 1-Mw green helium–neon laser emitting at 546 nm attached to a BX-50 microscope (Olympus Imaging America, Inc., Center Valley, PA, USA).

4.2.7 Automated area quantification and cell counting

MCF-7 cells seemed to aggregate in cell clusters within 3D microenvironments. Their morphologies were very different from MRC-5 cells; MCF-7 presented relatively rounded and less spread morphology and fibroblast are distinct in having a clearly recognized nucleus with long-tail cell bodies expressing α-SMA. These techniques were used to provide a quantification of proliferative rates for each cell type.

Cell number and area was counted using automated segmentation software. To differentiate MRC-5 and MCF-7 cells in the co-culture sample, both TO-PRO3 red and FITC green fluorescent (GF) images were taken and merged. MRC-5 cells were distinguished from MCF-7 cells by virtue of their elongated shape and α-SMA expression. In the MCF-7 cell growth assay, a nucleus size exclusion strategy was applied during the cell counting procedure. MRC-5 cells displayed a more elongated nuclei staining than MCF-7 cells and MCF-7 cells are more circular, thus they could be differentiated during the counting process. Therefore, we collected the red circular images and then analyzed the MCF-7 cell

number and area. We calibrated this counting method with a hand counting method to validate the software. Both methods gave consistent MRC-5 cell number, however the software had a systematic under counting of the MCF-7 cells. So, the values given are accurate within a measured bias. A detailed description can be found in Appendix A, section 2.

4.2.8 Mechanical testing

The experimental protocol is the same as that used in our previous study (Qayyum & Insana 2012b). In brief samples were mechanically tested using a TA.XT Plus Texture Analyzer System with a 1 kg load cell (Texture Technologies Corp., Scarsdale, NY, USA) and a compressive indentation procedure with 1 hour following delivery of IR. The fluid medium was removed from the top of the sample before testing with a 5-mm-diameter spherical indenter. The indenter was pressed into the sample surface at low velocity, 10^{-1} mm/min and to a depth of 2.5 mm. Force (F) and displacement (d) were recorded by the instrument to estimate sample stiffness.

4.2.9 Statistical analysis

Analysis of variance (ANOVA) was performed using R software to determine the significance of differences at a α = 0.05 level. Observed differences among mean sample groups were evaluated with post-hoc analysis, including Tukey HSD.   This method was similar to one done earlier in section 3.2.9.

4.3 Results

4.3.1 Cell viability and proliferation

Calibration curves

The 3 cell types (MCF-7, MRC-5 and CAFs) underwent the MTT assay to measure metabolic activity.   All three cell types were plated into 96 well plates in serial dilutions ranging from 5,000 –

120,000 cells/µl. To calibrate our system, we first ran a standard curve for each cell type. This was done

by plating the full range of cell densities in a 96 well plate and allowing time for attachment, but not

propagation. We then added the MTT assay to acquire the exact absorbance level per each well. The

assay was allowed to incubate for 4 hours, before the medium was removed and the dye was dissolved

with 100 µl of DMSO. The optical density was measured at 570 nm using a photospectrometer. The data

in Fig. 18 indicates a logistic curve relationship between absorbance signal and cell number, and there is

a range in which this relationship is linear. For each cell type the linear range was determined from

Figure 18 and found to be from 10,000 to 30,000 cells. A logistic curve behavior was observed for the

following reason; at the lower ranges there is less direct cell contact and less paracrine signaling leading

to lower metabolic activity and thus lower absorbance (Range < 5000 cells). At the linear range, MTT

absorbance increases linearly with cell density. Cells are close enough to each other for paracrine

signaling to occur and are more metabolic activity (range 10,000 to 30,000 cells). Cells make contact

with other cells through the cell surface by means of specific glycolipids and glycoproteins embedded in

the membrane. This signaling mechanism is important in cell recognition. In addition to these contact

interactions cells have to communicate with each other to relate the need for metabolites, fuel

molecules, growth and cell division. These interactions are based on the release of chemical substances

which travel to target cells. At the target cell, these messenger molecules attach themselves via a highly

specific interaction to membrane bound receptors. This in turn leads to the activation of certain

enzymes inside the cell initiating a particular cellular response.

   If there are too many cells, there are two potential problems. The first is that an unwanted

variable of media depletion is added to the experiment. The cells quickly use up the vital nutrients in the

media and their growth rate decreases. Second is the limitation of the equipment, where absorption

measurements are saturated above a reading of 4 so that we cannot distinguish between all numbers

greater than 50,000 cells/µl. Fibroblast and CAFs were limited by their cell density and size within the
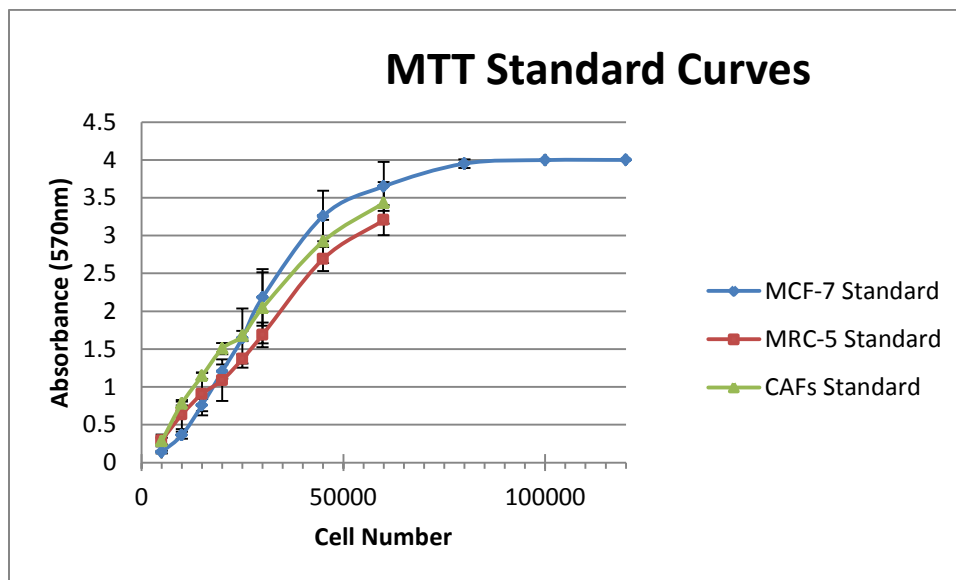
well to maximum of 60,000 cells/well.

Figure 18 Standard curves, for cells plated in a serial dilution ranging from 5,000 to 120,000 cells/µl were incubated for 4 hours with MTT as described in Materials and Methods. At the end of the MTT-incubation period, the formazan crystals were dissolved in DMSO. During the experiment the formazan/dimethyl sulphoxide solution was kept in the dark at room temperature. The data indicate a relationship between absorbance signal and cell number, and there is a range in which this relationship is linear.

4.3.2 Absorbance as a measure of cell proliferation

Provided that the sample measurements are within the linear part of the absorbance curve, cell

number can be determined by observing the absorbance of a test sample after the desired time period.

We established a relationship between absorbance seen from the MTT assay over a 5 day period and

cell counting from confocal imaging of IF stained samples as estimated from the area calculation of MCF-

7 cells over 5 days. From the linear curve of absorbance versus cell area cluster (Fig. 19) we can

establish that absorbance is an indication of cell proliferation and that the metabolic activity per cell is
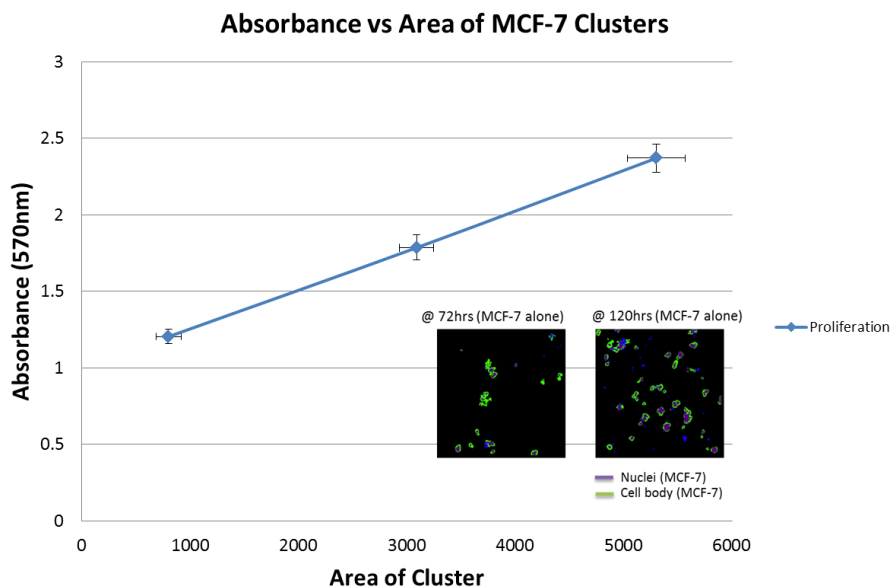
not changing significantly.

Figure 19 Absorbance from MTT assay for an initial plating density of 20,000 cells/µl at day 0, 3, and 5 days for MCF-7 cells versus the area over 0, 3 and 5 days from IF staining. INSET: Automated output of the area for samples at 72 and 120 hours. Error bars indicate one standard error of the mean (SEM).

The interpretation of figure 18 for the MCF-7 cells would indicate the proliferative nature of the cells. As a function of time from days 0, 3 and 5 days the cell number is increasing along with the metabolic activity. The R^2 value of the linear fit is 0.9999. This suggests that absorbance and cluster area are linearly related. The increase in absorbance signal in the MTT assay is a result of the proliferation of the MCF-7 within the well plates. If the conversion of the MTT assay, which indicates metabolism, per cell is constant, then the increase in cluster area should track the increase in absorbance. Thus tracking metabolic activity would indicate proliferation since cell cluster area is going up.

4.3.3 Response for all the cell types under calibration curves

Even when calibration curves of the number of cells counted versus absorbance values obtained with the MTT assay are derived from the linear portion of standard curve, the slope of the calibration curves are different for different cell lines (Fig. 18). This suggests different capacities of cells to produce

formazan, possibly as a result of different morphology and growth characteristics of these various cell lines. The steeper the slope, i. e., the higher the amount of formazan produced per cell, the higher the absorbance value up to which the relationship between cells counted and absorbance is linear. Growth rate and morphology of cells in culture also seem to play a role. For the CAFs there seems to be higher rate in metabolic activity than MRC-5 fibroblast at the same number of cells plated.

4.3.4 Metabolic activity and Fractionation

The results of our investigation on the metabolic activity of the control samples show proliferation of cells, and unlike the IF staining the MTT assay can distinguish between viable and dead cells.   MCF-7 cells seem to be the most sensitive to radiation, where the higher dose fractions induced the greater reduction in metabolic activity. As shown in Figure 20a*,* the surviving fraction remained constantly lower than the untreated controls, indicating that MCF-7 cells are highly sensitive to radiation (overall *p* <0.05). Based on this result, the next studies were conducted by examining MRC-5 fibroblasts under normal conditions and CAFs by inducing differentiation with TGF-β1. Results are expressed as the change in rate of metabolic activity over 5 days (Fig. 20 a,b,c). Normal MRC-5 fibroblasts are more radioresistant than MCF-7 cells. It is significant to note that CAFs are the most radioresistant of the three cell types (Fig. 20c).
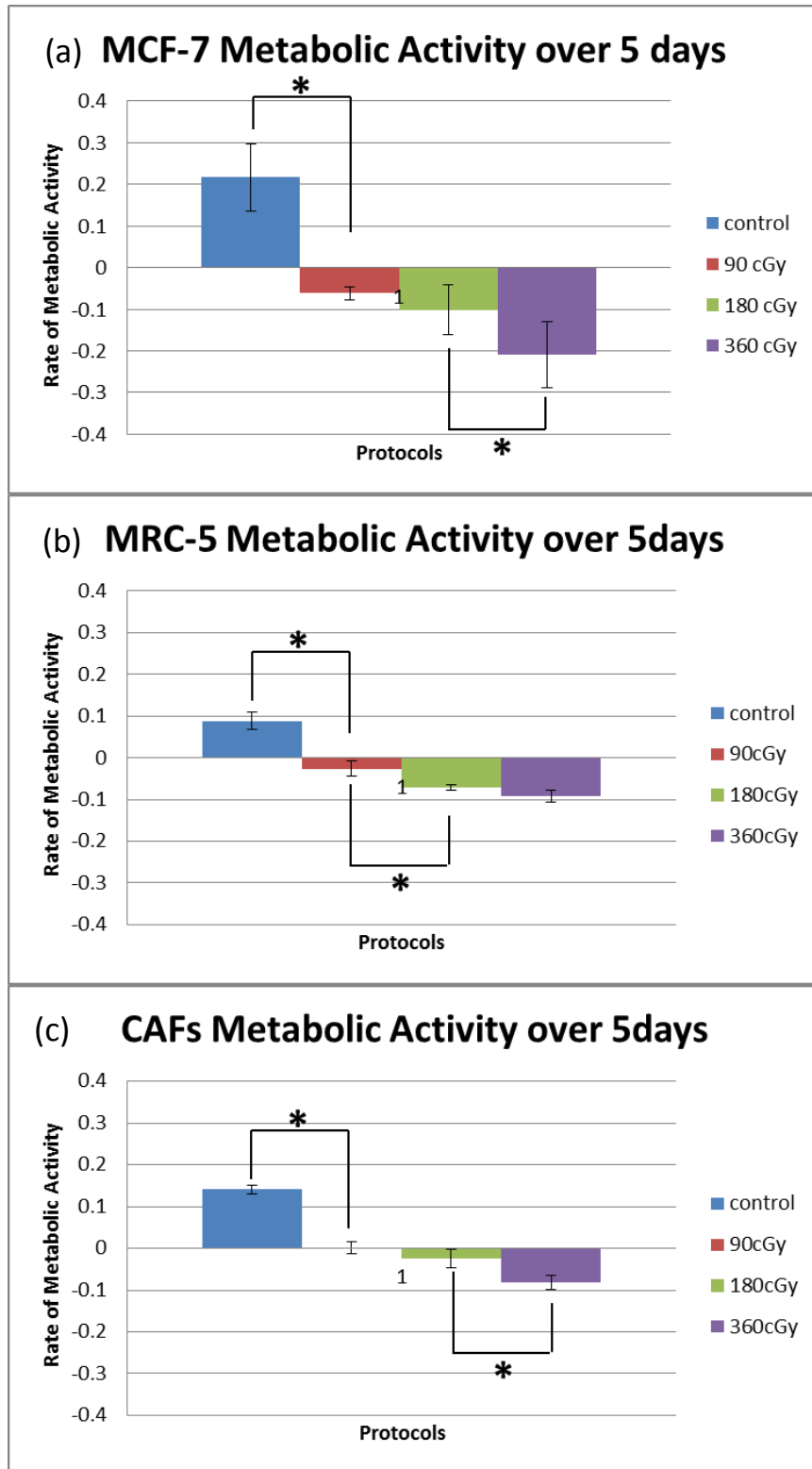
Figure 20 Metabolic activity of MCF-7, MRC-5 and CAFs. Error bars indicate one standard error of the mean (SEM). *indicates statistical significance at the p < 0.05 level. Significance was taken of adjacent values as well as protocols. Details of activity calculations can be found in Appendix C under calculation of absorbance rate section.

From figure 20, we see that the absorbance, determined by the formazan concentration, normally decreases with increasing radiation dose as was reported previously (Bromley et al. 2006).   If decisions are based on cancer cells alone, plot (a) would be used, using 180 cGy fractions would save the patient some extra risk. The microenvironment also consists of CAFs, from plot (c) it is apparent that a standard fraction gives a small response; however if a higher dose is used, it would cause higher cancer cell death and if tolerated by the patient a fourfold increase in CAFs reduction would be achieved. This method would help in the clinical decision making process. This is possible as seen in studies, such as the START trails referenced earlier which favor use of hypofractionated (i.e., larger fraction size) breast irradiation because it provides excellent long-term local control and limited late morbidity as well as benefits of convenience and cost.

4.3.5 Stromal Fibroblasts Stimulate Breast Carcinoma Cell Growth

To characterize the behavior of collagen co-culture in a 3D environment, MCF-7 cells were embedded in collagen gels, with or without the addition of MRC-5 fibroblasts. Based on preliminary studies, a 3:1 ratio was chosen of MRC-5 and MCF-7 cells, respectively, to be used throughout the investigation. Since the MTT assay, as performed in our study, provides information on total cells viability (overall metabolic activity) and not the spatial orientation of cells or activity, we detected the area of MCF-7 cells by the IF staining, in which MCF-7 and MRC-5 fibroblast cells can be easily identified, counted and measured. As MCF-7 cells proliferate they cluster which makes it difficult to count, so an initial quantitative assessment of cell growth was performed by measuring the total area occupied by MCF-7 cell clusters. An initial assessment of the MCF-7 alone indicated an increase in cluster area over the 5 days.
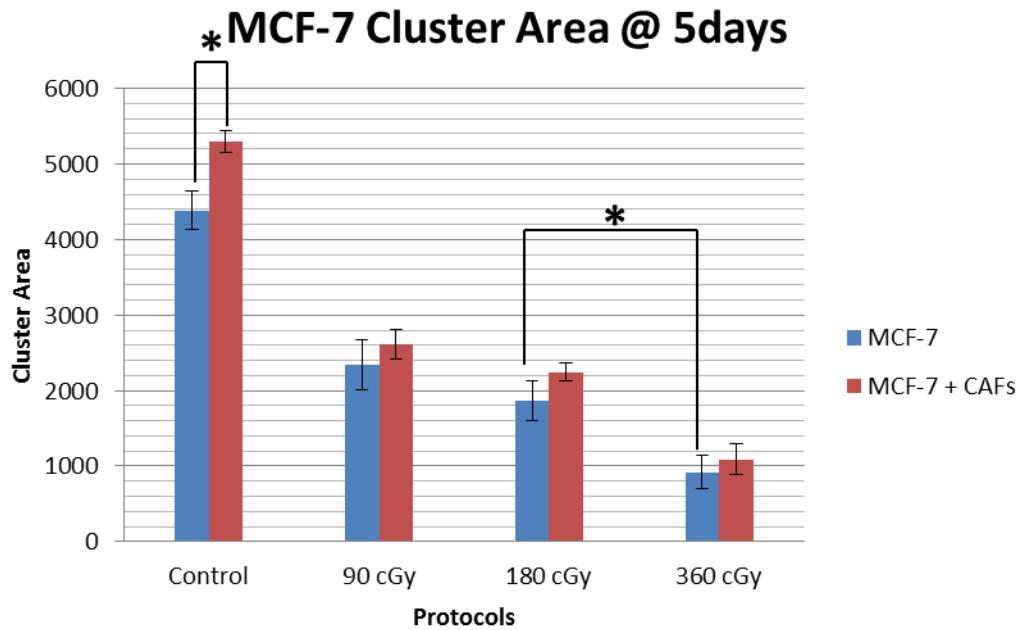
Figure 21 MCF-7 Cluster area over a 5 day period under control and IR fractionations. The presence of MRC-5 induced MCF-7 cell growth, resulting in large, irregular, and partially branched epithelial cell clusters.

In contrast, the presence of MRC-5 fibroblast induced a significantly greater MCF-7 cell growth, resulting in larger and more abundant MCF-7 cell clusters (Fig. 22). MCF-7 cells were identified and distinguished from MRC-5 by morphological differences as stated earlier. MCF-7 cell clusters composed of one cell to more than a hundred cells were included in the analysis. A quantitative assessment of epithelial cell numbers revealed that the presence of MRC-5 fibroblasts caused a highly significant growth stimulation of the MCF-7 cells from day 3 onward. To determine whether the software area is an acceptable surrogate measure of cell number, MCF-7 nuclei were counted manually in randomly selected clusters and the number of nuclei was correlated with the absolute software area. Analysis demonstrated that cell numbers were consistently under counted by the automated cell counting software method (A detailed description of this process can be seen in Appendix A).

4.3.6 Co-culture response to IR

Co-culture samples were exposed to 5 sequential daily fractions of either 90, 180 and 360 cGy/fraction, for a total dose of 450, 900 and 1800 cGy. The number of cells, as indicated by cluster area, that result as a consequence of these radiation treatments during treatment on day 5 are illustrated in Fig. 21. Each fraction scheme of radiation were sufficient to inhibit MCF-7 cells growth when cultured alone, though the higher fraction of 360 cGy induced the greatest reduction in MCF-7 cluster area. However, in the co-cultures exposed to the same amount of radiation, the average numbers of MCF-7 area were larger, though not a significant difference at $p > 0.05$. With the high fraction dose of 360 cGy, the damage was much more pronounced than the lower fraction doses; there was a significant difference ($p < 0.05$) in MCF-7 area (Fig. 21). This further demonstrated stromal component, such as CAFs impact the response of MCF-7 cells to radiation.

4.3.7 Fibroblast ability to contract after IR

We went on to investigate the functional status of irradiated cells, with particular emphasis on stiffness, which have been shown to influence tumor invasiveness and angiogenesis (Baker et al. 2010). If we just have fibroblasts we get stiffness when incorporated into collagen. Now if we add growth factor, which we know from our previous experience, will transform the cells and produce an increase in stiffness more than double the control because the fibroblast are being activated (Figure 22). Now if we create co-culture, we are not adding growth factors but we are aware cancer cells also produce growth factors. So, we can see almost the same response as that with growth factor. By stimulating the co-culture with growth factor, we see an added impact on the stiffness. The stiffness values all seem to bunch around 2.5 to 3 N/m stiffness range. We attribute this is to the active contraction that the growth factor is causing the fibroblast cells to contract which is making our sample stiff. Once we irradiate these samples at the early stage where cell arresting is leading to a decrease in stiffness, however with

increasing the dose we are causing crosslinking of the matrix leading to stiffness. We must keep in mind

that radiation has a passive effect – which causes crosslinking as seen in figure 10. This reduction, we

think is the deactivating of the cells, where fibroblasts are either actively contracting or not. All fraction

sizes caused a decrease in stiffness. However a significant difference in stiffness was found between the

lower fractions of 90cGy and 180cGy to the 360 cGy fraction size, which we attribute to the passive

impact of radiation on the collagen matrix leading to crosslinking. Overall, these results indicate that

while CAFs appear to survive high radiation doses, however their contraction capacity is considerably

compromised.
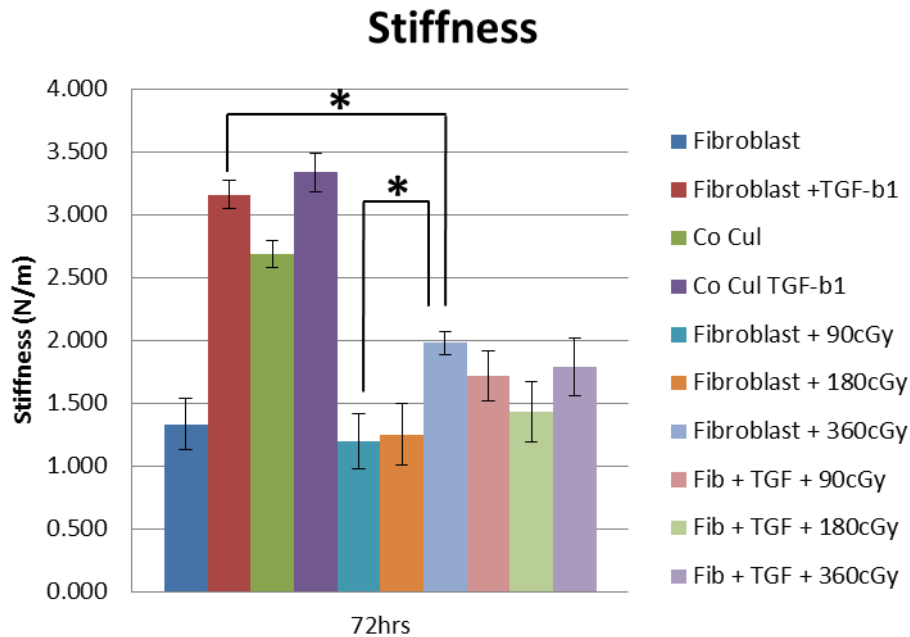
Figure 22 Measurements of sample stiffness (a), total cell number per sample (b), and cell activation ratio (c) for collagen gel samples (Groups 3 and 4) formed with fibroblast cells and without TFG-β1. Group 4 samples are given three daily IR fractions at the three times indicated. Each bar in the stiffness results is taken from measurements on N=6 samples (mean ± 1 SE). Cell numbers (b) and activation ratios (c) are for N=4 samples. No radiation was given to the control samples. * indicates statistical significance at the p < 0.05 level.   INSET: IHC-stained confocal fluorescent images for (i) a non-irradiated sample and (ii) a sample irradiated with 2 fractions of 180 cGy. Both samples were imaged after 48 hours.

Our data shows that radiation doses exert advantageous inhibitory effects on the proliferative, contracting capacity on CAFs, thus hindering some of their pro-malignant properties.

4.3.8 Post treatment evaluation of cancer cells

The clinical bench mark of treatment efficiency is post treatment survival of five years. Even though, we did not look at the bench mark, we extrapolated by doubling the time after exposure of radiation. This will be an indication as to what occurs when we turn off the radiation and observe the effects. The 90cGy fraction size was not evaluated because it is not clinically relevant for early state breast cancer; just the standard of 180cGy and doubling of the standard (360cGy) was used. The cancer cell cluster area post treatment is depicted in Figure 23, which represents the MCF-7 cluster area. Without any radiation, the MCF-7 cell cluster area increased and kept growing. However, samples after radiation showed a decrease in the MCF-7 area. Five days post-treatment the cells started decreasing in size due to delayed cell death response. Samples which had growth factor TGF-β1 seemed to have a larger MCF-7 cluster area. Radiation-induced apoptosis can be mediated by either of two pathways: intrinsic or extrinsic. Activation of the cascade of caspases is common to both pathways. Targets for cleavage by caspases include proteins involved in DNA repair, DNA replication, cytoskeleton regulation, and the nuclease that causes DNA fragmentation.
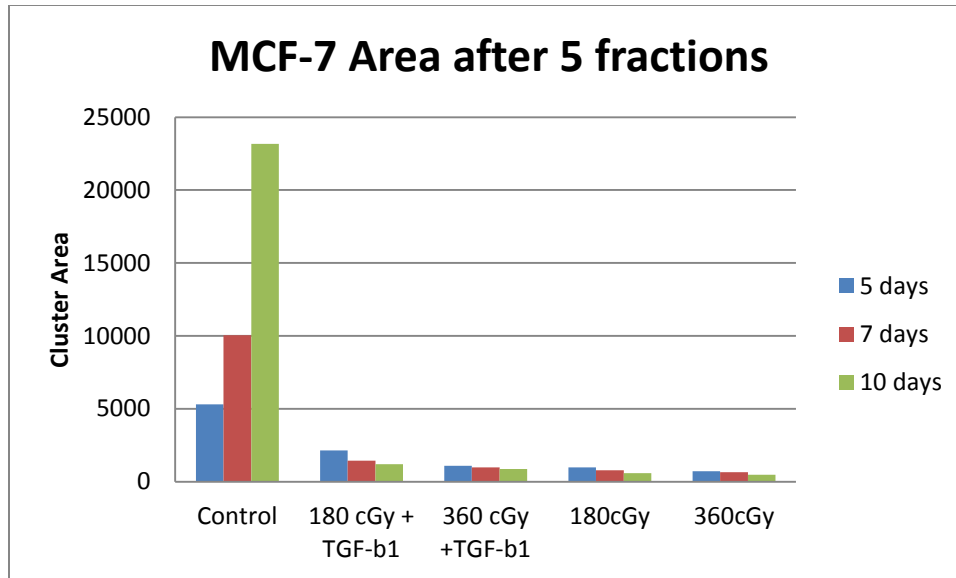
MCF-7 Area after 5 fractions

Figure 23 Cluster area post treatment. Without any radiation, the MCF-7 cell cluster area increased and kept growing. However, samples after radiation showed a decrease in the MCF-7 area. Five days post-treatment the cells started decreasing in size due to delayed cell death response.

4.3.9 Reactive Stroma response of stiffness

For the non-treatment condition, we observed that the parameter of stiffness does not continue to increase. Co-culture past day seven shows that stiffness starts to decrease due to cancer cell cluster size increasing faster than fibroblasts' growth and contraction (Fig. 24). This may be due to the increased presence of MCF-7 extracting nutrition present in the culture leading to the diminished role of MRC-5 fibroblast. In regards to post-treatment, stiffness of the co-culture was reduced for all fractionation schemes. Radiation damage is largely manifested by the loss of cellular reproductive integrity. Some cells undergo apoptosis (triggered death), which would not show morphologic evidence of radiation damage until they attempt to divide. Irradiation causes reduction of stiffness by deactivating the cells, causing fibroblasts to be active or inactive. For the slight increase in stiffness that was observed for the samples with growth factor, it was perhaps due to growth factors leading to contraction of residual fibroblasts post-treatment.
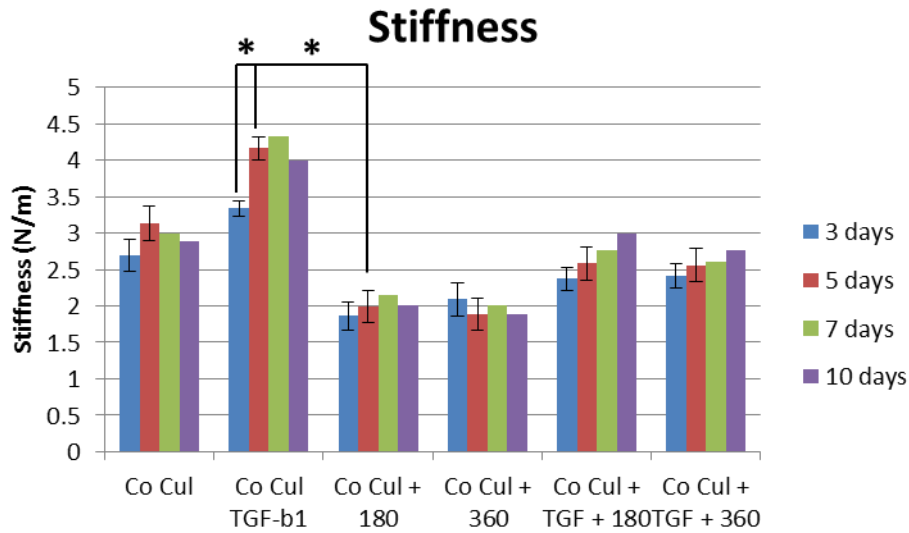
Figure 24 Stiffness response post treatment. Co-culture past day 7 days stiffness starts to decrease due to cancer cell cluster size increase. Irradiation causes reduction of stiffness by deactivating the cells (Fibroblast – on or off). For irradiated samples with growth factor leads to contraction of residual fibroblasts.

4.4 Discussion

We see our investigation as a new approach between radiobiology and radiotherapy. In the past radiobiology was looking at specific diseases or cell types not under natural conditions. We wanted to generalize these conditions and developed a 3D co-culture model to evaluate the dose fractionation schemes relevant to clinical practices.

Clinical studies look at recurrence rate, patient susceptibility and 5 year survival rates. However, we are looking at an abstract view of component interactions coupled with responses to radiation therapy, the signaling between stromal cell types and cancer cells in their environment.

The focus of therapy is the cancer cells, but nonetheless in our study we found the microenvironment to also be important in that if not suppressed it may harbor any residual disease,

reigniting tumor growth. So, the feature space of fibroblast activation, stiffness and proliferation are important parameters within the matrix that derive fibroblast conversion and stiffness responses.

Myofibroblasts or CAFs have been found in a variety of normal tissues and various pathological situations, including wound-healing, fibromatosis, and stromal reaction to epithelial tumors (Morishima et al. 2001). We found fractionation studies with MRC-5 fibroblasts and CAFs indicate that higher fraction doses may be more effective early on in preventing cancer harboring environments. Higher fraction schemes inhibit contractility in CAFs and prevent differentiation in fibroblasts, thereby metabolically uncoupling tumor cells from their surrounding stroma.

The conclusion that MRC-5 fibroblasts definitively modulated the response of MCF-7 cells to radiation relies on two main considerations. First, using the MTT assay on different cell types, CAFs were found to be most resistant to radiation in terms of metabolic activity i.e., for all fractionation schemes on both days 3 and 5 (Fig. 19). The observation that CAFs were resistant and MCF-7 cells were sensitive, suggesting that the target of interest should also include the CAFs and not only MCF-7 cells. These observations bring forward a new concept that tumor cells and their reactive stroma should not be merely seen as a morphologic domain but also as a functional domain with a genuine metabolic cooperation between the cancer cells and newly formed CAFs. Second, by the cell counting and area clusters performed on collagen gels, the number and size of MCF-7 clusters from the gels containing mixed MCF-7 and MRC-5 fibroblast cells were significantly increased compared with the number and size of the clusters from the gels containing MCF-7 cells alone (Fig. 20). Taken together, these results suggest that fibroblasts and cancer cells in co-culture become metabolically coupled, resulting in the development of a "symbiotic" relationship. As seen in figure 20 the area of MCF-7 increases with co-culture than in cell culture alone.

Putting this information together, the metabolic activity, as indicated and explained in Fig. 19 and based upon IF staining directs the importance of biochemical fluxes within the microenvironment consisting of tumor and stromal components. The distinctly different but complementary metabolic function of MCF-7 cells and CAFs shows a complex spatial organization compatible with synergistic support to each other. Indeed, many investigators stressed the unique characteristics of CAFs (Olumi et al. 1999; Desmouliere et al. 2004). These are, in essence (together with the ECM), the main component of stromatogenesis (i.e., the process of new stroma formation occurring concurrently with tumor cell invasion and angiogenesis). The newly formed stroma not only provides tumor cells with a substrate suitable for tumor cell growth and proliferation but also offers them metabolic support essential for cancer cell survival. These findings direct attention to the stromal components along with the tumor, which might give rise to an improved therapeutic ratio.

Tumors are characterized by ECM remodeling and stiffening (Levental et al. 2009). Our experimental results both improve our basic understanding of mechanobiology of the microenvironment, metabolic activity, as well as identify relevant therapeutic responses. Many investigators have found breast cancer tissue to be as sensitive to fraction size as dose-limiting healthy tissues (Owen et al. 2006; Abram et al. 2008; Prosnitz et al. 2009). Fibroblasts, CAFs and the factors they produce are important targets for RT and prove to be useful prognostic markers. These findings confirm that radiotherapy schedules can be evaluated through metabolic activity, stiffness and differentiation changes.

Expanding beyond cancer cells by including the microenvironment and looking at interactions provides new insights into long term sustainability of tumor regeneration.   Evaluation of alternative fractionation techniques i.e. Hypofractionation may result in a useful alternative to standard breast cancer RT. There is value in a technique which reduces the treatment time while maintaining cosmetic

and functional control, if by adjusting fraction size from standard protocols does not adversely affect stiffness or differentiation changes.

This proposed technique provides a useful tool to systematically optimize radiotherapy and sheds important insight into the complex problem of dose-time fractionation. The presented feature spaces outlined earlier allow us a better understanding of the influence of various biological parameters on RT treatment of cancer. This may provide a practical tool to obtain the optimal total dose, overall treatment time, fraction sizes, and intervals for each disease site. In summary, though clinical decisions cannot be derived from cell culture studies, nonetheless targeting CAFs as a therapeutic strategy against cancer is an intriguing concept that requires further research.

The development of Intensity Modulated Radiation Therapy (IMRT) (Fig. 25), results in greatly improved dose distributions, with more limited doses to normal tissues for comparable tumor doses. One of the most important advances has been in IMRT as a type of 3-D conformal radiotherapy which supports complex beam delivery schemes. IMRT produces high dose conformation to target with normal tissue avoidance and subsequent potential benefit to both reduced normal tissue toxicity and dose escalation to tumor to increase local control. The beam can be moved while the patient is fixed in one position. The patient does not have to be in close contact with beam structure which makes it easier to implement complex beam movements together with simple and comfortable patient positions. The IMRT computer planning implements an inverse sequence of the normal planning process used in conventional radiation therapy. The conventional approach to radiation is to try to develop an appropriate treatment plan for the tumor by trial and error simulations on a computer. Sophisticated IMRT computer technology is used to determine the best way to achieve this result, thus shaping the dose cloud to the tumor. This suggests the attractive possibility of increasing the dose per fraction. These techniques can greatly reduce the duration and cost of therapy and may minimize the effects of

accelerated tumor repopulation triggered by RT itself. It is therefore appropriate and safe to embark on

such non-standard fractionation clinical practices.
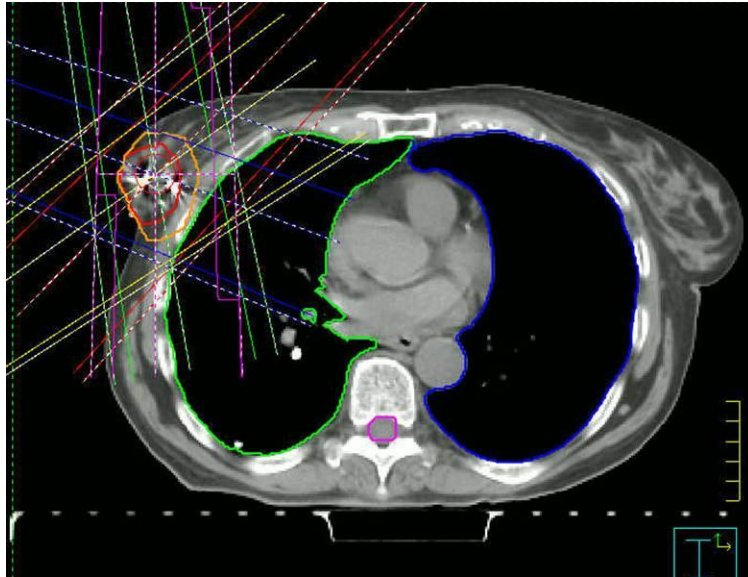
Figure 25 Boost irradiation (IMRT) at the site of tumorectomy, 1600 cGy over 8 fractions. Rationale of this strategy is most local recurrences appear close to the tumorectomy cavity and spare the patient late radiation morbidity. Courtesy of Provena United Samaritans.

CHAPTER 5

CONCLUDING REMARKS

5.1 Conclusions

The overall objective of this research is to develop a model for 3D cell culture in order to better understand the effects of fractionation in radiation therapy for breast cancer. My specific aims are as follows. (1) To systematically map 3D stromal cell culture responses to fractionated radiotherapy (the effects of fractionation schemes on collagen matrix stiffness and fibroblast activation were studied using this culture model). (2) To establish a 3D cell co-culture model by incorporating more breast tissue components such as a cancerous mammary cell line into a fibroblast-collagen gel to mimic more natural signaling conditions. The purpose of this was to produce co-cultures that will be used to deliver fractionated courses of radiation prescriptions that enable measurements of the cellular microenvironment. (3) In addition, I exposed a co-culture model to altered fractionation schemes to process optimized dose per fraction for eradication of residual disease. We tracked a feature space that includes collagen matrix stiffness, fibroblast activation and epithelial cell proliferation. The parameters may eventually provide a metric for clinical decision-making. Acquiring the data stated in this thesis has improved our understanding of IR fractionation on a subset model of residual diseases. With more research in this data we may be able, as I had intended, to optimize clinical decision making. However, at the conclusion of this thesis project such clinical decisions cannot be definitive.

I have reached my short term goals but in order to reach my long term goal I have to extend this study to develop animal models. This will increase the level of complexity and realism of this research at the cost of some clinical control being lost. However, using my understanding of cell culture as

developed in this research, I would be equipped to assemble a theory on the data produced in the more

advance models. Once data from an animal model is analyzed, we can apply that data to formulate in-

vivo patient trials. Thus, data collected from previous models can be used to study and evaluate data

gathered in patient trials.

Currently patients at treatment centers are receiving treatments based on modern techniques

that better shape the radiation dose distribution to the target volume (e.g., IMRT based on computed

tomography of the breast and surrounding normal tissues). As a physicist at Provena Covenent Hospital,

I noticed that treating patients with breast cancer using these modern techniques makes it possible to

deliver an effective dose of radiation to the tumor volume with reduced toxicity to surrounding tissue.

As such we are able to deliver higher doses of radiation with little or no increase in toxicity. This

observation was based on an evaluation of patients receiving an IMRT boost after their conformal

treatment. These patients did not have an adverse reaction to the elevated dose directed at the tumor

region. These methods have been fully adopted at this cancer institute and it has become apparent that

the delivery of higher doses by conformal radiotherapy and IMRT has led to a significant improvement in

the treatment of patients with breast cancer. These clinical practices significantly increase the rate of

local tumor control without an increase in treatment-related side effects.

However, it cannot be conclusively stated that achieving significant improvement in the

therapeutic ratio depends only on advances in the technology of radiation delivery. It is important to

understand the mechanisms that govern the sensitivity of cancer cells and normal tissues to radiation.

This will make it possible to improve the therapeutic ratio and, hence, the probability of obtaining

permanent tumor control without the result of severe injury to normal tissues.

Further research using animal models and clinical trials are needed to test the safety and efficacy of cancer treatments that target the cancer cell and the wound healing pathway utilized by the cancer cell to proliferate and metastasize.

5.2 Future Outlook

This study is an initial step in my career plans to study stromal modulation of epithelial tumors. It is also my objective to integrate basic science experiments and engineering tools into clinical practice. As such, I plan to translate the knowledge acquired from the laboratory experiments conducted in pursuit of this thesis into clinical standards. In a larger context, the elucidation of a microenvironment controlled cancer behavior and its control mechanisms can provide major guiding principles in the search for biomarkers of improved therapeutic ratios.

Imaging tools

This data can potentially be used to develop a device that is able to diagnose the microenvironment with the parameters of stiffness, activation and proliferation.

Physical forces coupled with bimolecular signals cause certain cell behaviors as demonstrated by our cultures, such as the differentiation leading to contraction and thus stiffness of matrix. Within our culture, cancer cell proliferation occurs and irradiation leads to crosslinking of the matrix, stromal cell activation and deactivation. How can we turn this into a diagnostic tool, which may be able to look at stromal cell activation? Any molecular imaging tool that can lock onto a fibroblast when it is converting is an indicator of stromal cell activity. There might not be a method currently available; however, we have the ability to measure stiffness as a parameter for stromal activation. We can measure stiffness locally on the order of resolution of an imaging system, such as ultrasound which is on the order of a millimeter. Though, stiffness is an elastic modulus and a static value, which has a low specificity;

however the viscous component which is the dynamic parameter may be more telling. So, it may not be

enough to only look at stiffness but also evaluate the dynamic component of viscous response of the

microenvironment. So, there are methods to look at the static response as I have done, but to study the

viscous dynamics there is shear wave imaging. Shear wave imaging is one of the dynamic methods in

quantitatively evaluating the elastic parameters of the tissue. It utilizes the phase velocity and

attenuation coefficient information of the propagated shear waves in tissue to reconstruct mechanical

properties. This might be an important application of the stiffness mapping to give us an assessment of

the microenvironment surrounding a cancer cell post-surgery. For example, looking at the relationship

between activation and stiffness (figure 14) we can be able to determine the nature of the stromal

environment.

The Role of Molecular Imaging in Evaluating Tumor Response to Targeted Radiotherapy

Positron emission tomography (PET) has become one of the most important molecular imaging

modalities in clinical oncology. This success is primarily based on the ability of PET to measure and

visualize the increased glucose metabolism of cancer tissue by using the radiolabeled glucose analogue

18F-fluorodeoxyglucose (FDG). However, our findings have important implications for re-interpreting

the PET scans of human tumors using Fluoro-2-deoxy-D-glucose (F-2-DG), as glucose uptake was

previously thought to be solely the domain of cancer cells. Instead, here we see that CAFs show

increased metabolic activity, just as cancer cells do under identical culture conditions. Thus, increased

PET glucose avidity may actually be a surrogate marker for a reactive stroma, allowing the rapid

detection of a lethal reactive microenvironment.

Staging of cancer patients has evolved as the most important clinical application by providing an

accurate assessment of the localization, extent and spread of disease. FDG-PET can assess tissue glucose

utilization with high reproducibility (Figure 26). Following therapy, the decrease of tumor glucose

utilization correlates with the reduction of viable tumor cells, however it may be more telling of the

reactive stroma that is a result of post treatment. Thus, FDG-PET may allow for the assessment of

therapy response by determining the viability of residual masses after completion of treatment.

Figure 26 Axial PET/CT slice of a patient with an inflammatory carcinoma of the right breast showing increased activity diffusely through the breast and involvement of both axillary level I and internal mammary lymph nodes. (Courtesy of Provena United Samaritans)

APPENDIX A

AUTOMATED CELL COUNTING

(1) MRC-5 Fibroblast only

Phenotypically, activated fibroblasts are characterized as expressing large amounts of α-Smooth

Muscle Actin (α-SMA). To observe differentiation of fibroblast cell, Immunofluorescence (IF) staining

was done. Confocal imaging resulted in number of images that required α-SMA-stained cells and nuclei

counting to quantify activation ratios. Here, we developed an automated segmentation method to

recognize and count two different types of staining from a confocal image. The percentage of cells

expressing α -SM Actin was determined by a computerized Count Activated Cells Thresholding image

analysis program, developed by our lab. It was used to maintain a constant threshold for determining

positive differentiation of cells, represented in figure 27. In order to count the total cell number and

activated cell number, we detected red fluorescence regions (nuclei, representing total cell number) and

green fluorescence regions (α-SMA, representing activated cell number) in the images from confocal

microscope. The activation ratio was defined by

$$Activation\ Ratio = \frac{Number\ of\ Activated\ Fibroblasts}{Total\ Number\ of\ Fibroblasts} = \frac{Number\ of\ (GF \cap RN)}{Number\ of\ RN}. \quad (1)$$

Where Number of Green fluorescence represents α-SMA and the denominator indicates the total

number of red nuclei and intersection of green cell bodies. Since both red and green fluorescence

regions in the images are brighter than background, but the level and pattern of noise vary from image

to image. To reject image noise while identifying valid fluorescent objects to be counted, 2-stage

Percentile (P-tile) thresholding is applied to the images (Doyle 1962). The P-tile threshold value was set

to be 50 percent greater than background noise. The fluorescence of interest was the area with values above the P-tile threshold. The fluorescence we are interested in is assumed to be present in the area above the P-tile threshold value. To eliminate the artifacts, we restrict the candidate objects by their intensity and size. For each candidate object, we collect pixels (B) surrounding the object, and the intensity threshold value is determined as AVG(B) + STD(B) where AVG($\bullet$) and STD($\bullet$) represent average and standard deviation of $\bullet$. The size threshold value is computed as 0.5 * S_{median} where S_{median} is the median size of all candidate objects. Have detected both red and green fluorescence, we count the number of total and activated cells. The total number of cells in an image is the total number of red fluorescence objects, and the activated cell is the red fluorescence object where more than 30% of the pixels in the object are also designated to have green fluorescence.
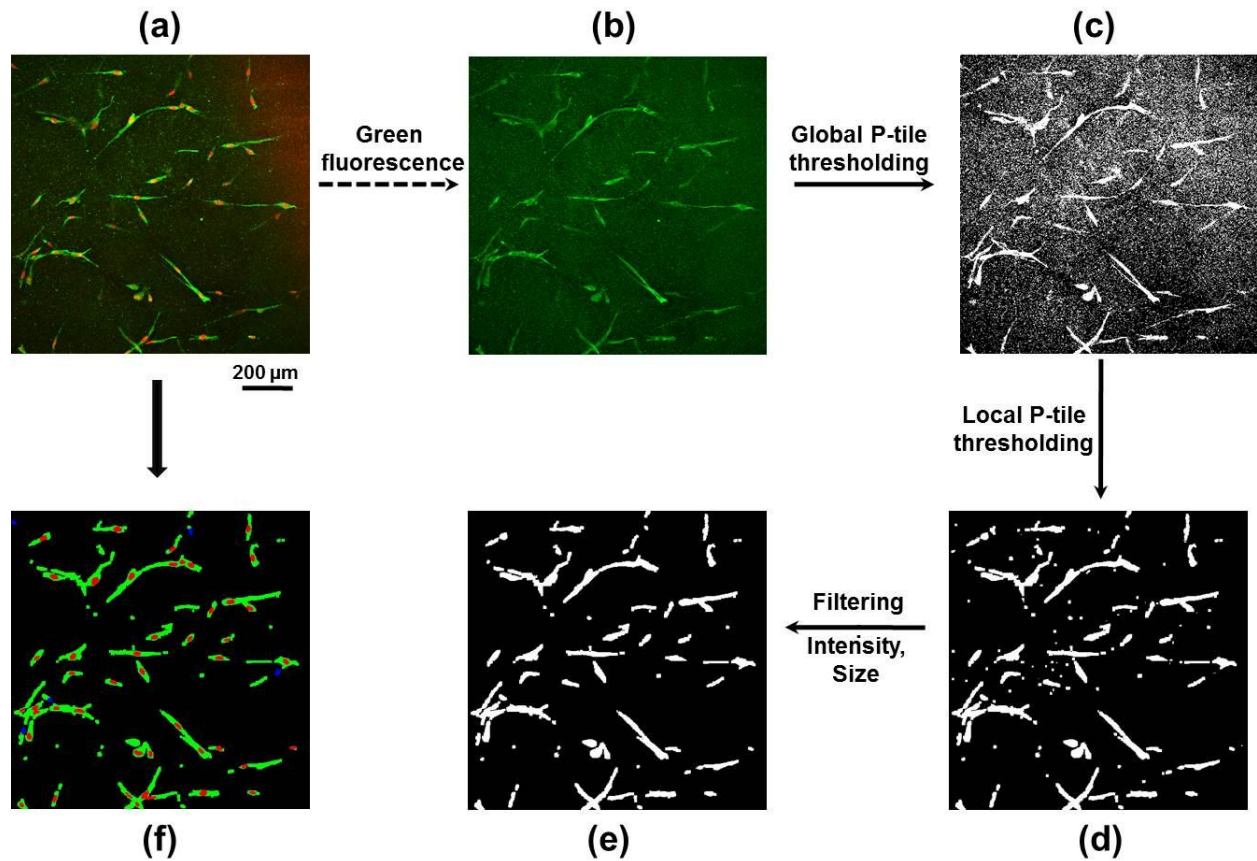
Figure 27 Automated cell counting and cell activation ratio calculation. (a) Confocal fluorescence microscopy image (20×). α-SMA is shown in green and nuclei are in red. Green cell bodies that meet the threshold criteria are counted as activated. (b)-(e) show results of the automated segmentation method applied to a green fluorescence image. The same method was used for red fluorescence images (not shown here). (b) Input image of green fluorescence. (c) Global P-tile thresholding. (d) Local P-tile thresholding. (e) Intensity and size restriction. (f) Computer generated image for automated cell counting. α-SMA is shown in green; nuclei are in red for cells with α-SMA and in blue for cells without α-SMA. (Acknowlege: R. Bharagava & J.T. Kwak)

(2) Co-culture study – Automated Area quantification and cell counting

We detect red fluorescence regions (representing nuclei of MCF-7 and MRC-5 cells) and green fluorescence regions (representing activated MRC-5 cells) in the images of confocal microscopy. Both red and green fluorescence regions in the images are brighter than background, but the characteristics of the fluorescence are different and the level and patterns of noise vary from images to images. To handle noise and better represent the candidate fluorescence objects, we adopt the concept of scale-space theory. Fluorescence should exist as meaning objects over certain ranges of scale and be robust to

the scale variation within the ranges, but not noise. Accordingly, we generate a number of Gaussian smoothed images with varying sizes ($\sigma = 1.6 \times 2^k, k = 1,2,3,4$) and add them to the original image. Nuclei and green fluorescence of MCF-7 are relatively round or elliptical and MRC-5 fluorescence has an elongated shape. As cell grows, nuclei tend to clump together and to look like one large cluster. In these cases, the detection is confounded and often makes many false positives, i.e., identifying background areas as nuclei.

2.1 Nucleus Detection

To detect nuclei, we first obtain the initial segmentation of the objects by Otsu method (Otsu 1979) which is a global thresholding technique. Since global thresholding may not be optimal, the true nuclei may be (partially) missed. To compensate for the possible lose, an iterative region growing method is used; the initial threshold value is th_0=AVG(O)±STD*(O), and at iteration i, the threshold value is updated as th_i = AVG(O) ±(1-0.1*i)*STD(O) where O is the pixels of the identified area and AVG and STD are the average and standard deviation of the area, respectively. For each identified candidate areas, we group similar pixels together by applying multi-threshold segmentation method based on MHFFCM (Wang et al. 2006). In principle, given n data points $X = \{x_i\}_{i=1}^n$, it generates an optimal partition by minimizing the following objective function:

$$J_f = \sum_{j=1}^{c} \sum_{i=1}^{n} [\mu_j(x_i)]^b \|x_i - m_j\|^2$$

where c, b, $\mu_j(x_i)$, and m_j denotes the number of groups, the exponential weight factor, the membership degree of x_i to jth group, and the center of jth group, respectively. For an image, data points are generated at each intensity level and contain intensity and spatial information. For instance, at intensity level i, $x_i = \{mx_i, my_i, s_i, f_i, i, mr_i, sr_i\}$ is defined where mx_i and my_i denote the average horizontal and vertical coordinates, respectively. s_i and f_i are designated as standard deviation of the

location of all pixels with the intensity level *i* and frequency of the intensity level *i*, respectively. mr_i and sr_i represent average and standard deviation of the distances from the center of all pixels with the intensity level *i*, respectively. Then, individual nucleus is identified. Ordering clusters in ascending order of the average intensity $G = \{G_1, G_2, \dots, G_c\}$, the roundness of the cluster(s) is computed as adding new cluster at a time according to the order and identify the union of clusters (*g**) resulting in the best roundness score.

$$g^* = \underset{g \in \cup\, G}{\mathrm{argmax}}\, Roundness(g)$$

$$Roundness(g) = \frac{Qhull\_ratio(g) + Bound\_ratio(g)}{2}$$

where *Qhull_ratio* and *Bound_ratio* denote a ratio between the area of a cluster and the areas of convex hull and minimum bounding circle of the cluster, respectively. We require the size of the nucleus to be >0.5 * N_{median} where N_{median} is the median size of all candidate objects.

2.2 Green Fluorescence Detection

We segment green fluorescence of MCF-7 by applying the same method with nuclei, but different rules are invoked to remove artifacts: $r_{major/minor} < 5.0$, $Roundness > 0.7$ and size > 10 pixels. $r_{major/minor}$ is a ratio of major and minor axes. Then, the detected segments are removed from the original image, and Otsu's method and iterative region-growing method are applied to find candidate areas of green fluorescence of MRC-5. For the candidate areas, the size and shape are examined: size > 10 pixels and $r_{major/minor} > 1.5$.

2.3 Count Activated Cells

Since a series of images are taken, it is likely that the same cells appear in the adjacent images. If such cells exist, we only use the nucleus which has the largest intensity in the original image. Using the

segmented nucleus and green fluorescence, we identify the activated cells: if >30% of the pixels of

nucleus are the areas of the green fluorescence, the nucleus is designated as the nucleus of an activated

cell.

3. Calibration of Automated Cell and Area quantification

Tumor cells were identified and distinguished from fibroblasts by Immunofluorescence labeling

for nuclei and cell body. The immunofluorescently stained gels were then analyzed by image analysis.

Carcinoma cell clusters composed of one cell to more than a hundred cells were included in the analysis.

3.1 Cell number for automated counting calibration

To determine whether the nuclei and cell body area is an acceptable surrogate measure of cell

number, carcinoma nuclei were counted manually in selected clusters and the compared with software

counting. The results can be seen in figure 28, which indicates at low cell number there is agreement

between the techniques, however at larger number of cells the software systemically under counts as

compared to the hand counting.
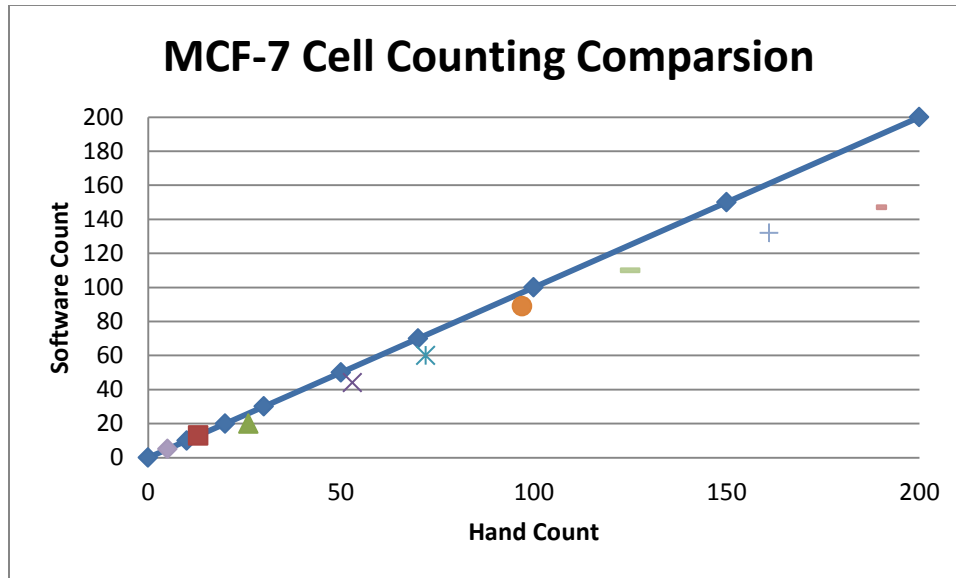
MCF-7 Cell Counting Comparsion

Figure 28 MCF-7 cell counting under control conditions. Selected immunofluorescence images were chosen to which ranged from 1 to 200. The results are plotted for software counting and hand counting. The software systemically under counted in larger number of cells

3.2 Calibration of Area and cell number

An initial quantitative assessment of cell growth was performed by measuring the total area occupied by carcinoma cell clusters.
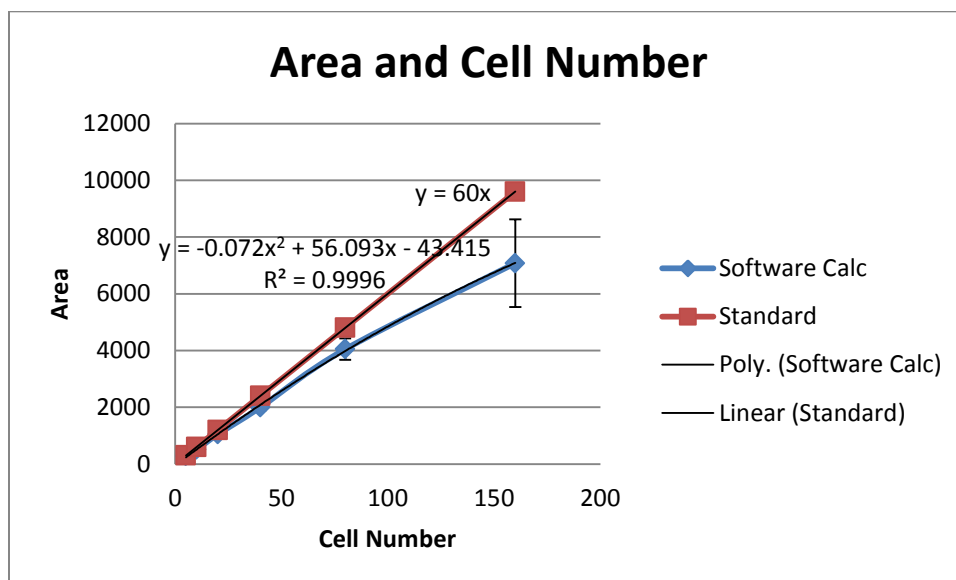

Area and Cell Number

$y = 60x$

$y = -0.072x^2 + 56.093x - 43.415$
$R^2 = 0.9996$

Figure 29 Relationship between MCF-7 cell cluster area and cell number.

A standard curve was generated by assessing the area of a size MCF-7 cell and extrapolating the area

that multiple cells would occupy for up to 150 cells, which was fit to a linear line. Then the software

computation of the area for cells ranging up to 150 was plotted and fit to a 2nd polynomial (Figure 29).

Using the two fitted equations we find that the difference at lower range of cells is small. However, at

large cell numbers the bias between the standard and software calculated curves gets larger.

APPENDIX B

DESIGNING A TREATMENT PLAN

The goal of radiotherapy treatment planning is to justify an effective treatment that will deliver a precise irradiation dose to the target volume without causing damage to the surrounding normal tissues. Therefore patient positioning, target volume definition and irradiation field placement are very critical steps while planning the irradiation process.

1. Collect patient's CT data including attached aluminum markers.

2. CT data set is transferred to a Virtual Simulator. The physician defines the tumor volume and the organs at risk and she/he will place the necessary fields relative to the tumor volume.

3. The simulation plan and the CT data are transferred via DICOM (Digital image and Communication in Medicine) server to the Treatment Planning System (TPS) for dose calculation and final treatment plan optimization.

4. Verify patient position on LINAC before irradiation.

5. Perform treatment on the treatment machine (Linear Accelerator or LINAC).
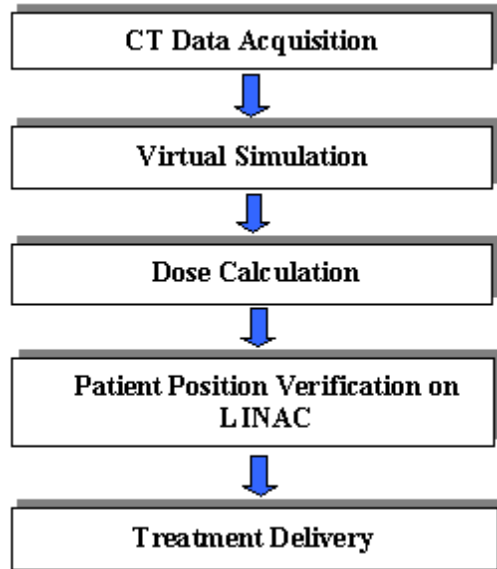
Figure 30 Current clinical routine for external beam treatment delivery

The breast is prescribed 4500 cGy for five weekly fractions for a total of 25 fractions each with 180cGy per day. The use of energy greater than 6 MV photons for these patients would have resulted in under dose to the superficial tissue just below the skin surface. Therefore, two tangential off-parallel fields of 6 MV photons, each with wedges, were designed. Because of the breast shape is irregular and the volume of the breast tissue decreases towards the nipples, wedges are used on beams for breast cancer patients. Different wedges are used depending on the specific patient breast shape, as shown in the figure 34 below. In addition, the off-parallel tilt reduced the amount of beam deviation into the lungs. The dose within the target volume is also kept to within 10% dose variance in keeping with common standards.

Below is the procedure for completing a dosimetry plan for breast cancer external beam radiation therapy. Figure 31 shows patient setup. The user can modify basic setup as well as couch removal and laser localization. Figure 32 shows the counters including regions of interest and display options. Figure 33 allows the user to assign points of interest such as the isocenter. Figure 34 shows the

beams. Figure 35 allows the user to compute dose and assign a dose grid and well as dose computation
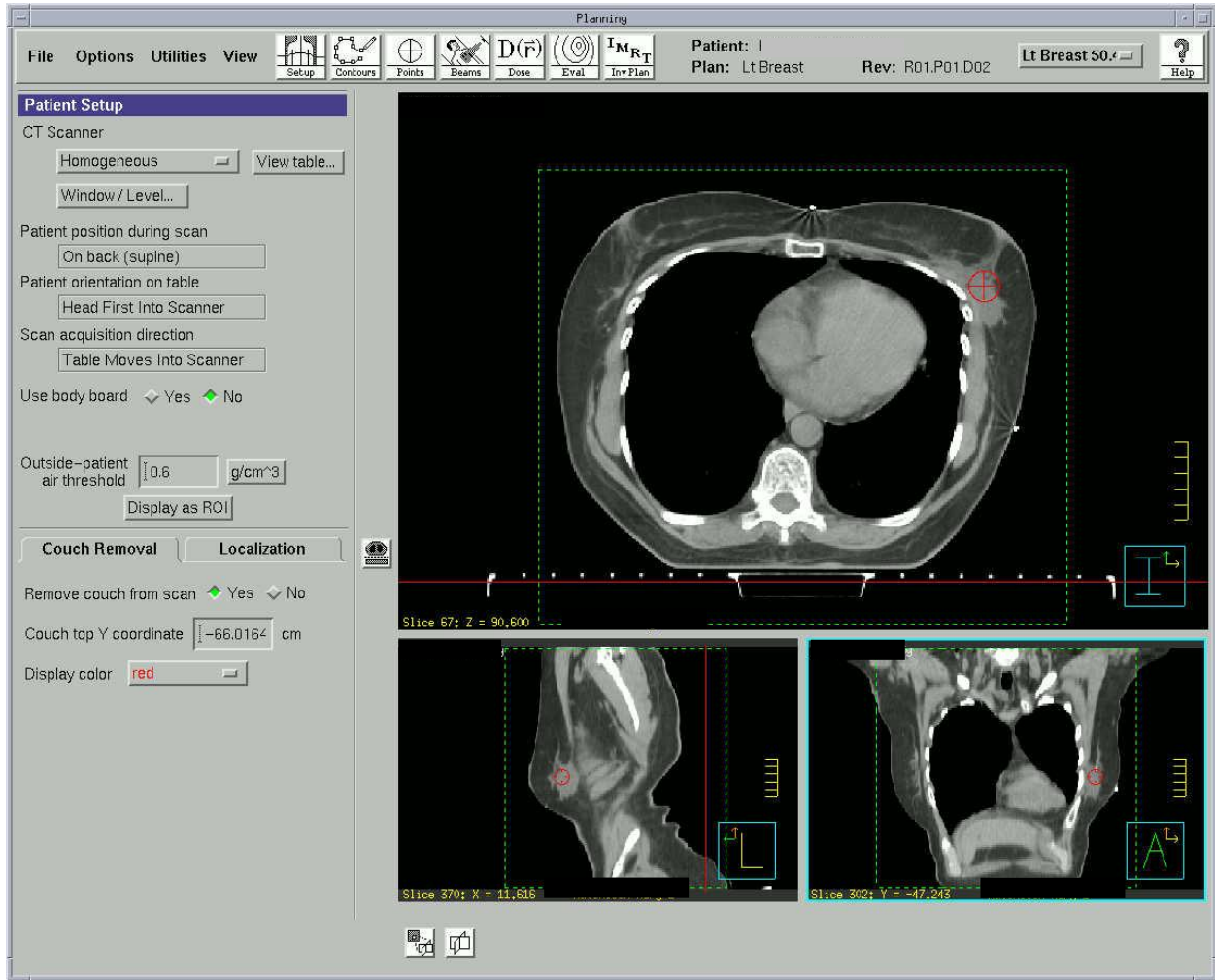
method.

Figure 31 Patient positioning and treatment fields for treating the intact breast using a three-field isocentric technique. The 3-window layout of the system showing CT slices (from superior to inferior). On the left side the parameter controls windows, the top window is the transverse view, the lower left is the sagittal view and the lower right is the coronal view.
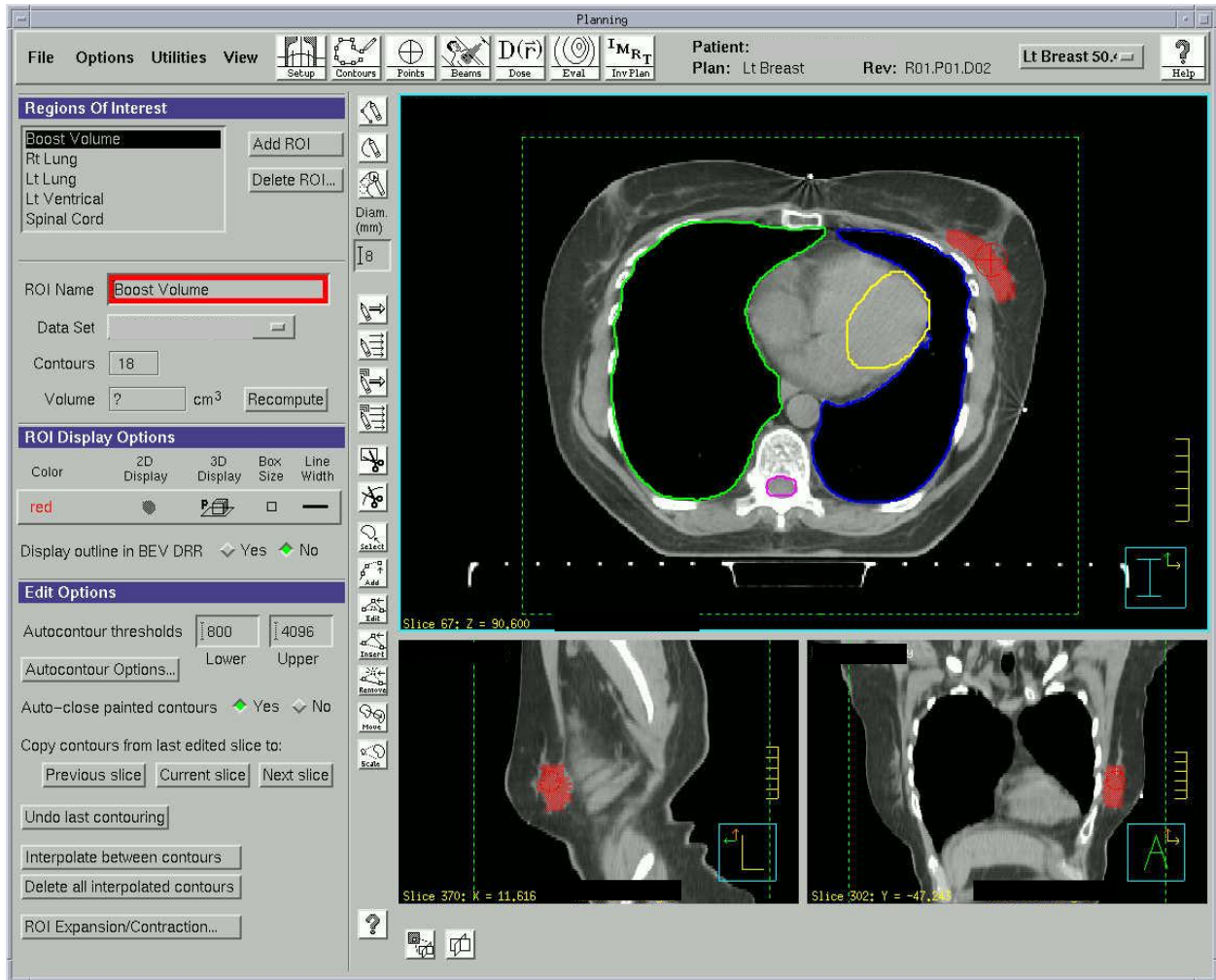
Figure 32 Contouring of a tumor bed and incision site on 3-D treatment planning. Colored contours of the lumpectomy region shown in red contour. As pictured are regions of interest such as the lungs (green and blue), spinal cord (purple) and heart (yellow).
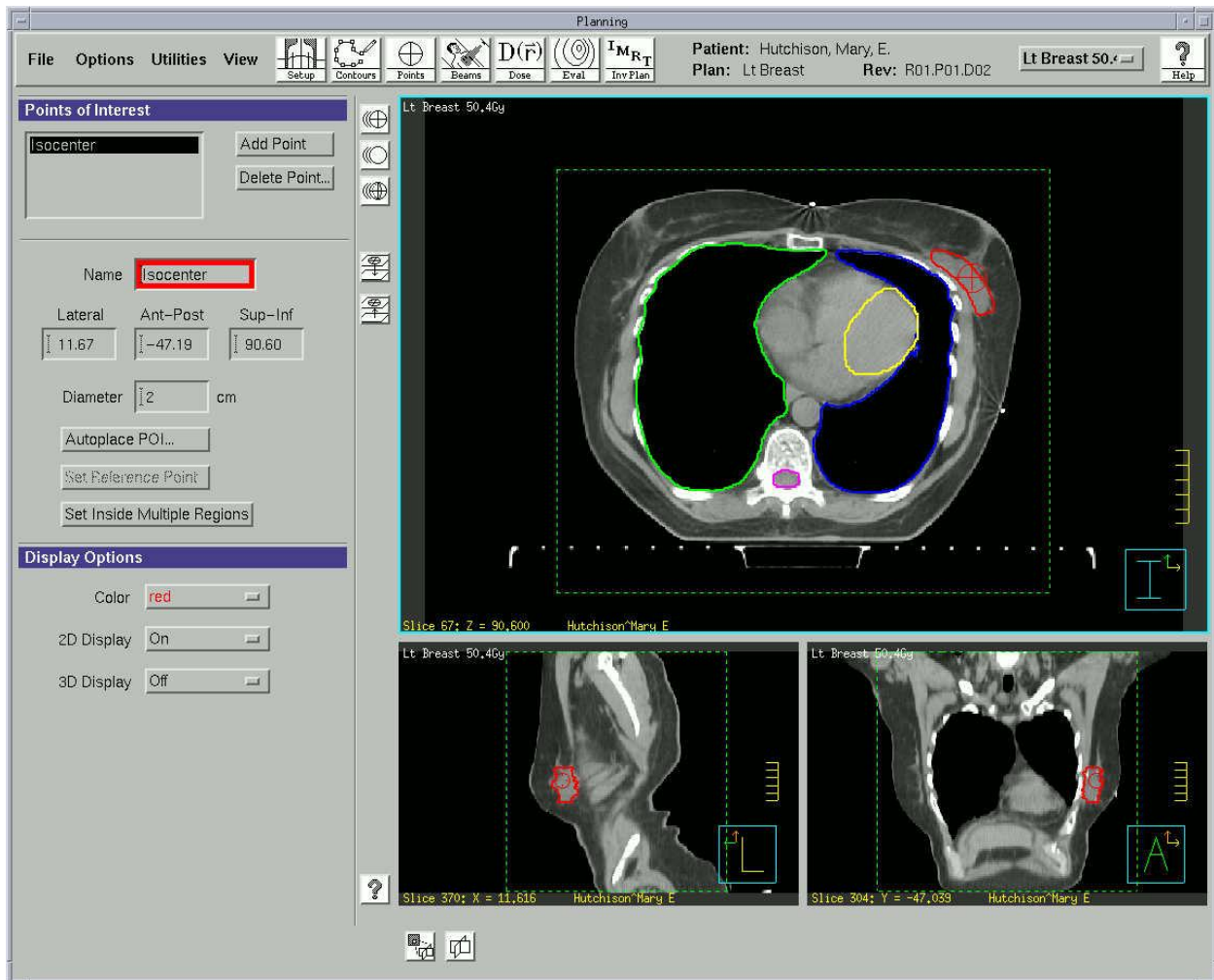
Figure 33 An isocenter (red crosshair) is placed within the gross tumor volume to allow user to assign localization for treatment planning and patient positioning during treatment.
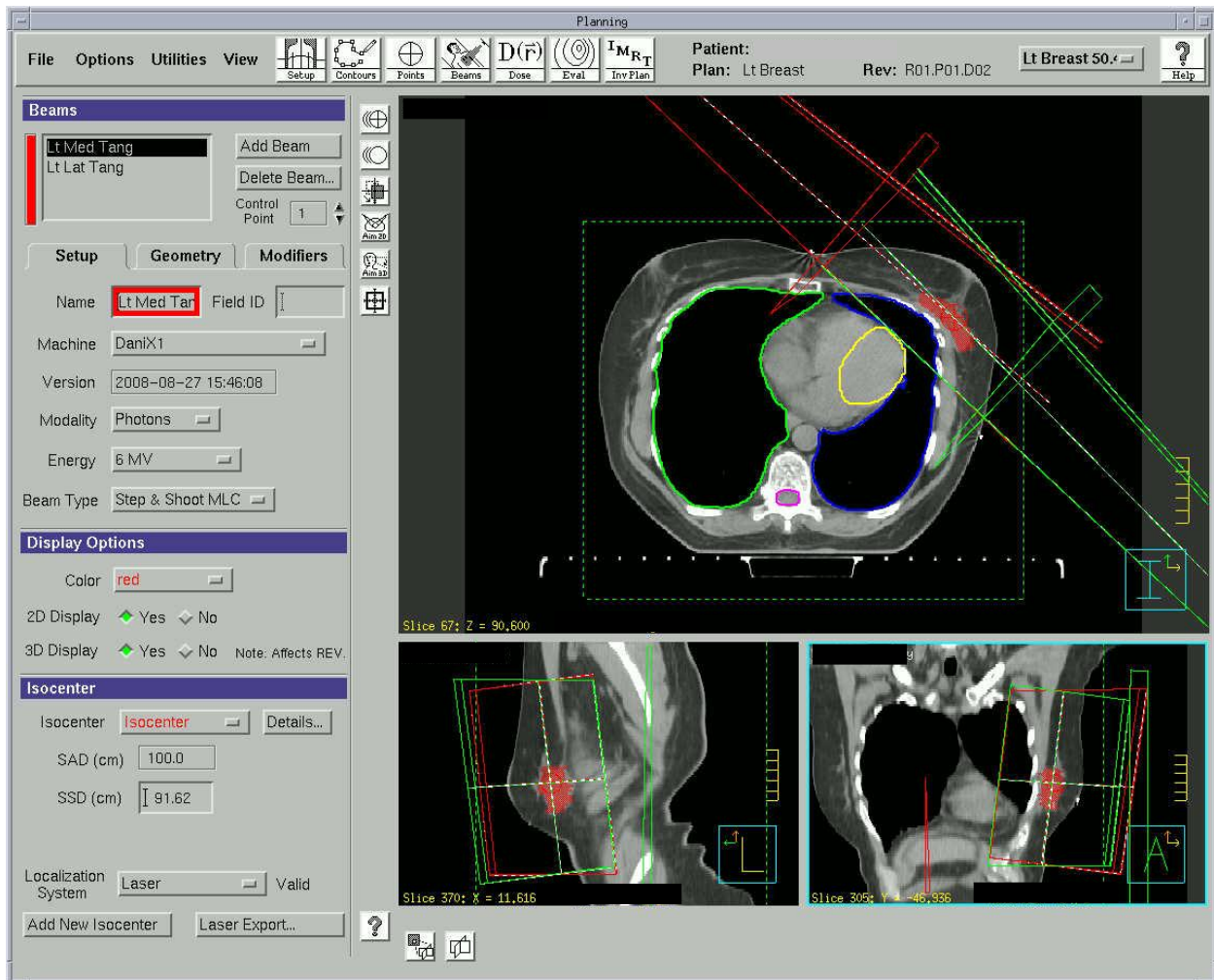
Figure 34 Two-field technique for treatment of the breast, intermediate step in development of tangent pair. After opposing medial field, the new lateral field has a diverging deep edge. Additional gantry rotation will result in the desired coplanar deep field edge.
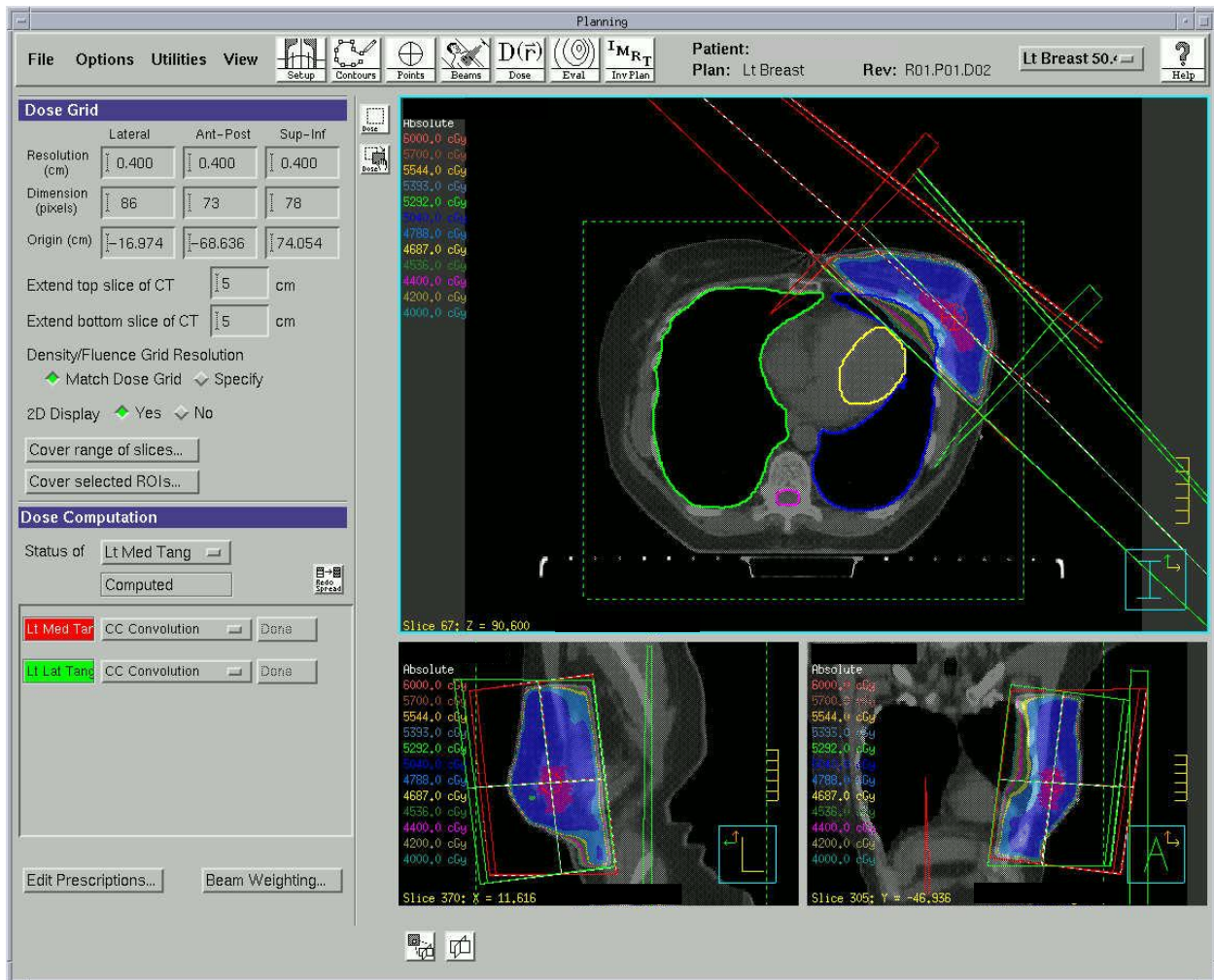
Figure 35 Left-sided tumor in lateral breast, showing minimal irradiation of the heart and lung in the tangential fields. Shown is the dose distribution for a prescribed at a depth of 5 cm. Dose distribution of tangential fields created using lung inhomogeneity corrections and forward planning, with additional medial and lateral segments added to improved homogeneity (not done for this patient). Isodose color key: *blue, 100% of prescribed dose*.

APPENDIX C

MTT ASSAY

The non-radioactive, colorimetric assay system using MTT was first described by Mossman and co-workers (Biedler et al. 1973). It is used for the measurement of cell proliferation in response to growth factors, cytokines and nutrients as well as for the measurement of cytotoxocity (Pieters et al. 1990). MTT, 3-[4,5-dimethylthiazol-2-yl]-2,5-diphenyl tetrazolium bromide, is a yellow tetrazolium salt which can be transformed into purple colored formazan crystals by metabolic active cells. This cellular reduction involves the pyridine nucleotide cofactors NADH and NADPH (Slater 1963). The larger the number of mitochondria, the more MTT will be transformed into formazan. The photometric measurement of a 96-well plate is performed with a spectrophotometer. Since reduction of MTT can only occur in metabolically active cells, the level of activity is a measure of the viability of the cells. MTT provides sensitive and reproducible indices of growth as well as sensitivity in individual cell lines over the course of multiple passages.

The method described in Protocol can be performed using standard laboratory equipment and individual reagents. MTT assay where purchased from Sigma (St. Louis, MO) and were used according to the manufacturer's instructions. The method is described for cells in a 96-well plate. Prior to performing experiments, a standard curve for a given cell type by MTT assay of known numbers of cells over a range of approximately 5000–120000 was done.

Advantages of the MTT assay are that responses of cell lines which do not grow as colonies can be measured, and moreover it is less time consuming and less prone to personal interpretations because of the automated read-out. With calibration curves it is possible

1) To overcome the absence of a linear relationship between cell number and the higher absorbance values, 2) To extend the range of values, and 3) To correct for the differences in formazan production between cell lines.

PROTOCOL:

THE MTT ASSAY

EQUIPMENT, MATERIALS AND REAGENTS

Spectrophotometer: Emax reader (Molecular Devices, Wokingham, UK) with software Softmax PRO. MTT stock solution 5 mg ml−1: dissolve 50 mg MTT in a total volume of 10ml phosphate-buffered saline. Solution was stored at −20°C. Working concentration MTT solution: 0.5 mg ml^{-1} MTT in PBS. Dimethylsulfoxide (DMSO) were purchased from ATCC (Rockville, MD, USA).

METHOD

1. Incubate cells seeded in the wells of a 96-well plate with test growth factors for the desired time periods. Aspirate medium and add 30 μl per well of 0.5 mg ml−1 MTT solution. Incubate for 4 hours at 37°C in the tissue culture incubator.

2. Remove medium and add 100 μl per well of DMSO. Measure absorbance at 570 nm with a reference wavelength in the spectrophotometric plate reader. Calculate cell numbers from absorbance using the standard curve.

Calculation of Absorbance rate:

Once a linear range was found from the standard curves, we chose the 20000 cell concentration to observe for a 5 day period since in fell within linear range of 10000 to 30000 cells.   The absorbance values at day 0, 3 and 5 were plotted and the slope taken to derive a rate of absorbance changes over

the period of time (Figure 36). What is plot in the figure is the number of cells that where plated initially at day 0 and allowed to grow over day 3 and 5 and then measured.
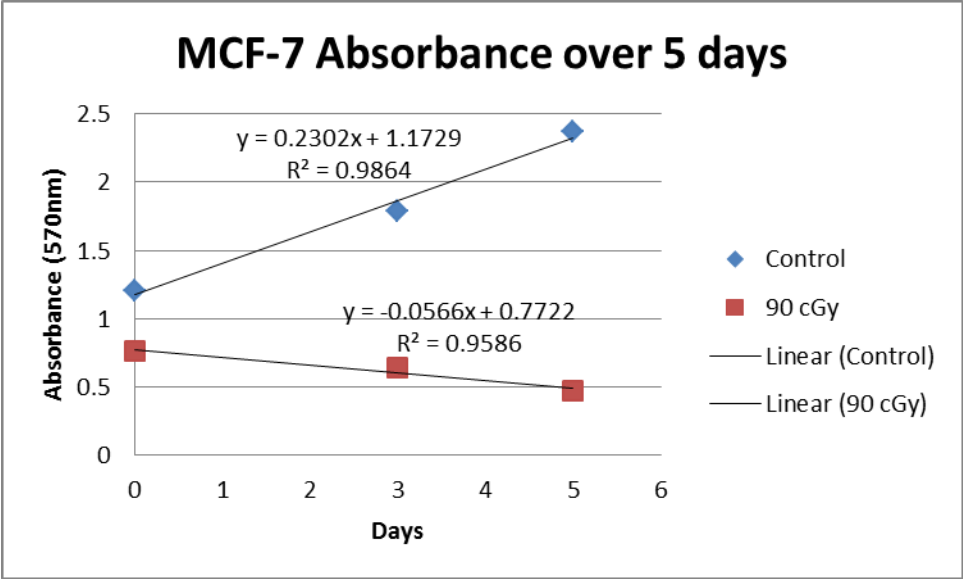

Figure 36 The MTT assay done on the well plate containing an initial value of 20,000 cells observed over a 5 day period for control and irradiation sample.

REFERENCES

Abram WP, Clarke J, McAleer JJA, Graham JD, Riddle P, Goodman S, Tomlinson M, Counsell KBR, Elyan SAG, Owen JR, Lavery B, Sugden E, Dobbs J, Whittaker S, Brammer C et al. 2008. The UK Standardisation of Breast Radiotherapy (START) Trial A of radiotherapy hypofractionation for treatment of early breast cancer: A randomised trial. Lancet Oncology 9(4): 331-341.

Allinen M, Beroukhim R, Cai L, Brennan C, Lahti-Domenici J, Huang HY, Porter D, Hu M, Chin L, Richardson A, Schnitt S, Sellers WR, Polyak K 2004. Molecular characterization of the tumor microenvironment in breast cancer. Cancer Cell 6(1): 17-32.

Amadeu TP, Coulomb B, Desmouliere A, Costa AM 2003. Cutaneous wound healing: myofibroblastic differentiation and in vitro models. Int J Low Extrem Wounds 2(2): 60-8.

Andre F, Berrada N, Desmedt C 2010. Implication of tumor microenvironment in the resistance to chemotherapy in breast cancer patients. Current opinion in oncology 22(6): 547-551.

Bagely RG ed. 2010. The Tumor Microenvironment. 1st ed. New York, Springer. 300 p.

Baker DG, Masterson TM, Pace R, Constable WC, Wanebo H 1989. The influence of the surgical wound on local tumor recurrence. Surgery 106(3): 525-532.

Baker EL, Lu J, Yu D, Bonnecaze RT, Zaman MH 2010. Cancer cell stiffness: integrated roles of three-dimensional matrix stiffness and transforming potential. Biophysical Journal 99(7): 2048-57.

Barcellos-Hoff MH 2008. Cancer as an emergent phenomenon in systems radiation biology. Radiation and Environmental Biophysics 47(1): 33-8.

Barcellos-Hoff MH 2010. Stromal mediation of radiation carcinogenesis. Journal of Mammary Gland Biology and Neoplasia 15(4): 381-7.

Barcellos-Hoff MH, Dix TA 1996. Redox-mediated activation of latent transforming growth factor-beta 1. Molecular Endocrinology 10(9): 1077-83.

Barcellos-Hoff MH, Costes SV 2006. A systems biology approach to multicellular and multi-generational radiation responses. Mutation research 597(1-2): 32-8.

Barcellos-Hoff MH, Park C, Wright EG 2005. Radiation and the microenvironment - tumorigenesis and therapy. Nat Rev Cancer 5(11): 867-75.

Baum M, Demicheli R, Hrushesky W, Retsky M 2005. Does surgery unfavourably perturb the "natural history" of early breast cancer by accelerating the appearance of distant metastases? European Journal of Cancer 41(4): 508-515.

Belletti B, Vaidya JS, D'Andrea S, Entschladen F, Roncadin M, Lovat F, Berton S, Perin T, Candiani E, Reccanello S, Veronesi A, Canzonieri V, Trovo MG, Zaenker KS, Colombatti A, Baldassarre G, Massarut S 2008. Targeted intraoperative radiotherapy impairs the stimulation of breast cancer cell proliferation and invasion caused by surgical wounding. Clinical Cancer Research 14(5): 1325-1332.

Bergamaschi A, Kim YH, Kwei KA, La Choi Y, Bocanegra M, Langerod A, Han W, Noh DY, Huntsman DG, Jeffrey SS, Borresen-Dale AL, Pollack JR 2008. CAMK1D amplification implicated in epithelial-mesenchymal transition in basal-like breast cancer. Molecular oncology 2(4): 327-39.

Biedler JL, Helson L, Spengler BA 1973. Morphology and growth, tumorigenicity, and cytogenetics of human neuroblastoma cells in continuous culture. Cancer research 33(11): 2643-52.

Bissell MJ 2006. Extracellular matrix remodeling in mammary gland branching morphogenesis and breast cancer. In: Davies JA ed. Branching Morphogenesis. New York, Springer Science. Pp. 126-142.

Bissell MJ, Radisky DC, Rizki A, Weaver VM, Petersen OW 2002. The organizing principle:

microenvironmental influences in the normal and malignant breast. Differentiation 70(9-10):

537-546.

Bloomer WD, Adelstein SJ 1982. The mammalian radiation survival curve. Journal of nuclear medicine :

official publication, Society of Nuclear Medicine 23(3): 259-65.

Bromley R, Davey R, Oliver L, Harvie R, Baldock C 2006. A preliminary investigation of cell growth after

irradiation using a modulated x-ray intensity pattern. Physics in Medicine and Biology 51(15):

3639-3651.

Calinski T 1981. PRINCIPLES AND PROCEDURES OF STATISTICS - A BIOMETRICAL APPROACH, 2ND

EDITION - STEEL,RGD, TORRIE,JH. Biometrics 37(4): 859-860.

Camara O, Rengsberger M, Egbe A, Koch A, Gajda M, Hammer U, Jorke C, Rabenstein C, Untch M,

Pachmann K 2007. The relevance of circulating epithelial tumor cells (CETC) for therapy

monitoring during neoadjuvant (primary systemic) chemotherapy in breast cancer. Annals of

oncology : official journal of the European Society for Medical Oncology / ESMO 18(9): 1484-92.

Carlson MA, Longaker MT 2004. The fibroblast-populated collagen matrix as a model of wound healing:

a review of the evidence. Wound Repair and Regeneration 12(2): 134-147.

Castelló-Cros R, Khan DR, Simons J, Valianou M, Cukierman E 2009. Staged stromal extracellular 3D

matrices differentially regulate breast cancer cell responses through PI3K and beta1-integrins.

BMC Cancer 9.

Chiarugi P, Pani G, Giannoni E, Taddei L, Colavitti R, Raugei G, Symons M, Borrello S, Galeotti T, Ramponi

G 2003. Reactive oxygen species as essential mediators of cell adhesion: the oxidative inhibition

of a FAK tyrosine phosphatase is required for cell adhesion. Journal of Cell Biology 161(5): 933-

44.

Cukierman E, Pankov R, Stevens DR, Yamada KM 2001. Taking cell-matrix adhesions to the third

     dimension. Science 294(5547): 1708-12.

Demicheli R, Valagussa P, Bonadonna G 2001. Does surgery modify growth kinetics of breast cancer

     micrometastases? British Journal of Cancer 85(4): 490-492.

Desmouliere A, Guyot C, Gabbiani C 2004. The stroma reaction myofibroblast: a key player in the control

     of tumor cell behavior. International Journal of Developmental Biology 48(5-6): 509-517.

Diegelmann RF, Evans MC 2004. Wound healing: an overview of acute, fibrotic and delayed healing.

     Frontiers in bioscience : a journal and virtual library 9: 283-9.

Dobaczewski M, Gonzalez-Quesada C, Frangogiannis NG 2010. The extracellular matrix as a modulator of

     the inflammatory and reparative response following myocardial infarction. Journal of Molecular

     and Cellular Cardiology 48(3): 504-511.

Doyle W 1962. Operation useful for similarity-invariant pattern recognition. Journal of the Association

     for Computing Machinery 9: 259-267.

Eck SM, Cote AL, Winkelman WD, Brinckerhoff CE 2009. CXCR4 and matrix metalloproteinase-1 are

     elevated in breast carcinoma-associated fibroblasts and in normal mammary fibroblasts exposed

     to factors secreted by breast cancer cells. Molecular cancer research : MCR 7(7): 1033-44.

Engler AJ, Sen S, Sweeney HL, Discher DE 2006. Matrix elasticity directs stem cell lineage specification.

     Cell 126(4): 677-89.

Fillmore CM, Kuperwasser C 2008. Human breast cancer cell lines contain stem-like cells that self-renew,

     give rise to phenotypically diverse progeny and survive chemotherapy. Breast Cancer Research

     10(2).

Fisher B, Anderson S, Bryant J, Margolese RG, Deutsch M, Fisher ER, Jeong JH, Wolmark N 2002. Twenty-

     year follow-up of a randomized trial comparing total mastectomy, lumpectomy, and

lumpectomy plus irradiation for the treatment of invasive breast cancer. The New England journal of medicine 347(16): 1233-41.

Fowler JF 2001. Biological factors influencing optimum fractionation in radiation therapy. Acta Oncologica 40(6): 712-717.

Goh BK, Yong WS 2004. Eighteen-year results in the treatment of early breast carcinoma with mastectomy versus breast conservation therapy. Cancer 100(8): 1766; author reply 1767.

Gouk SS, Lim TM, Teoh SH, Sun WQ 2008. Alterations of human acellular tissue matrix by gamma irradiation: Histology, biomechanical property, stability, in vitro cell repopulation, and remodeling. Journal of Biomedical Materials Research Part B-Applied Biomaterials 84B(1): 205-217.

Grinnell F 1994. Fibroblasts, myofibroblasts, and wound contraction. J Cell Biol 124(4): 401-4.

Grinnell F 2003. Fibroblast biology in three-dimensional collagen matrices. Trends in cell biology 13(5): 264-9.

Gunderson LL, Tepper JE 2007. Clinical Radiation Oncology, Elsevier Churchill Livingstone.

Guo S, Dipietro LA 2010. Factors affecting wound healing. Journal of dental research 89(3): 219-29.

Hakenjos L, Bamberg M, Rodemann HP 2000. TGF-beta1-mediated alterations of rat lung fibroblast differentiation resulting in the radiation-induced fibrotic phenotype. International Journal of Radiation Biology 76(4): 503-9.

Hall EJ 1994. Radiobiology For The Radiologist. Philadelphia, J.B. Lippincott.

Hall JA, Knaus, John V. ed. 2003. An Atlas of Breast Disease. New York, Parthenon Pub. Group.

Hellevik T, Pettersen I, Berg V, Winberg JO, Moe BT, Bartnes K, Paulssen RH, Busund LT, Bremnes R, Chalmers A, Martinez-Zubiaurre I 2012. Cancer-associated fibroblasts from human NSCLC survive ablative doses of radiation but their invasive capacity is reduced. Radiation oncology 7(1): 59.

Herskind C, Rodemann HP 2000. Spontaneous and radiation-induced differentiationof fibroblasts. Experimental Gerontology 35(6-7): 747-55.

Hinz B, Mastrangelo D, Iselin CE, Chaponnier C, Gabbiani G 2001. Mechanical tension controls granulation tissue contractile activity and myofibroblast differentiation. The American journal of pathology 159(3): 1009-20.

Hockel A, Dornhofer N 2005. The hydra phenomenon of cancer: Why tumors recur locally after microscopically complete resection. Cancer research 65(8): 2997-3002.

Holliday DL, Brouilette KT, Markert A, Gordon LA, Jones JL 2009. Novel multicellular organotypic models of normal and malignant breast: tools for dissecting the role of the microenvironment in breast cancer progression. Breast cancer research : BCR 11(1): R3.

Holloway CL, Panet-Raymond V, Olivotto I 2010. Hypofractionation should be the new 'standard' for radiation therapy after breast conserving surgery. Breast 19(3): 163-7.

James ML, Lehman M, Hider PN, Jeffery M, Hickey BE, Francis DP 2010. Fraction size in radiation treatment for breast conservation in early breast cancer. The Cochrane Database of Systematic Reviews(11): CD003860.

Johnston SR 2009. Enhancing the efficacy of hormonal agents with selected targeted agents. Clinical Breast Cancer 9 Suppl 1: S28-36.

Kalluri R, Zeisberg M 2006. Fibroblasts in cancer. Nature Review Cancer 6(5): 392-401.

Kalyanam S, Yapp RD, Insana MF 2009. Poro-viscoelastic behavior of gelatin hydrogels under compression-implications for bioelasticity imaging. Journal of Biomechanical Engineering 131(8): 081005.

Kantarjian H, , Koller, Charles A.Wolff, Robert A. ed. 2006. The MD Anderson manual of medical oncology. New York, McGraw-Hill Medical Pub. Division.

Kaplan RN, Riba RD, Zacharoulis S, Bramley AH, Vincent L, Costa C, MacDonald DD, Jin DK, Shido K, Kerns SA, Zhu Z, Hicklin D, Wu Y, Port JL, Altorki N et al. 2005. VEGFR1-positive haematopoietic bone marrow progenitors initiate the pre-metastatic niche. Nature 438(7069): 820-827.

Kass L, Erler JT, Dembo M, Weaver VM 2007. Mammary epithelial cell: Influence of extracellular matrix composition and organization during development and tumorigenesis. The International Journal of Biochemistry & Cell Biology 39(11): 1987-1994.

Lacroix M, Leclercq G 2004. Relevance of breast cancer cell lines as models for breast tumours: an update. Breast Cancer Research and Treatment 83(3): 249-289.

Levental KR, Yu H, Kass L, Lakins JN, Egeblad M, Erler JT, Fong SF, Csiszar K, Giaccia A, Weninger W, Yamauchi M, Gasser DL, Weaver VM 2009. Matrix crosslinking forces tumor progression by enhancing integrin signaling. Cell 139(5): 891-906.

Mannino M, Yarnold J 2009. Effect of breast-duct anatomy and wound-healing responses on local tumour recurrence after primary surgery for early breast cancer. The lancet oncology 10(4): 425-429.

Marcu LG 2010. Altered fractionation in radiotherapy: from radiobiological rationale to therapeutic gain. Cancer Treatment Review 36(8): 606-14.

Martinez-Outschoorn UE, Lin Z, Trimmer C, Flomenberg N, Wang C, Pavlides S, Pestell RG, Howell A, Sotgia F, Lisanti MP 2011. Cancer cells metabolically "fertilize" the tumor microenvironment with hydrogen peroxide, driving the Warburg effect: implications for PET imaging of human tumors. Cell Cycle 10(15): 2504-20.

Morishima Y, Nomura A, Uchida Y, Noguchi Y, Sakamoto T, Ishii Y, Goto Y, Masuyama K, Zhang MJ, Hirano K, Mochizuki M, Ohtsuka M, Sekizawa K 2001. Triggering the induction of myofibroblast and fibrogenesis by airway epithelial shedding. American journal of respiratory cell and molecular biology 24(1): 1-11.

Muriel V 2002. The biological basis of fractionation in radiotherapy. Clinical and Translational Oncology 4(3): 161-166.

Nemade R 2008. Diseases and Disorders. In: Horobin W ed. Cancer. Tarrytown, Marshall Cavendish Corp. . Pp. 323.

Nguyen TD, Maquart FX, Monboisse JC 2005. Ionizing radiations and collagen metabolism: from oxygen free radicals to radio-induced late fibrosis. Radiation Physics and Chemistry 72(2-3): 381-386.

Olsen CJ, Moreira J, Lukanidin EM, Ambartsumian NS 2010. Human mammary fibroblasts stimulate invasion of breast cancer cells in a three-dimensional culture and increase stroma development in mouse xenografts. BMC Cancer 10: 444.

Olumi AF, Grossfeld GD, Hayward SW, Carroll PR, Tlsty TD, Cunha GR 1999. Carcinoma-associated fibroblasts direct tumor progression of initiated human prostatic epithelium. Cancer research 59(19): 5002-11.

Orimo A, Gupta PB, Sgroi DC, Arenzana-Seisdedos F, Delaunay T, Naeem R, Carey VJ, Richardson AL, Weinberg RA 2005. Stromal fibroblasts present in invasive human breast carcinomas promote tumor growth and angiogenesis through elevated SDF-1/CXCL12 secretion. Cell 121(3): 335-48.

Otsu N 1979. THRESHOLD SELECTION METHOD FROM GRAY-LEVEL HISTOGRAMS. Ieee Transactions on Systems Man and Cybernetics 9(1): 62-66.

Owen JR, Ashton A, Bliss JM, Homewood J, Harper C, Hanson J, Haviland J, Bentzen SM, Yarnold JR 2006. Effect of radiotherapy fraction size on tumour control in patients with early-stage breast cancer after local tumour excision: long-term results of a randomised trial. Lancet Oncology 7(6): 467-71.

Park CC, Bissell MJ, Barcellos-Hoff MH 2000. The influence of the microenvironment on the malignant phenotype. Molecular medicine today 6(8): 324-9.

Paszek MJ, Zahir N, Johnson KR, Lakins JN, Rozenberg GI, Gefen A, Reinhart-King CA, Margulies SS, Dembo M, Boettiger D, Hammer DA, Weaver VM 2005. Tensional homeostasis and the malignant phenotype. Cancer Cell 8(3): 241-54.

Pavlides S, Vera I, Gandara R, Sneddon S, Pestell RG, Mercier I, Martinez-Outschoorn UE, Whitaker-Menezes D, Howell A, Sotgia F, Lisanti MP 2012. Warburg meets autophagy: cancer-associated fibroblasts accelerate tumor growth and metastasis via oxidative stress, mitophagy, and aerobic glycolysis. Antioxidants & redox signaling 16(11): 1264-84.

Petersen OW, Lind Nielsen H, Gudjonsson T, Villadsen R, Ronnov-Jessen L, Bissell MJ 2001. The plasticity of human breast carcinoma cells is more than epithelial to mesenchymal conversion. Breast Cancer Research 3(4): 213-7.

Pieters R, Loonen AH, Huismans DR, Broekema GJ, Dirven MW, Heyenbrok MW, Hahlen K, Veerman AJ 1990. In vitro drug sensitivity of cells from children with leukemia using the MTT assay with improved culture conditions. Blood 76(11): 2327-36.

Pinsky RW, Rebner M, Pierce LJ, Ben-David MA, Vicini F, Hunt KA, Helvie MA 2007. Recurrent cancer after breast-conserving surgery with radiation therapy for ductal carcinoma in situ: Mammographic features, method of detection, and stage of recurrence. American Journal of Roentgenology 189(1): 140-144.

Polyak K, Kalluri R 2010. The role of the microenvironment in mammary gland development and cancer. Cold Spring Harbor perspectives in biology 2(11): a003244.

Prosnitz LR, Horton J, Wallner PE 2009. Accelerated partial breast irradiation: caution and concern from an ASTRO task force. International Journal of Radiation Oncology, Biology, & Physics 74(4): 981-4.

Qayyum MA, Insana MF 2012a. Stromal responses to fractionated radiotherapy. International Journal of Radiation Biology 88(5): 383-392.

Qayyum MA, Insana MF 2012b. Stromal responses to fractionated radiotherapy. International Journal of
Radiation Biology.

Qin J, Li L 2003. Molecular anatomy of the DNA damage and replication checkpoints. Radiation Research
159(2): 139-48.

Rao AK, Ziegler YS, McLeod IX, Yates JR, Nardulli AM 2008. Effects of Cu/Zn superoxide dismutase on
estrogen responsiveness and oxidative stress in human breast cancer cells. Molecular
Endocrinology 22(5): 1113-24.

Rave-Frank M, Virsik-Kopp P, Pradier O, Nitsche M, Grunefeld S, Schmidberger H 2001. In vitro response
of human dermal fibroblasts to X-irradiation: relationship between radiation-induced clonogenic
cell death, chromosome aberrations and markers of proliferative senescence or differentiation.
International Journal of Radiation Biology 77(12): 1163-74.

Rodemann HP, Blaese MA 2007. Responses of normal cells to ionizing radiation. Seminars in Radiation
Oncology 17(2): 81-88.

Ronnov-Jessen L, Petersen OW, Bissell MJ 1996. Cellular changes involved in conversion of normal to
malignant breast: importance of the stromal reaction. Physiological Reviews 76(1): 69-125.

Rossi L, Reverberi D, Podesta G, Lastraioli S, Corvo R 2000. Co-culture with human fibroblasts increases
the radiosensitivity of MCF-7 mammary carcinoma cells in collagen gels. International Journal of
Cancer 85(5): 667-673.

Schulz W 2005. Cancer Therapy

Molecular Biology of Human Cancers. Springer Netherlands. Pp. 449-488.

Shen KC, Miller F, Tait L, Santner SJ, Pauley R, Raz A, Tainsky MA, Brooks SC, Wang YA 2006. Isolation and
characterization of a breast progenitor epithelial cell line with robust DNA damage responses.
Breast Cancer Research and Treatment 98(3): 357-364.

Shieh AC 2011. Biomechanical forces shape the tumor microenvironment. Annals of Biomedical
Engineering 39(5): 1379-89.

Slater TF 1963. Studies on a succinate-neotetrazolium reductase system of rat liver. II. Points of coupling
with the respiratory chain II. Points of coupling with the respiratory chain. BBA - Biochimica et
Biophysica Acta 77(C): 365-382.

Sotgia F, Del Galdo F, Casimiro MC, Bonuccelli G, Mercier I, Whitaker-Menezes D, Daumer KM, Zhou J,
Wang CG, Katiyar S, Xu H, Bosco E, Quong AA, Aronow B, Witkiewicz AK et al. 2009. Caveolin-1(-
/-) Null Mammary Stromal Fibroblasts Share Characteristics with Human Breast Cancer-
Associated Fibroblasts. American Journal of Pathology 174(3): 746-761.

Storz P 2005. Reactive oxygen species in tumor progression. Frontiers in Bioscience 10: 1881-96.

Stuelten CH, DaCosta Byfield S, Arany PR, Karpova TS, Stetler-Stevenson WG, Roberts AB 2005. Breast
cancer cells induce stromal fibroblasts to express MMP-9 via secretion of TNF-alpha and TGF-
beta. Journal of cell science 118(Pt 10): 2143-53.

Su G, Blaine SA, Qiao D, Friedl A 2007. Shedding of syndecan-1 by stromal fibroblasts stimulates human
breast cancer cell proliferation via FGF2 activation. The Journal of biological chemistry 282(20):
14906-15.

Tagliabue E, Agresti R, Carcangiu ML, Ghirelli C, Morelli D, Campiglio M, Martel M, Giovanazzi R, Greco
M, Balsari A, Menard S 2003. Role of HER2 in wound-induced breast carcinoma proliferation.
Lancet 362(9383): 527-533.

Thibeault SL, Gray SD, Bless DM, Chan RW, Ford CN 2002. Histologic and rheologic characterization of
vocal fold scarring. Journal of voice : official journal of the Voice Foundation 16(1): 96-104.

Tomasek JJ, Gabbiani G, Hinz B, Chaponnier C, Brown RA 2002. Myofibroblasts and mechano-regulation
of connective tissue remodelling. Nature reviews. Molecular cell biology 3(5): 349-63.

Tsuchiya Y, Sawada S, Yoshioka I, Ohashi Y, Matsuo M, Harimaya Y, Tsukada K, Saiki I 2003. Increased surgical stress promotes tumor metastasis. Surgery 133(5): 547-55.

Ungefroren H, Sebens S, Seidl D, Lehnert H, Hass R 2011. Interaction of tumor cells with the microenvironment. Cell Communication and Signaling 9.

Vaidya JS, Tobias JS, Baum M, Keshtgar M, Joseph D, Wenz F, Houghton J, Saunders C, Corica T, D'Souza D, Sainsbury R, Massarut S, Taylor I, Hilaris B 2004. Intraoperative radiotherapy for breast cancer. The lancet oncology 5(3): 165-73.

Van Dyk J 1999. The modern technology of radiation oncology: a compendium for medical physicists and radiation oncologists, Medical Physics Pub.

Veronesi U, Cascinelli N, Mariani L, Greco M, Saccozzi R, Luini A, Aguilar M, Marubini E 2002. Twenty-year follow-up of a randomized study comparing breast-conserving surgery with radical mastectomy for early breast cancer. The New England journal of medicine 347(16): 1227-32.

Wachsberger P, Burd R, Dicker AP 2003. Tumor response to ionizing radiation combined with antiangiogenesis or vascular targeting agents: exploring mechanisms of interaction. Clinical cancer research : an official journal of the American Association for Cancer Research 9(6): 1957-71.

Wang J, Fan J, Laschinger C, Arora PD, Kapus A, Seth A, McCulloch CA 2005. Smooth muscle actin determines mechanical force-induced p38 activation. The Journal of biological chemistry 280(8): 7273-84.

Wang Z, Chen J, Dou L 2006. A new multi-threshold segmentation method based on MHFFCM. Pp. 195-200.

Weaver VM, Petersen OW, Wang F, Larabell CA, Briand P, Damsky C, Bissell MJ 1997. Reversion of the malignant phenotype of human breast cells in three-dimensional culture and in vivo by integrin blocking antibodies. The Journal of cell biology 137(1): 231-45.

Weinberg RA 2007. The Biology of Cancer. New York, Garland Science, Taylor & Francis Group LLC.

Wipff PJ, Hinz B 2009. Myofibroblasts work best under stress. Journal of bodywork and movement
therapies 13(2): 121-7.

Xu J 2010. Characterization and modeling of cell activation upon TGF-beta 1 stimulation in a 3-D culture
system. Unpublished thesis, University of Illinois at Urbana-Champaign, Urbana.

Yamada KM, Cukierman E 2007. Modeling tissue morphogenesis and cancer in 3D. Cell 130(4): 601-10.

Yang Y, Xing L 2005. Optimization of radiotherapy dose-time fractionation with consideration of tumor
specific biology. Medical physics 32(12): 3666-3677.

Yu H, Mouw JK, Weaver VM 2011. Forcing form and function: biomechanical regulation of tumor
evolution. Trends in cell biology 21(1): 47-56.